THE PIVOTAL ROLE OF FIBROCYTES ON FOREIGN BODY REACTIONS

by

DAVID WILLIAM BAKER

Presented to the Faculty of the Graduate School of

The University of Texas at Arlington in Partial Fulfillment

of the Requirements

for the Degree of

DOCTOR OF PHILOSOPHY

THE UNIVERSITY OF TEXAS AT ARLINGTON

August 2013

Acknowledgements

I would like to take this opportunity to thank a number of individuals who have helped to guide and shape my development as a researcher here at UT Arlington. I would first like to thank my dissertation committee, Dr. Kytai Truong Nquyen, Dr. Chi-Chun Tsai, Dr. Ramesh Saxena, Dr. Lei Shi, and Dr. Liping Tang, for their guidance, insight, and suggestions during the development of this dissertation. I would like to further express my gratitude to my advisor Dr. Liping Tang for his encouragement, his demand for excellence, and his wisdom in guiding prior works and the outline of this dissertation.

In addition, I would like to thank several members of the regenerative medicine lab group whose assistance has been instrumental for the development of this dissertation and my prior works. I would like to acknowledge Dr. Hong Weng and Dr. Jinhui Shen for their assistance with animal studies. In addition, I would also like to acknowledge the work of Dr. Jun Zhou for his fabrication of the imaging probes and other microparticles used in this work. My sincerest thanks to Dr. Yi-Ting Tsai for her technical assistance with, and time spent on, *in vivo* imaging, as well as Dr. Ashwin Nair for his patience and insight in discussing problems and solutions. Lastly from the laboratory I would like to thank Dr. Paul Thevenot for his help and guidance in getting me started during the early part of my research.

Finally, I would like to thank my family for their support and understanding. To my wife, Jordan Baker, I would like to express my deepest appreciation for her patience and companionship. I would also like to thank my parents, David and Janice Baker, who have always believed in me. Without the support and love of my family this work would not have been possible.

July 12, 2013

Abstract

THE PIVOTAL ROLE OF FIBROCYTES

ON FOREIGN BODY REACTIONS

David W Baker, PhD

The University of Texas at Arlington, 2013

Supervising Professor: Liping Tang

Fibrocytes are circulating connective tissue precursor cells that were first described in 1994 by Bucala *et al*. as mediators of the innate immune response [1]. Recently the notion of a fibrocyte has not only gained widespread acceptance, but these cells have been identified to participate in a number of disease and pathologic states including aberrant wound repair, fibrosis of organs, cardiovascular disease, and even normal aging. Despite these advancements, little was known about the response of these dynamic cells to biomaterial implants and foreign body reactions. The main focus of my thesis work has therefore focused on investigating fibrocyte-mediate responses, and identifying cellular interactions and the role of fibrocytes during the foreign body response. Our results support that fibrocytes are vital and primary contributors to collagen deposition and expansion of encapsulating fibrotic matrix and scar formation. This thesis summarizes our efforts on the development of several strategies to alleviate fibrocyte driven fibrotic responses.

In the first approach macrophage interactions were investigated through the development of a dual, near infrared, imaging probe modality to non-invasively investigate the role of macrophage polarization on implant-associated fibrotic tissue reactions in real time. Two polyethylene glycol based probes were fabricated to detect

M1 and M2 macrophages around biomaterial implants and infection. Using antagonistic compounds to block specific cytokine activators, we find that fibrocyte accumulation is linked to macrophages and responsive to transforming growth factor beta (TGF-β) signaling related to alternative macrophage activation. In addition, we found that stabilizing mast cells drastically reduce fibrocyte and fibrocyte-derived collagen production around PLGA implants. Deeper investigation using mast cell depleted and reconstituted mice irrevocably demonstrates that the degree of mast cell activation can dictate subsequent fibrocyte responses.

In addition to cellular mediate mechanisms, micropillar implants are used to passively modify fibrocyte activation. Very interestingly fibrocytes were found to be more responsive to topographical changes, specifically spacing and height, of PDMS micropillar implants than fibroblasts or macrophages. The cellular responses were found to correlate with the histological outcomes of fibrosis including granulation tissue formation and collagen production. Lastly, it has recently been shown that fibrocytes possess a multi-potency for several lineages including adipocytes. The potential for differentiation however had not been investigated *in vivo*. Through the use of mini-osmotic pumps, the potential for directing fibrocyte differentiation *in vivo* was assessed by delivering specific differentiation agents. The results presented in this thesis provide strong support for novel strategies to resolve or treat complications of the foreign body response and excessive fibrosis to existing medical implants.

Table of Contents

Acknowledgements iii

Abstract iv

List of Illustrations x

List of Tables xii

Chapter 1 Introduction 1

1.1 Background 1

1.2 Acute Inflammatory Responses and Fibrosis 3

1.2.1 Macrophage Polarization and Tissue Responses 4

1.2.2 Fibroblasts and Myofibroblasts 6

1.2.3 Fibrotic Tissue Formation 7

1.3 Fibrocytes 8

1.3.1 Origin and Properties of Fibrocytes 8

1.3.2 Identification and Isolation of Fibrocytes 9

1.3.3 Fibrocytes in Disease Models and Wound Healing 10

1.4 Strategies and Aims of This Dissertation 11

1.4.1 Mast Cells Responses and the Alteration of Fibrocyte Recruitment 12

1.4.2 Macrophage Polarization and the Influence on Fibrocytes 12

1.4.3 Topographical Cues and Passive Alteration of Fibrocyte Responses 13

1.4.4 Fibrocyte to Adipocyte Differentiation and the Fibrotic Response 13

Chapter 2 Fibrocytes and Implant-Mediated Fibrotic Tissue Responses 14

2.1 Introduction 14

2.2 Fibrocytes at the Interface and their Role in Biomaterial-mediated Responses 14

2.2.1 Purpose 14
2.2.2 Materials and Methods 15
2.2.3 Results 18
2.2.4 Conclusion 25
2.3 Mast Cell Stimulation Dictates Fibrocyte and Fibrotic Responses 26
2.3.1 Purpose 26
2.3.2 Materials and Methods 27
2.3.3 Results 29
2.3.4 Discussion 32
2.4 Mast Cell Deficiency and Reconstitution on Implant-Associated Fibrotic Reactions 32
2.4.1 Purpose 32
2.4.2 Materials and Methods 33
2.4.3 Results 34
2.4.4 Discussion 36
Chapter 3 Implant-Associated Macrophage Responses and Polarization 39
3.1 Introduction 39
3.2 Macrophage Depletion Leads to Reduced Fibrocyte Responses and Collagen Production 41
3.2.1 Purpose 41
3.2.2 Materials and Methods 41
3.2.3 Results 42
3.2.4 Discussion 45
3.3 Development of Optical Imaging Probes for Monitoring Macrophage Polarization 46

3.3.1 Introduction 46
3.3.2 Materials and Methods 48
3.3.3 Results 54
3.3.4 Discussion 63
3.4 Influence of Macrophage Polarization on Fibrotic Reactions 66
3.4.1 Introduction 66
3.4.2 Materials and Methods 67
3.4.3 Results 70
3.4.4 Discussion 76
Chapter 4 Strategies to Alleviate Fibrocyte-Mediated Fibrosis 81
4.1 Introduction 81
4.2 Topographical Cues and Alteration of Fibrocyte Responses 83
4.2.1 Introduction 83
4.2.2 Materials and Methods 84
4.2.3 Results 88
4.2.4 Discussion 99
4.3 Fibrocyte to Adipocyte Differentiation and the Fibrotic Response 101
4.3.1 Introduction 101
4.3.2 Materials and Methods 103
4.3.3 Results 106
4.3.4 Discussion 113
Chapter 5 Summary and Conclusion 116
5.1 Summary 116
5.2 Future Perspectives 119
References 121

Biographical Information 136

List of Illustrations

Figure 1.1 Current model of tissue injury and repair 4

Figure 1.2 Alternative model of tissue injury and repair 8

Figure 2.1 Culture and identification of splenic derived fibrocytes. 20

Figure 2.2 *In vivo* migration of cultured fibrocytes to biomaterial implants. 21

Figure 2.3 FACS analysis of wound fluid after chimeric bone marrow transplant. 22

Figure 2.4 Time course study of fibrocyte accumulation and collagen production. 24

Figure 2.5 Correlation between recruited fibrocyte numbers and collagen percentage. . 25

Figure 2.6 Histological staining for mast cell stabilizing and destabilizing agents. 31

Figure 2.7 Histological responses for mast cell stabilizing and destabilizing agents. 31

Figure 2.8 Cellular responses for mast cell stabilizing and destabilizing agents. 32

Figure 2.9 Histological staining for mast cell deficiency and reconstitution. 35

Figure 2.10 Histological responses for mast cell deficiency and reconstitution. 36

Figure 2.11 Cellular responses for mast cell deficiency and reconstitution. 36

Figure 3.1 NIR labeled fibrocyte migration to control and macrophage depleted mice 43

Figure 3.2 Histological identification of fibrocytes and collagen production 44

Figure 3.3 Histograms of fibrocyte and collagen response to macrophage depletion 45

Figure 3.4 M1 and M2 cellular influx to PLA implants 53

Figure 3.5 Characterization of folate- and mannose-based probes 55

Figure 3.6 Differentiation of macrophage and cytotoxicity of imaging probes 57

Figure 3.7 In vitro characterization of folate- and mannose based probes 58

Figure 3.8 M1 M2 probe assessment in an extremes model of device-centered infection 60

Figure 3.9 M1 M2 probe assessment in a subtle model of biomaterial responses 62

Figure 3.10 Correlation of folate- and mannose-based probe intensity with M1 M2 cells. 62
Figure 3.11 HPLC absorbance spectrum of SB431542 and SB203580 69
Figure 3.12 Scaffold fabrication and drug release kinetics 71
Figure 3.13 Effect of various cytokine antagonists on fibrocyte and polarized macrophage reactions in the acute response. 73
Figure 3.14 Chronic response of microbubble scaffold implants. 74
Figure 3.15 Two week histological response of SB431542 and SB203580 76
Figure 3.16 Two week histological response of SB431542 and SB203580 76
Figure 4.1 Overview of micropillar fabrication 86
Figure 4.2 Analysis of differential *in vitro* response of macrophages and fibroblasts 90
Figure 4.3 SEM images of cellular proliferation at 3 days for select pillar substrates 92
Figure 4.4 Histological analysis of tissue response to micropillar implants 94
Figure 4.5 Analysis of cellular responses to micropillar implants 95
Figure 4.6 Selected correlations of fibrocytes with histological tissue responses. 96
Figure 4.7 Collagen alignment to micropillar implants 99
Figure 4.8 In vitro differentiation of fibrocytes to adipocytes. 107
Figure 4.9 Histological analysis of fibrocyte to adipocyte differentiation 109
Figure 4.10 Analysis of lipid and collagen accumulation surrounding implants 110
Figure 4.11 Identification of fibrocytes during adipogenic differentiation in vivo. 111
Figure 4.12 Quantification of fibrocytes during adipogenic differentiation 112
Figure 4.13 Quantification of myofibroblasts during adipogenic differentiation 113

List of Tables

Table 3.1 Summary of localized release of cytokine antagonists on macrophage and fibrotic responses. 78

Table 4.1 Dimensional analysis of pillar substrates 88

Table 4.2 Summary of tissue response to micropillar implants. 97

Chapter 1

Introduction

1.1 Background

Governing the biomaterial mediated tissue response is critically importance for the future design and improvement of many medical devices. With almost daily advances in biomedical materials including novel polymers and intricate fabrication methods, there is a high demand to understand and improve implant biocompatibility to enhance efficacy, safety, and regenerative properties. Unfortunately, almost all biomedical implants are plagued with significant adverse reactions with localized tissue contact. The functional success or failure of these devices is invariably a function of the host tissue response, often termed the “foreign body response”. This response involves varying degrees of immune, inflammatory, and fibrotic reactions, often regulated by interactive biomaterial, protein, and cellular events.

An account of the foreign body response has been well established in many previous reports [2-5]. The complex processes however are not entirely understood. In brief, almost all medical implants are quickly covered (within seconds to minutes), with a layer of plasma proteins following exposure to bodily fluids or blood [6]. Within a few hours to several days, implants are surrounded by a large number of immune cells and a small number of fibroblast-like cells. A few weeks later, collagen-rich fibrotic capsules form and isolate the medical device from the surrounding host tissue. Since implants are encapsulated by adsorbed plasma proteins, and a dense population of inflammatory cells (neutrophils and macrophages), forms prior to fibrotic tissue formation, it is generally believed that biomaterial:protein interactions drive biocompatibility. In addition, it is highly regarded that biomaterial-mediated inflammatory responses drive subsequent fibrotic tissue formation. We should temper this however by pointing out that while immune and

inflammatory cell populations are known to release a plethora of pro-inflammatory and pro-fibrotic cytokines, none of these cells are directly responsible for the collaganous matrix formation resulting in the fibrotic capsule.

This report focuses on the cellular interactions primarily and directly responsible for the formation of the collagen-rich fibrotic capsule in the foreign body response. Our studies have revealed that a circulating connective tissue cell, termed “fibrocyte,” plays a critical and previously underestimated role in the foreign body response. These cells are highly migratory with a dynamic and plastic phenotype and were found to be directly related to the collagen production and accumulation surrounding biomaterial implants. Since mast cells are known to initiate inflammatory responses, we hypothesized, and show for the first time, that mast cell stabilization or degranulation substantially alters the fibrocyte-mediate response. In addition, we have confirmed that macrophages are an important modulator of fibrotic tissue reactions, and suggest a positive relationship between macrophages and fibrocytes. Further investigation shows that macrophage polarization is an important determinant for fibrocyte recruitment and activation around biomaterials. We therefore propose the following sequence of cellular events during foreign body reactions. First, (1) biomaterial implants prompt mast cell activation and release of pro-inflammatory cytokines. This is followed by, (2) the localized release of cytokines which trigger the recruitment of inflammatory cells, including macrophages which lean towards an M1 pro-inflammatory phenotype. Subsequently, (3) activated neutrophils and M1 macrophages release many inflammatory products and enzymes to destroy surrounding tissue which is quickly followed by fibrocyte recruitment. Immigrated fibrocytes, (4) proliferate at the implant site in an inflammatory setting and are further stimulated to differentiate into myofibroblasts producing collagenous tissues. Finally, (5) the changing microenvironment, stimulates an increase in the percentage of

macrophages that possess an M2 phenotype. The release products of M2 macrophages then slow down fibrotic tissue production to form permanent fibrotic capsules.

By understanding these cellular mediated interactions we continue to investigate strategies to overcome fibrocyte dominated fibrotic reactions. To further explore strategies to mitigate fibrocyte driven responses we must first appreciate the connections between inflammation and fibrosis.

1.2 Acute Inflammatory Responses and Fibrosis

It is well recognized that the extent of inflammation and the persistence of inflammatory cells and products surrounding the implant has a substantial influence on the subsequent host fibrotic response. There is evidence to support this claim in both the acute and chronic inflammatory reactions. In the acute phase of inflammation, mast cell degranulation is known to increase vasodilation facilitating neutrophil infiltration and monocyte diapedesis, as well as subsequent fibrosis around silicone implants [2, 7-8]. Additionally, adherent phagocytes have been shown to produce and release significant amounts of pro-inflammatory and pro-fibrotic cytokines, such as interleukin-1β (IL-1β) and tumor necrosis factor -α (TNF-α) [3, 9-12]. With prolonged inflammation, it has been shown that by suppressing the activation, but not the presence of phagocytes with corticosteroids, the formation of fibrotic tissue can be dramatically reduced [13-17]. Furthermore, recent research of wound healing reactions has shown that that phagocyte responses, and associated inflammatory products, are essential to fibrotic reactions [18-23]. In many cases, macrophages become activated to destroy the potential pathogen (the implant), however the continued presence of the implant often contributes to a long-term overstimulation of macrophages leading to chronic inflammation and the resultant poor wound healing/ regenerative capabilities. As a result of continued inflammation, it is

generally accepted that fibroblast proliferation and collagen production are influenced by many of the phagocyte-derived proteins including, platelet activating factor, platelet-derived growth factor-α, IL-1β and TNF-α, resulting in the fibrosis of the implant [3, 9-12]. In normal repair however, macrophages are observed to shift from classical activation to an alternative activation state (termed macrophage polarization), down regulating inflammation and up regulating fibroblast proliferation and activation to produce extracellular matrix and promote repair (Figure 1).

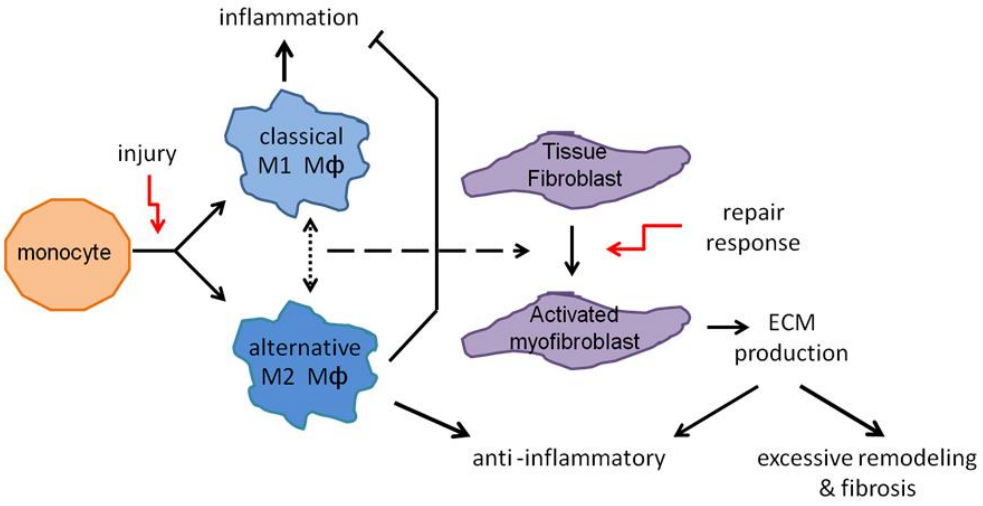

Figure 1.1 Current model of tissue injury and repair
In current models of tissue repair circulating monocytes enter the tissue in response to injury and undergo phenotypic changes to become macrophages. Macrophages possess a plasticity of multiple phenotypes shown to effect both tissue destruction (M1) and repair (M2). During the repair response macrophages stimulate tissue fibroblasts to proliferate and activate to enhance production of extracellular matrix. With an increased inflammatory response or profibrotic environment the mechanisms shift toward excessive remodeling and fibrosis

1.2.1 Macrophage Polarization and Tissue Responses

As previously mentioned immune/ inflammatory cells such as neutrophils and, macrophages are known to prompt the release of a variety of pro-inflammatory and pro-

fibrotic cytokines which drive the resultant tissue response [2, 24-27]. While neutrophils are undoubtedly one of the first cell types to arrive at the biomaterial interface, their numbers decrease significantly one week after material implantation [28]. In fact, the neutrophils peak influx is short lived, up to 24 hours, with a dominating presence for less than a few days [2, 5]. Two weeks after implantation no myeloperoxidase-positive neutrophils are found at the implant sites suggesting that most of the residual neutrophils are no longer activated and functional [29].

Macrophage's on the other hand are widely recognized as the driving force in perpetuating immune responses and chronic inflammation [2, 4-5]. Macrophages are derived from monocytes which develop from a common myeloid progenitor cell in the bone marrow [30]. These circulating monocytes enter the tissues, and upon arrival at the implantation site, undergo a phenotypic change to become macrophages either through steady state turnover or through differentiation [4, 30]. In recent years, there has been great emphasis on the plasticity of functional phenotypes or polarization of macrophages which are mainly thought to exist within a range of functional subsets [31]. These subsets are commonly categorized as M1 classically activated cells or M2 alternatively activated cells. It has been shown that these subtypes tend to react in a pro-inflammatory or regulatory nature respectively (although not exclusively), influencing both tissue destruction and regeneration [31-32].

In terms of tissue regeneration and fibrosis, this macrophage paradigm introduces an interesting concept. While substantial research efforts have demonstrated macrophage adhesion, activation, cytokine expression and secretion with *in vitro* studies on biomaterials, few studies have implicated a polarization response and resulting interactions *in vivo*. Recently one study examined the role of macrophages in the remodeling process of biologically derived surgical mesh materials after implantation. The

authors found that higher ratios of M2/M1 macrophages were associated with more positive remodeling outcomes [30]. Additionally they hypothesize that the constructive remodeling outcome may be due to the recruitment of different cell populations with materials that elicit an M1 or an M2 response [30]. It remains mostly unknown however, how alterations in macrophage responses and macrophage polarization (pro-inflammatory M1 cells and pro-regenerative M2 cells) will influence fibrocytes and the fibrotic response to the implant.

1.2.2 Fibroblasts and Myofibroblasts

Several cytokines released by activated macrophages including interleukin-1β (IL-1β), tumor necrosis factor-α (TNF-α), platelet activating factor, and platelet-derived growth factor (PDGF), have been shown to initialize the recruitment and activation of fibroblasts, which may lead to localized collagen production [10-11, 33-34]. Fibroblasts however, often have organ-specific functions in promoting tissue homeostasis such as extracellular matrix and cytokine production [35]. Furthermore fibroblasts are often quiescent in tissue and must activate to myofibroblasts before participating in wound healing or tissue remodeling [36]. Myofibroblasts, the activated phenotype of fibroblasts, are well known to be responsive for increased collagen production and are ultimately responsible for wound contraction and closure [37-38]. Myofibroblasts have also been shown to participate in foreign body reactions [38-40]. However, the source of myofibroblasts remains unclear at best. Studies have suggested that myofibroblasts may arise from resident tissue populations [38], dedifferentiate from epithelial cells through epithelial-mesenchymal transition [36], or differentiate from a precursor cell such as the fibrocyte [39, 41-42]. In addition, it is not entirely clear how the inflammatory mediators affect fibrotic cell responses in the case of foreign body reactions.

1.2.3 Fibrotic Tissue Formation

The continued presence of the implant in tissue is perceived by the host as a persistent source of inflammatory stimuli which often leads to chronic inflammation. As a result, the initial protein adsorption and fibrin clot formed during acute inflammation is converted into a granulation tissue [43]. Granulation tissue development encompasses a wide variety of growth factors and cytokines which promote the formation of new blood vessels through angiogenesis. At the same time, fibroblasts are thought to activate to myofibroblasts producing proteins which replace the granulation tissue with a structural extracellular matrix comprised of collagen, elastin, glycoproteins and proteoglycans. The circulating fibrocyte offers an alternative mechanistic paradigm during this shift from inflammation to fibrosis. It has been suggested, that rather than resulting from the actions of macrophages and fibroblasts alone, tissue remodeling may also be influenced by fibrocytes adopting the phenotype of macrophages or fibroblasts (Figure 2) [35]. At either rate, the continuation of extracellular matrix production often results in the implant becoming walled off by a thick collagenous fibrous capsule preventing interaction with the surrounding tissue [44-45].

This process is associated with the failure of many types of devices, such as a variety of biosensors [13, 46-48], drug delivery systems [49-50], spine/joint [51-53], breast [54-56], and eye implants[57-58], as well as neural electrodes [59-60]. In example, glucose sensors have been found to lose functionality due to fibrous encapsulation of sensor implants [61]. The role of fibrocytes at the material interface presents an alternative mechanism of tissue repair and remodeling with the potential to improve the safety and efficacy of such devices.

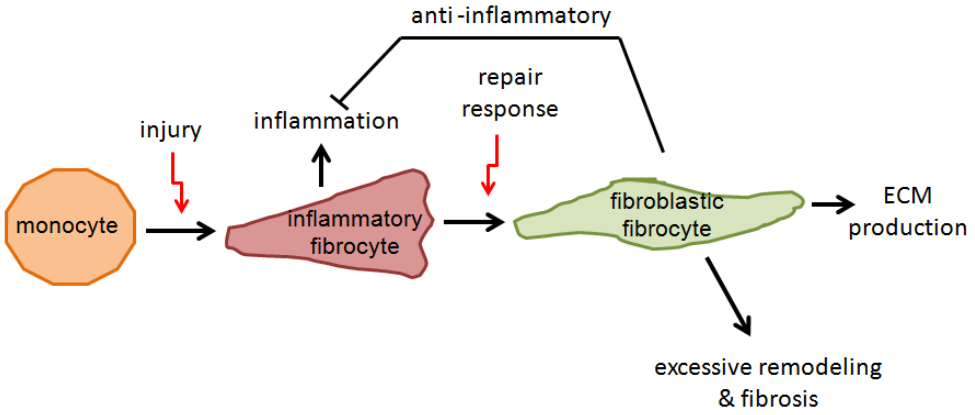

Figure 1.2 Alternative model of tissue injury and repair
In an alternative model of fibrocyte mediate repair, fibrocytes are thought to differentiate from a monocyte precursor cell. These initial fibrocytes are inflammatory in nature and can act directly on the inflammatory response similar to macrophages. During the repair response fibrocytes respond to environmental cues with a shift in phenotype to regulate extracellular matrix production and fibrosis becoming anti-inflammatory similar to activated fibroblasts.

1.3 Fibrocytes

1.3.1 Origin and Properties of Fibrocytes

Fibrocytes are mesenchymal cells that are thought to derive from monocyte precursors in the bone marrow [39, 62]. Their biology and interactions have primarily come understudy recently, however the term "fibrocyte" was first used to describe a circulating monocyte-derived cell type capable of expressing fibroblastic properties in 1994 [1]. More recent study of the fibrocyte has lead to the notion of a dual modality, with the inflammatory features of a macrophage and the remodeling properties of a fibroblast [35]. During the acute inflammatory response, fibrocytes have been shown to increase production of inflammatory cytokines such as IL-6 and IL-8 and down regulate fibrotic markers such as collagen production [63]. Additionally fibrocytes may also function to activate cytotoxic $CD8^+$ T cells through antigen-presentation [64-65]. After arrival at a wound site, fibrocytes can participate in fibrotic reactions through differentiation to

myofibroblasts and secretion of collagen, vimentin, and other proteins which influence the developing fibrotic matrix [39, 42, 66]. Furthermore, and very interestingly fibrocytes have recently been shown to possess differential plasticity with the ability to differentiate not only to myofibroblasts but also adipocytes [67-68], osteoblasts [69], and chrondocytes [69].

1.3.2 Identification and Isolation of Fibrocytes

Fibrocytes have been found to express several leukocyte (CD45, CD90), monocyte (CD13, CD11b), co-stimulatory (CD80,CD86), progenitor (CD34), and integrin (CD18, CD61) markers as well as extracellular matrix proteins (collagen, vimentin) and glycosminoglycans (hyaluronan, perlecan) which have been reviewed elsewhere [35, 62, 70]. Generally it is accepted that fibrocytes may be identified by expression of either the hematopoietic progenitor marker CD34, or the leukocyte common antigen CD45, in conjunction with collagen or vimentin [71]. It has been shown however that as fibrocytes differentiate to myofibroblasts they decrease expression of hematopoietic markers CD45 and CD34 while increasing expression of α-SMA [72-74]. In fact, culture of human fibrocytes from peripheral blood showed that CD34 levels drop dramatically after 1 week in culture [74]. In this same experiment, CD45 levels began to drop after 2 weeks in culture reaching a threefold reduction after 3 weeks, however collagen 1 levels remained constant and α-SMA levels rose during the three weeks of culture [74].

For the culture of fibrocytes in vitro peripheral blood mononuclear cells may be isolated and differentiated into fibrocytes. This is often accomplished through purification by Ficoll density centrifugation [74], and or removal of the contaminating cells by Dynabead purification [70, 75]. For murine studies however, blood from multiple mice must be pooled together to obtain an adequate number of cells due to the low number of circulating monocytes found in blood [75-76]. More recently, fibrocytes have been shown

to differentiate from the splenic reservoir of monocytes [76-77]. With proper conditioning, a larger number of cells may be isolated and differentiated to fibrocytes from a single mouse spleen. Additionally it was found that using serum free media, with the addition of interleukin-13 (IL-13) and macrophage colony stimulating factor (M-CSF), significantly enhances fibrocyte differentiation as well as reducing the time needed for culture from 14 days down to 5 [76]. This source has the potential to generate substantial numbers of fibrocytes from a small number of animals for research studies.

1.3.3 Fibrocytes in Disease Models and Wound Healing

While fibrocytes are thought to only make up a small fraction of circulating leukocytes, there is evidence to support a greatly increased number in several disease states. This is true for lung diseases such as asthma [42, 78] and pulmonary fibrosis [74, 79-83], skin diseases like nephrogenic systemic fibrosis [84], renal fibrosis [85-86] hepatic fibrosis [87], cardiovascular disease [88], and even normal aging [89]. In several of these fibrotic models such as pulmonary and renal fibrosis as well as dermal wound healing [70], fibrocytes have been indentified to correlate directly with the amount of collagen production in the tissue. Interestingly, in a liver fibrosis model the development of fibrosis was increased in aged mice over young mice which correlated with an increased number of fibrocytes [87]. On the other hand, it has been suggested that enumeration of circulating fibrocytes may serve as a biomarker for disease progression in chronic lung disease such as asthma and pulmonary fibrosis [71].

Fibrocytes express several extracellular matrix proteins and properties, such as expression of pro-angiogenic and pro-inflammatory factors, that are critical in wound repair [71]. They can differentiate to myofibroblasts and increase expression of α-SMA, however the level to which this occurs in different wound setting and stages of repair remains unclear. In would healing it has been postulated that fibrocytes can rapidly enter

the site of tissue injury and can reach up to 10% of the inflammatory cell infiltrate [90]. In this response the chemokines CCL21 and CXCL12 seem to play an important role in inducing fibrocyte recruitment [74-75].Fibrocytes have been identified in several aberrant wound healing models such as hypertropic scars and keloids which develop as a consequence of extensive burn injury [62, 90]. In fact it has been demonstrated that the differentiation of fibrocyte from peripheral blood monocytes is significantly higher in burn patients than in normal individuals [90]. This increase may be linked to increased cytokine expression including TGF-β as a result of injury [90].

While it is clear that fibrocytes play an important role in different aspects of inflammatory/ fibrotic diseases and wound healing, their role in the foreign body response remains largely undetermined. In this dissertation we focus our efforts on identifying and characterizing the fibrocyte-mediated inflammatory and fibrotic effects in foreign body reactions. We then investigate several strategies to alleviate fibrosis through mitigation of the fibrocyte response.

1.4 Strategies and Aims of This Dissertation

The aim of this dissertation is to illuminate and examine the involvement of fibrocytes in foreign body reactions. In the course of our investigation, we specifically focus on immune/inflammatory cellular mediated responses and the resultant interactions with fibrocytes and the fibrotic outcome. The definitive goal is to not only identify fibrocyte mediated cellular reactions but to propose and implement strategies to alter or mitigate these processes with the objective of resolving fibrotic responses and enhancing regeneration. The summary of these aims is further described below.

1.4.1 Mast Cells Responses and the Alteration of Fibrocyte Recruitment

Since mast cell activation is accountable for the recruitment of inflammatory cells to the implantation site [91-92], and the presence of mast cells around the implant has been related to the degree of fibrotic encapsulation [93], we hypothesized that mast cell activation and subsequent fibrocyte responses are directly associated with the fibrotic pathogenesis of biomaterial implants. To test this hypothesis we conducted two independent studies to analysis the degree of mast cell involvement in fibrocyte recruitment and activation. The first study investigated the use of chemical mediators to induce mast cell degranulation or mast cell stabilization with localized release from PLGA film implants. While this study supports our hypothesis, the use of chemical mediators could have unknown effects on fibrocytes directly. In our second investigation we conclusively examine the mast cell connection to fibrocytes by using mast cell depleted and subdermally reconstituted mice.

1.4.2 Macrophage Polarization and the Influence on Fibrocytes

Many studies support the notion that the degree of inflammation (primarily macrophage cells) leads to the level of the fibrotic or healing outcome of an implant [18, 21, 23]. In addition, macrophage polarization has been increasingly studied due to the contrasting roles of M1 and M2 cells to elicit inflammation or to improve tissue regeneration [2, 32, 94-97]. Despite of the improvements in understanding inflammatory responses, the interaction and mutual influence between polarized macrophage and fibrocytes are mostly unclear. To illuminate these potential interactions we develop a dual modality imaging probe to monitor M1 and M2 responses to biomaterial implants *in vivo*. Through imaging and histological identification of macrophage polarization, we proceed to analyze how M1 and M2 cells influence the accumulation of fibrocytes over time and the resultant fibrotic response at two weeks.

1.4.3 Topographical Cues and Passive Alteration of Fibrocyte Responses

Surface topography has been shown in many studies to alter cellular and tissue responses, although the mechanisms and processes governing such reactions are not entirely understood. Specific patterned topography may be one strategy to alter the inflammatory fibrotic response to an implant through passive mechanical cues. To determine the role of fibrocytes on biomaterial-associated fibrotic tissue formation, poly-dimethylsiloxane micropillars with different surface morphology (pillar heights and pillar distances) were implanted in the subcutaneous cavity [98]. Through the use of histological analysis we investigate the relationships between inflammatory cells, fibroblasts, and fibrocytes in comparison to fibrotic tissue reactions such as capsule thickness, density, granulation tissue, angiogenesis, and collagen production. Specifically we evaluate how micropillar topography may be an alternative strategy to antagonistic agents in altering or mitigating fibrotic responses via fibrocyte interactions.

1.4.4 Fibrocyte to Adipocyte Differentiation and the Fibrotic Response

We have previously stated that fibrocytes have been shown to be multi-potent for several lineage including myofibroblasts [39, 41-42], adipocytes [67, 99], chondrocytes [100], and osteoblasts [100]. This multi-potency may be another potential strategy to passivate the fibrocyte response during fibrosis, or to enhance regeneration of tissue specific implants. This study primarily focused on the potential for directing fibrocyte differentiation surrounding implants *in vivo*. After confirming differentiation potential *in vitro*, we utilized mini-osmotic pumps to study the differentiation potential *in vivo*.

Cumulatively, our results indicate that inflammatory stimuli may be altered through several mechanistic cellular-mediated events to greatly influence the activation and proliferation of fibrocytes at the interface dictating the degree of fibrosis to the medical implant.

Chapter 2

Fibrocytes and Implant-Mediated Fibrotic Tissue Responses

2.1 Introduction

The involvement of fibrocytes in several inflammatory and fibrotic diseases has been eluted in many recent works. Their role in the foreign body response however remains largely undetermined. We hypothesize that fibrocytes play an important role on biomaterial mediated fibrotic reactions and that their recruitment or activation may be tuned to alter the pro-fibrotic or pro-regenerative response to the implant. Before these interactions can be altered however we must first understand the role of fibrocytes and the level of interaction around biomaterial implants. In this chapter we aim to identify the source of fibrocytes using a chimeric bone marrow model. To illuminate the degree of participation in the foreign body response we analyze the cellular influx and collagen production around PLGA subcutaneous implants over time. We then further show that fibrocyte responses are linked to the inflammatory response by studying the initial mediating influence of mast cells on the fibrotic outcome.

2.2 Fibrocytes at the Interface and their Role in Biomaterial-mediated Responses

2.2.1 Purpose

All biomaterial implants prompt a host response initiating varying degrees of inflammatory, immune, and fibrotic tissue reactions [4]. Although resident tissue fibroblasts have been implicated in fibrotic tissue formation, the source and method of activation of these quiescent cells into collagen producing myofibroblasts is not clear. Coincidentally, many recent studies have uncovered that circulating fibroblast progenitor cells -fibrocytes- play a dominate role in fibrotic reactions. Therefore we first set out to determine the source and level of involvement of fibrocytes around biomaterial implants.

We were primarily interested in ascertaining whether cultured fibrocytes would home to the site of biomaterial-mediated inflammation and whether a direct link could be established with the degree of fibrocyte accumulation and collagen production. Furthermore as suggested by previous works, we ascertain whether biomaterial-associated fibrocytes are migrating from the bone marrow.

2.2.2 Materials and Methods

2.2.2.1 Fibrocyte Culture and Labeling

Fibrocytes were harvested from the spleens of Balb/C mice based on a published procedure [76-77, 101]. Briefly, the spleen is harvested and then finely diced in a culture hood before being digested with collagenase (Invitrogen, Grand Island, NY) and hyaluronidase (Sigma) for 30 minutes at 37^{o}C. RPMI media (Sigma) is then used to dilute the sample for cell straining and centrifugation. The sample is then re-suspended in 1ml of red blood cell lysis buffer (155 mM NH_4Cl, 12 mM $NaHCO_3$, 0.1 mM ethylenediaminetetraacetic acid) for 3 minutes at room temperature. Cell lysis is neutralized by the addition of 12ml phosphate buffer (PBS) and re-centrifugation two times before being cultured with DMEM media. The culture media consists of 85%DMEM, 15% L-929 conditioned media (as a source of macrophage colony stimulating factor) and the addition of 50ng/ml murine IL-13. Cells are cultured for 7 to 10 days with a media change every 3 days.

These cultured cells possess similar morphology and surface markers CD45+/ Col-1+/ α-SMA- (Santa Cruz Biotechnology), positively identified through immunohistochemistry, as previously observed for cultured fibrocytes (Figure 2-1) [1, 42, 65, 73-74]. For *in vivo* imaging cells were incubated with 5μM of near-infrared fluorophore (Xsight 761) (Carestream Health, New Haven, CT) for 3hrs. Following labeling, cells ($2x10^6$ cells in 200μl PBS) were administered by iv injection as described in the previous

work [102-103]. To simulate biomaterial implantation, animals were subcutaneously implanted with either poly-L-lactic acid (PLA) microparticles or poly-L-glycolic acid (PLGA) films, as previously described [104-106], for 24 hours prior to NIR-fibrocyte transplantation.

2.2.2.2 Imaging Model for Tracking Fibrocyte Migration

The in vivo imaging approach used for tracking fibrocyte migration has previously been established by our group as recently reported [103-104]. Briefly, whole body imaging analysis is performed using the KODAK *in vivo* FX Pro system (Kodak, USA) Fluorescence intensity was monitored at excitation wavelength of 760 nm and emission wavelength of 790 nm (f/stop, 2.5; no optical filter, 4x4 binning). After background correction, the region of interest (area of implantation) was selected and the mean fluorescence intensities for all pixels were calculated using Carestream Molecular Imaging Software, Network Edition 4.5 (Carestream Health) as established earlier [104, 107]. Migration of fibrocytes was studied by *in vivo* imaging over 48hrs.

2.2.2.3 Chimeric Bone Marrow Model

Since many studies have found that fibrocytes are blood-borne and migratory cells [1, 75, 108-109], we thus assume that implant-associated fibrocytes are recruited from blood stream. To test this hypothesis, we performed a chimeric bone marrow study. Briefly, female C57BL/6 mice (6-8 weeks old, n=6) (Taconic Farm, Hudson, NY) were whole body X-irradiated at 1000 cGy. Bone marrow cells were aspirated from the femur and tibia bones of one male enhanced green fluorescence protein (EGFP) transgenic mouse (6-8 weeks old, n=6) (Taconic Farm, Hudson, NY) and transplanted into one irradiated EGFP negative mouse through retro-orbital injection. All animals were cared for in compliance with the protocols approved by the Institutional Animal Care and Use Committee at the University of Texas at Arlington.

Using flow cytometry analyses, we assess the number of implant-associated fibrocytes over time. After transplantation for 6 weeks, the chimeric animals were subcutaneously implanted with perforated catheter tubes, also referred to as wound chambers, as previously described [1, 102-103]. Using this method, implant associated exudates can be recovered from live animals by aspiration with PBS at various time points, spaced three to four days apart. Cells are recovered from the exudates and the cellular composition was analyzed by flow cytometry staining of EGFP, CD45, and Collagen 1 to identify implant-associated fibrocytes.

2.2.2.4 Histological and Immunohistochemical Evaluation

To analyze cellular responses at different time points, we used PLGA films as model biomaterial implants. PLGA films (75:25, 113kDa, Medisorb Inc., Birmingham, AL) were fabricated as previously described [106], with a resulting thickness of ~1mm. Films were cut into 5 mm disks and stored at -20^{o}C until implantation. Mice were implanted with two films placed laterally on either side of a dorsal midline incision as described previously [103]. The films were tucked into the subcutaneous space approximately 15 mm away from the incision which was subsequently closed with sterilized stainless steel surgical clips.

For histological evaluation, film implants and surrounding tissue were removed at each respective time point and then embedded into optimal cutting temperature compound (Tissue-Tek, Sakura Finetek, Torrance, CA) for frozen sectioning. All histological sections were imaged under a Leica DMLP microscope (Leica, Wetzlar, Germany) equipped with a Qimaging Retiga Exi 1394 digital camera (Qimaging, Surrey, British Columbia, Canada). Inflammatory leukocytes were generally assessed by CD11b marker and fibrocytes were assessed by positive staining for CD45 and Collagen1 [105]. The amount of collagen production surrounding implants was assessed, to reflect the

extent of fibrotic tissue reactions, by Masson Trichrome staining [98, 105]. The quantification of cell numbers and collagen percentage was performed with NIH ImageJ as previously described [98, 103, 105].

2.2.2.5 Statistical Analysis

Statistics are performed with GraphPad (La Jolla, CA). For data sets with single comparisons, the Student's t-test was used. For data sets with multiple-group comparisons, one way analysis of variance, ANOVA, was used with a Dunnett post test. All results are reported as the means ± standard deviations and taken to be significant when *P<0.05 and **P<0.01. A linear regression analysis was used to assess the correlation between cell specific and tissue responses. The coefficient of determination (R^2) was calculated providing a measure of correlation.

2.2.3 Results

2.2.3.1 Fibrocyte Culture and Migration to Biomaterial Implants

For fibrocyte culture, cells harvested from the spleens of Balb/c mice and were grown in culture for 7 days. Fibrocyte characteristics were analyzed based on morphology and the expression of dual surface markers CD45 and Collagen 1. As expected, the majority of the cultured cells were found to be CD45+, Collagen 1+, and, equally important, to be stained negative for α-SMA, a common marker for myofibroblasts differentiation. Morphologically the majority of cells maintained a typical spindle shape with an oval shaped nucleus (Figure 2-1). The fibrocyte yield after 7 days in culture was found to be 72 ± 7.1%, while approximately 27 ± 8.8% of the cells were found to stain positive for α-SMA. Since fibrocytes have been shown to decrease CD45 expression and increase expression of α-SMA as they differentiate to fibroblasts or myofibroblasts all cell cultures were used after only 7 days in culture.

To determine the migratory ability of fibrocytes to biomaterial implants, fibrocytes labeled with NIR fluorophore Xsight761 were injected intravenously in mice bearing biomaterial implants. Real time imaging shows that injected fibrocytes do indeed migrate to the site of implantation over a 24 to 48 hour time point (Figure 2-2). The migratory response was also observed to increase over time. To confirm that fibrocytes would migrate to various biomaterial implants in the same fashion, both PLGA films and PLA particles were tested and compared against no-treatment control (PBS). The splenic derived fibrocytes transmigrated to the biomaterial implant as hypothesized regardless of material or configuration (PLGA scaffold vs. PLA particle). The PLA particles were observed to have increased fibrocyte migration which may be attributed to the higher surface area as previously described for migrating stem cells [102]. While this study clearly demonstrated that fibrocytes will migrate to an inflammatory site surrounding a subcutaneous biomaterial implant, the fibrocyte source is left to question. We therefore sought to answer this question using a chimeric bone marrow model.

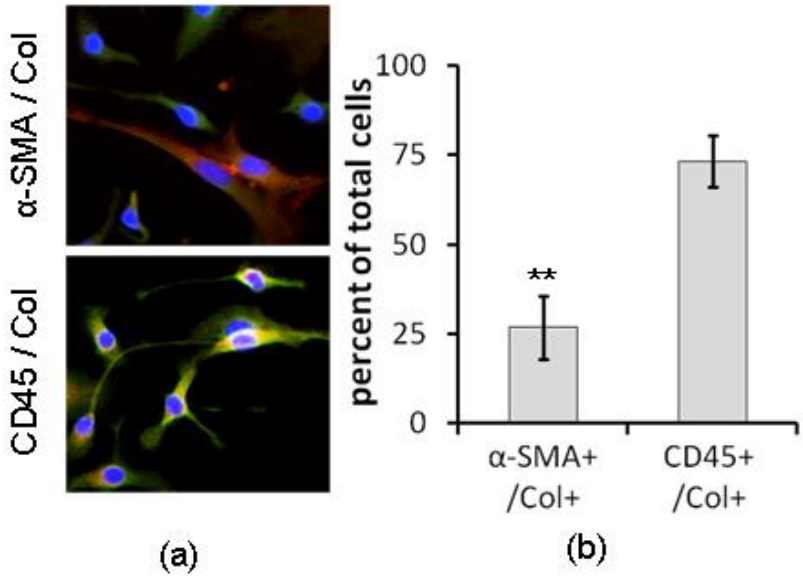

Figure 2.1 Culture and identification of splenic derived fibrocytes.
(a) Representative images are shown of positive staining of α-SMA (red) and collagen 1 (green) (top image), and CD45 (red) and collagen 1 (green) (bottom image). The overlay of CD45 and collagen appears yellow in the bottom image. DAPI is used to stain cell nuclei. Cells were derived from the spleens of Balb/c mice and cultured for 7 days on glass cover slips in serum free medium containing IL-13 and M-CSF. (b) Histogram showing the quantitative measurements of the respective cell types in culture. Statistics are performed with the student's test from n=6 replicates for each staining taken at 400x magnification, **P<0.01. This figure is adapted from reference [110] currently in submission.

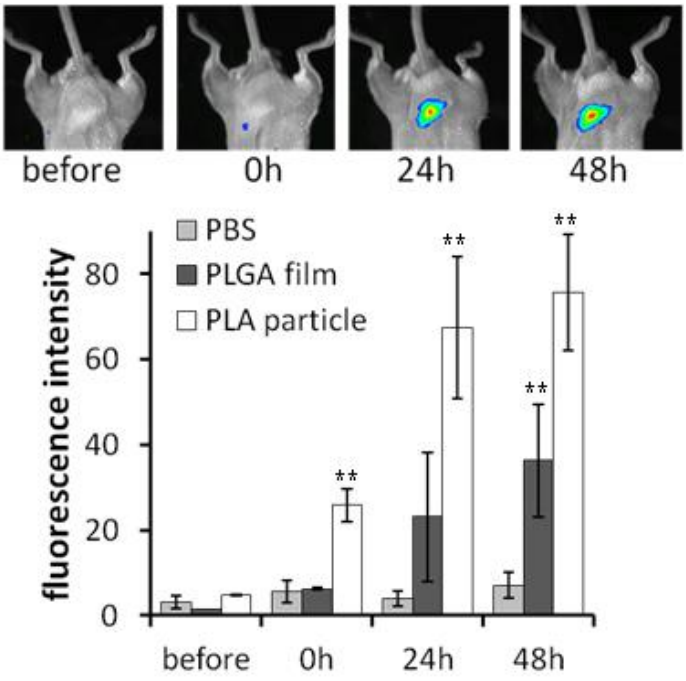

Figure 2.2 *In vivo* migration of cultured fibrocytes to biomaterial implants. Fibrocytes are labeled with NIR fluorophore Xsight761 and injected iv at $2x10^6$ cells in 200µl PBS 24 hours after implantation. Representative images show migration of fibrocytes to the site of PLA particle implantation over time. The histogram demonstrates that both PLGA film and PLA particles have an increased accumulation of fibrocytes over the PBS control. Studies were performed with n=3 mice for each implant type. Statistics are performed with ANOVA Dunnett comparisons to the PBS as the control at each respective time point and taken to be significant at *P<0.05 or **P<0.01. This figure is adapted from reference [110] currently in submission.

2.2.3.2 Identification of the Source(s) of Immigrated Fibrocytes.

During wound healing, fibrocytes are thought to migrate to the wound site from a circulating population recruited from the bone marrow [111]. We thus assumed that implant-associated fibrocytes have transmigrated from the bone marrow to the site of biomaterial implantation. To test this hypothesis, we used a wound chamber model in which perforated catheters were subcutaneously implanted as wound chambers to collect immigrated cells. In our chimeric enhanced green fluorescence protein expression model, we observed a 15 fold increase in fibrocyte accumulation from day 3 to day 10 following

subcutaneous implantation of catheter tubes (Figure 2-3 a). Closer evaluation of the fibrocyte population reveals a similar increase from 15% to 30% of the GFP+ fibrocyte population. This indicates that a substantial portion of the fibrocytes have derived from the newly transplanted chimeric bone marrow (Figure 2-3 b-c). It should be noted that in this model only 30% of the bone marrow cells were observed to express the GFP marker, indicating a reduced efficiency in the chimeric transplantation. Therefore the 30% of GFP+ fibrocytes observed at day 10 is indicative of 100% of what we expect to see from our model. Regardless of the efficiency of the chimeric bone marrow transplant, these results support that bone marrow is most likely the main source for the implant-associated fibrocytes.

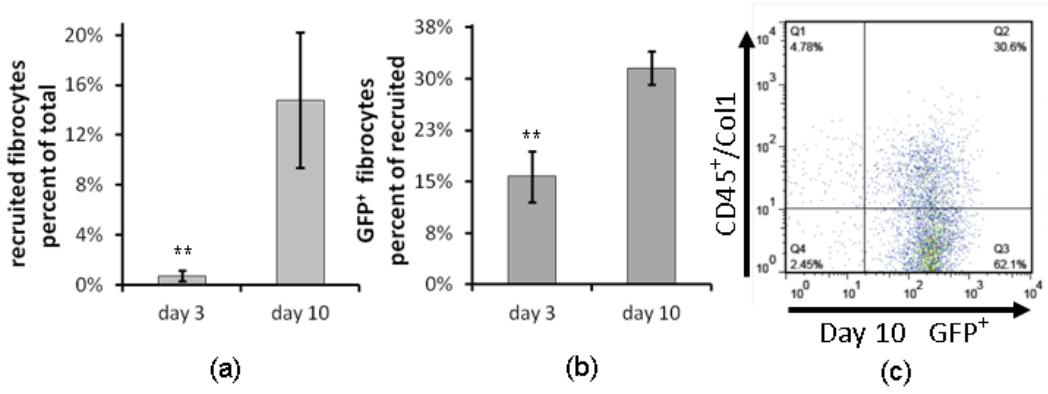

Figure 2.3 FACS analysis of wound fluid after chimeric bone marrow transplant. (a) Number of fibrocytes present in wound chamber exudates as a percent of total cells analyzed. (b) Number of GFP^+ fibrocytes as a percent of the total recruited fibrocyte population. (c) Representative FACS plot of GFP^+ fibrocytes (quadrant 2). Wound chamber fluid was analyzed at the respective time points after chimeric bone marrow transplantation for 6 weeks. Results are from n=6 mice. Statistics are performed with Student's t-test and taken to be significant at **P<0.01. This figure is adapted from reference [110] currently in submission.

2.2.3.3 Fibrocytes and Implant-Associated Fibrotic Tissue Responses.

To study the role of recruited fibrocytes on implant-associated fibrotic reactions, we conducted a time course study using PLGA film implants to analyze the cellular influx and collagen production over time. As anticipated, our study shows that shortly after biomaterial film implantation, a substantial number of fibrocytes accumulate at the implant site and are found to increase with time (Figure 2-4 a,b). The accumulation of immune/ inflammatory cells ($CD11b^+$) between the biomaterial and the native hypodermis reached the plateau 2 days after implantation. This dynamic interface contains cells having a granulocytic morphology up to about 4 days after implantation. Gradually, we observe an increase in spindle-shaped cells becoming more prominent in the layer immediately next to the implant by day 7 to 14. Interestingly, the influx of fibrocytes ($CD45^+$ /$Col1^+$) becomes significant at 4 days corresponding with an observed decrease in immune/ inflammatory cells after their peak at 1013 ± 100 cells/mm^2 on day 2. The influx of fibrocytes appears to follow the inflammatory cascade with a significant increase in fibrocyte numbers (121% increase) from day 4 to day 10 reaching a maximum at day 10 of 419 ± 86 cells/mm^2 (Figure 2-4 a,b). Critically, the increase in the fibrocyte number is precisely mirrored by the collagen content within the surrounding capsule.

Total collagen production is observed through Masson Trichrome staining (Figure 2-4 a,c). The collagen content shows a shift in the inflammatory and fibrotic response between day 7 and 10 with a doubling (21 ± 1.8% to 41 ± 3.9%) in the amount of collagen surrounding the biomaterial implant. Interestingly, we also observed a decrease in the capsule thickness (160 ± 19 μm at day 10, to 113 ± 16 μm at day 14) and CD11b+ inflammatory cells (727 ± 152 cells/mm2 at day 10, to 287 ± 77 cells/mm2 at day 14). To further link the fibrocyte influence on extracellular matrix/ collagen production, we established a correlation between the collagen tissue content (%) and fibrocyte cell

numbers within the developing fibrotic capsule. This correlation demonstrates a near linear relationship (R^2 = 0.902) indicating a strong link between fibrocyte recruitment and the shifting change from inflammation to fibrosis within the biomaterial interface (Figure 2-5). This shifting interaction of inflammatory cells and fibrocytes, and near linear correlation of fibrocytes and collagen content, clearly demonstrate an important role of recruited fibrocytes on the developing fibrotic matrix. Several questions still remain to be answered however including how fibrocytes are being recruited to the biomaterial implantation site, and what factors or cellular interactions are driving this recruitment?

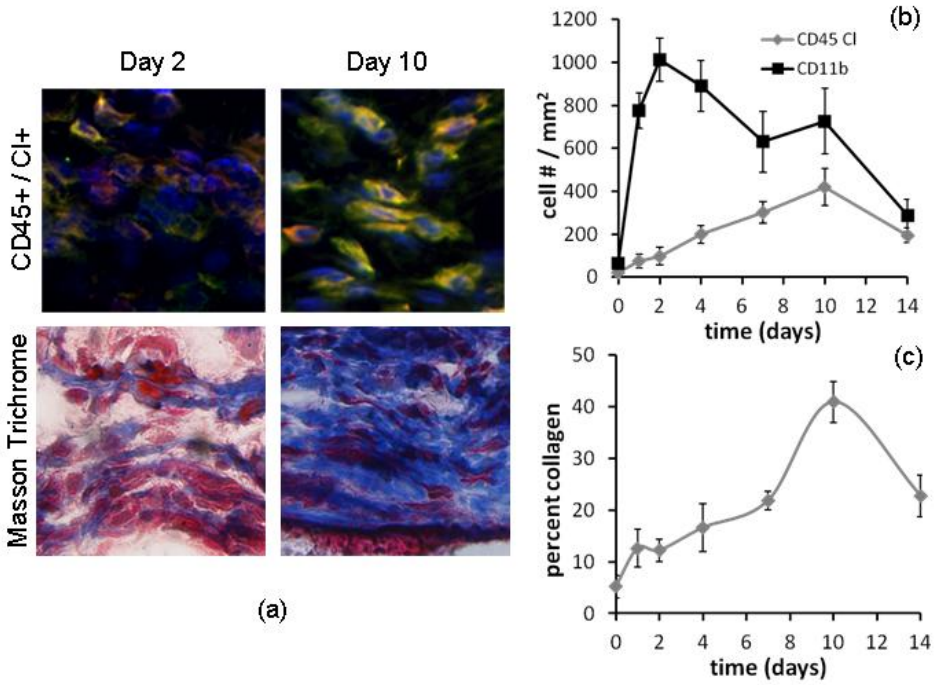

Figure 2.4 Time course study of fibrocyte accumulation and collagen production. (a) Panel of CD45/ collagen1 positive fibrocytes (yellow) and masson trichrome staining of collagen content (blue) at days 2 and 10 of the surrounding implant interface. (b) Plot of fibrocyte accumulation and immune/ inflammatory cell influx over time. (c) Plot of total collagen content in the developing fibrotic matrix over time. The figure is adapted from reference number [105]

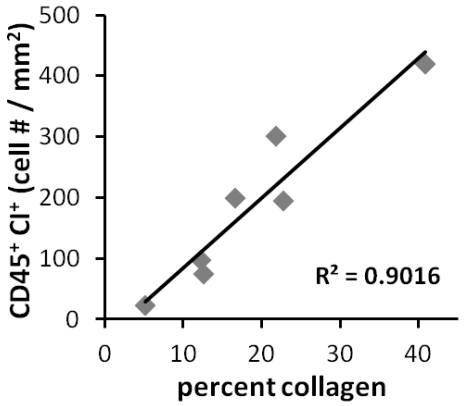

Figure 2.5 Correlation between recruited fibrocyte numbers and collagen percentage. A near linear trend is observed with a coefficient of determination $R^2 = 0.902$. The figure is adapted from reference number [105]

2.2.4 Conclusion

In alignment with our original hypothesis our studies have demonstrated that, in addition to macrophages/monocytes and polymorphonuclear neutrophils, a large number of in situ fibroblast-like cells are recruited to biomaterial implant sites [98, 105]. These fibroblast-like cells possess surface markers CD45+/ Collagen-1+/ α-SMA- resembling fibrocytes [71, 74, 87]. These cells can be isolated and cultured from the splenic reservoir [76]. *In vivo* imaging studies shows that fibrocytes home to the site of biomaterial-mediated inflammation regardless of material or configuration. Interestingly, we have found that fibrocytes migrate to the implant following the inflammatory cell influx and are directly related to the degree of collagen production around the implant. Furthermore, using a chimeric bone marrow model, we have identified that a substantial portion of the implant associated fibrocytes are derived from bone marrow. Our results support our original hypothesis that foreign body reactions drive the recruitment of fibrocytes originating from the bone marrow. Furthermore the results support the notion that

fibrocytes play an important, potentially underestimated role in biomaterial associated tissue responses.

2.3 Mast Cell Stimulation Dictates Fibrocyte and Fibrotic Responses

2.3.1 Purpose

It is well understood that mast cells are mediating and regulatory cells in the innate and adaptive immune response [112-115]. They secrete a number of mediators, including histamine and trypase, cytokines, such as IL-4, IL-6, IL-8, Il-10 and tumor necrosis factor alpha (TNF-α), chemokines, including RANTES, monocyte chemoattractant proteins (MCP-1 and MCP-3), and growth factors, such as fibroblast growth factor (FGF), transforming growth factor beta (TGF-β) and platelet-derived growth factor (PDGF) [116-117]. We have previously shown that histamine release from mast cells is critical for polymorphonuclear neutrophil and macrophage recruitment to polyethylene terephthalate implants [92]. Since fibrocyte migration is mediated by inflammatory signals [73-74] and mast cell activation is essential to biomaterial mediated inflammatory responses [92], we thus hypothesized that mast cell activation is responsible for facilitating biomaterial mediated fibrotic responses through fibrocyte interactions. In support of this, it has been suggested that the long term presence of mast cells at the implantation site may be related to the degree of fibrotic encapsulation [93]. Additionally, a recent study indicated that suppression of the mast cells response may lead to a reduced tissue reaction surrounding synthetic mesh implants [118]. The extent of biomaterial-mediated inflammatory responses may therefore be significantly reduced by mast cell inactivation.

In this section we investigate how the modulation of mast cell responses could change the fibrocyte and tissue reactions to biomaterial implants. For this, we determined

how mast cell stabilizing and destabilizing agents (cromolyn and compound 48/80 respectively) locally released from PLGA film implants would influence foreign body reactions.

2.3.2 Materials and Methods

2.3.2.1 Fabrication of Poly-L-Glycolic Acid Film Implants

All chemical were purchased from Sigma Aldrich (St Louis, MO) unless otherwise specified. The poly-L-glycolic acid (PLGA) films were fabricated as previously described with slight modifications to incorporate mast cell stabilization (cromolyn) and destabilization (compound 48/80) chemicals [92, 119-120]. For cromolyn embedded films, cromolyn salt (6 mg) was mixed with the polymer solution (~240 µg/implant with an intended release rate of ~640 µg/kg body wt/day) and cast into molds similar to control films. For compound 48/80 embedded films, compound 48/80 (10 mg) (~350 µg/implant with an intended release rate of ~1 mg/kg body wt/day) was dissolved in dimethylsulfoxide. The solution was then blended with the polymer solution and cast into molds. Release rates were quantified as previously described and found to be approximately 6.25 and 4.0 µg/day for compound 48/80 and cromolyn respectively [105]. All films were approximately 1mm thick, cut into 5mm disks, and stored at -20°C until implantation.

2.3.2.2 Animal Model and Implantation of PLGA Films

For implantation C57BL/6 mice (Jackson Labs) of equal age and sex were selected and anesthetized. As described earlier a dorsal midline incision was created and two implants of equal treatment condition (cromolyn, compound 48/80 or control) were implanted laterally on either side of the incision in the subcutaneous space. The incision was closed with surgical clips and the mice were monitored daily for irritation around the implant until explanation. All animals were cared for in compliance with the protocols

approved by the Institutional Animal Care and Use Committee at the University of Texas at Arlington.

2.3.2.3 Histological and Immunohistochemical Evaluation

The extent of the infiltrated cell layer was assessed by H&E staining. Fibrosis was assessed using both Masson Trichrome and Picrosirius Red staining. Picrosirius Red staining was visualized using polarized light microscopy where the percentage of red/yellow birefringence per total interface area may be quantified. Image J processing was used to quantify all histological tissue response as previously described [105, 121]. Briefly, all data is presented as the average of multiple counts taken from images captured on the skin side of the biomaterial interface (between the implant and hypodermis). Areas of equal value were assessed in all cases.

The density of inflammatory cells (CD45), fibrocytes (CD45 co-expressed with collagen I), and myofibroblasts (CD45 co-expressed with α-SMA), was assessed using immunohistochemistry as previously described [121]. In all cases the cell densities were calculated as the number of positive cells per area using Image J with areas of similar size. For all quantifications images were taken with a Leica microscope and imaged with a CCD camera (Retiga EXi, Qimaging, Surrey BC, Canada).

2.3.2.4 Statistical Analysis

Statistical analysis was performed with GraphPad (La Jolla, CA). All results are reported as the means ± standard deviations from n=6 mice for each treatment condition. We have assumed Gaussian distributions and performed parametric tests. Statistics were calculated with ANOVA using Bonferroni post test and taken to be significant when *$P<0.05$ and **$P<0.01$.

2.3.3 Results

To assess whether mast cells reactions are involved in fibrocyte recruitment and accumulation at the biomaterial interface we first released compound 48/80 and cromolyn from PLGA implants to destabilize or stabilize mast cell reactions respectively. Our histological results revealed significant differences in both the organization and thickness of the infiltrated cell layer around the interface at the two week time point (Figure 2-6). Specifically, activation of mast cells through localized release of compound 48/80 resulted in a 41% increase in cell number over the control and an approximate 30% increase in capsule thickness (Figure 2-7). Localized treatment with a mast cell stabilizer cromolyn on the other hand, resulted in a substantial decrease in overall cellular recruitment and fibrotic capsule thickness (an approximate 30% decrease was observed in capsule thickness from the control) (Figure 2-7).

Since we have previously linked fibrocytes to the amount of collagen production around biomaterial implants, we proceeded to analyze the collagen content after mast cell modification. For this we used both masson trichrome staining, for general collagen content, and picrosirius red staining to identify collagen 1 specifically. We looked specifically at collagen 1 as fibrocytes have been shown to secrete large amounts of collagen 1, vimentin, and other proteins in the fibrotic matrix [41-42, 66, 122-123]. Control PLGA films had random, discontinuous collagen I fiber deposition, produced primarily near the implant interface becoming segmented away from the implant. Compound 48/80 implants on the other hand had well formed collagen I bands, extending from the implant surface throughout the interface tissue aligned with the biomaterial interface. Cromolyn treated implants show a mixture of discontinuous collagen I bands with a significant decrease in deposition throughout the biomaterial interface (Figure 2-6). Collagen deposition shows the highest percentage in the compound 48/80 embedded implants (53

± 3.5%), followed by the PLGA unmodified films (37 ± 2.5%) and lastly the cromolyn embedded films (23 ± 2%) (Figure 2-7).

With the significant differences observed in both capsule thickness and collagen production, we proceeded to analyze the cellular contents of the fibrotic capsule including leukocyte, fibrocyte, and myofibroblasts density. The CD45+ leukocyte cell recruitment, as might be expected, shows an increase ($P<0.05$) with mast cell induced degranulation, using compound 48/80, in comparison to the control. Vice versa, there is an observed decrease in the leukocyte population in response to mast cell stabilization with cromolyn treatment (Figure 2-8). Compound 48/80 release is also observed to result in an elevated percentage of fibrocytes (CD45+/Col+) within the interface in comparison to the control unmodified films or cromolyn embedded films (471 ± 59, 373 ± 62, and 173 ± 32 cells/mm^2 respectively) (Figure 2-8). Finally analysis of the myofibroblasts population reveals similar reactions to the mast cell mediating chemicals. The myofibroblasts (CD45+/α-SMA+) population is reduced by cromolyn treatment and enhanced by compound 48/80 treatment (results are 296 ± 90 cells/mm^2 for cromolyn, 713 ± 192 cells/mm2 for compound 48/80, and 471 ± 94 cells/mm2 for PLGA controls). Interestingly in observing the fibrocyte or myofibroblast population the cells appear to be more localized to the biomaterial side, away from the hypodermis for both PLGA and cromolyn films, where in the compound 48/80 samples the cells are more dispersed throughout the capsule.

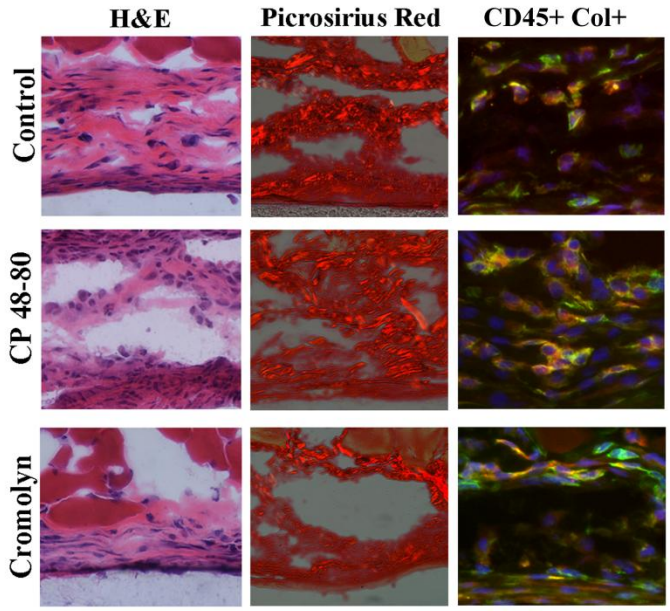

Figure 2.6 Histological staining for mast cell stabilizing and destabilizing agents. Panel shows representative images of histological staining for H&E (left column) and picrosirius red collagen 1 content (middle column). Immunohistochemical staining for CD45/Col reveals the presence of fibrocytes (yellow) (right column) surrounding PLGA films after subcutaneous implantation for 2 weeks. The figure is adapted from reference number [105]

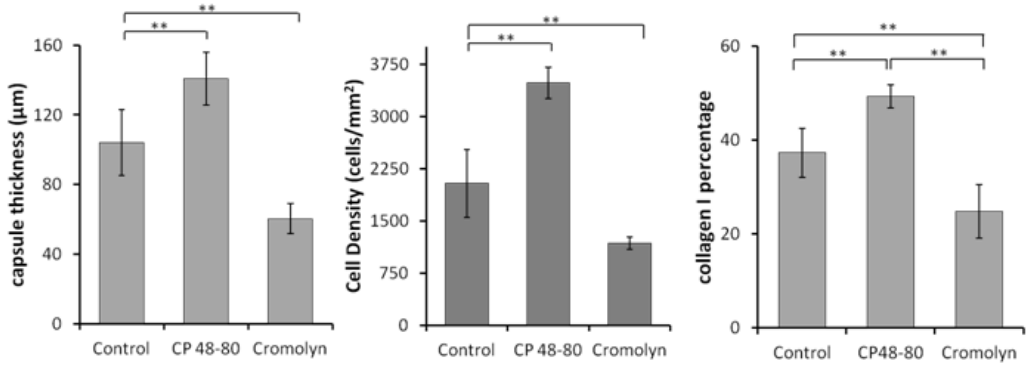

Figure 2.7 Histological responses for mast cell stabilizing and destabilizing agents. Histograms show quantification of capsule thickness, cell density, and collagen 1 percentage in the fibrotic capsule surrounding PLGA films after subcutaneous implantation for 2 weeks. Results are from n=6 mice. Significant differences were calculated by ANOVA with Dunnett comparisons and taken as significant at *P<0.05 and **P<0.01. The figure is adapted from reference [105]

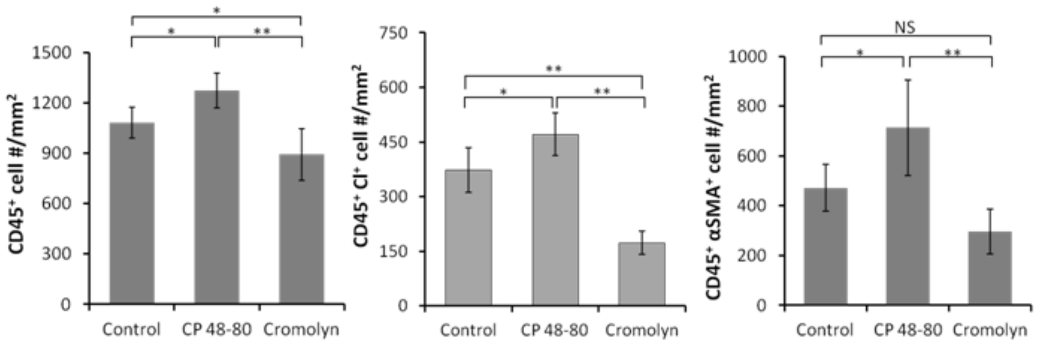

Figure 2.8 Cellular responses for mast cell stabilizing and destabilizing agents. Histograms show quantification of leukocyte numbers (CD45+), fibrocyte numbers (CD45+/Collagen+), and myofibroblast numbers (CD45+/α-SMA+) in the fibrotic capsule surrounding PLGA films after subcutaneous implantation for 2 weeks. Results are from n=6 mice. Significant differences were calculated by ANOVA with Dunnett comparisons and taken as significant at *P<0.05 and **P<0.01. The figure is adapted from reference [105]

2.3.4 Discussion

Our investigation thus far suggests that stabilization of mast cells will reduce fibrocyte/ myofibroblasts responses. Furthermore, the activation of mast cells will significantly increase fibrocyte/ myofibroblast responses and subsequent fibrotic reactions. We have thus identified that the chemical modification of the mast cell activation via compound 48/80 and cromolyn have a direct influence on fibrocyte-associated fibrotic tissue reactions to biomaterial implants. To further determine that the observed responses are solely the result of mast cell stimulation differences, we continued our investigation using a c-kit mast cell deficiency and reconstitution model.

2.4 Mast Cell Deficiency and Reconstitution on Implant-Associated Fibrotic Reactions

2.4.1 Purpose

Mast cell deficient mice and their dermally reconstituted counterparts were studied to rule out independent effects of agonistic and antagonistic agents on fibrocytes. WBB6F1/J-Kit^{W}/Kit^{W-v}/J mice were purchased from Jackson Labs as a model of mast cell

deficiency. By culturing mast cells from C57BL/6 wild type mice some of the WBB6F1/J-Kit^{W}/Kit^{W-v}/J mice could be subdermally injected with cultured mast cells to reconstitute a localized population of mast cells. The three sets of mice, mast cell deficient, reconstituted, and wild type controls, were then subjected to PLGA film implantation and analysis at two weeks as before for stabilization and destabilization agents.

2.4.2 Materials and Methods

2.4.2.1 Mast Cell Deficient Animal Model

For mast cell deficiency and reconstitution studies control C57BL/6 mice and mast cell deficient mice (WBB6F1/J-Kit^{W}/Kit^{W-v}/J, Jackson Labs) were used. Dermal reconstitution of mast cell deficient mice was achieved as previously described [92, 105]. Briefly, bone marrow flushes were taken from C57BL/6 control mice (n=8). Cells were cultured in 75cm^2 flasks in DMEM with 10% low IgG serum (Invitrogen, Carlsbad, CA) supplemented with 10ng/mL SCF (Prospec) and 10ng/mL IL-3 (Prospec). Every 3 days non-adherent cells were transferred into new flasks and supplemented with fresh mast cell differentiation media for 4 weeks. Mast cell phenotype was verified by toluidine blue staining. For reconstitution mast cells were subdermally injected into deficient mice at $3x10^6$ cells/ mouse in PBS. After six weeks, compound 48/80 was injected subcutaneously to verify peripheral mast cell engraftment through observed signs of inflammation.

2.4.2.2 Poly-L-Glycolic Acid Film Fabrication and Implantation

PLGA films (75:25, 113kDa, Medisorb Inc., Birmingham, AL) were fabricated as previously described [105-106]. For the mast cell deficiency and reconstitution studies only control films (free of chemical agents) were used. Implantation of films was similarly performed as described for the mast cell stabilization/destabilization study previously discussed (Please see 2.3.2.1).

2.4.2.3 Histological and Immunohistochemical Evaluation

All histological analysis was performed as previously described in this chapter for the mast cell stabilization/destabilization studies (Please see 2.3.2.3).

2.4.2.4 Statistical Analysis

All statistical analysis was performed with GraphPad (La Jolla, CA) as previously described. The results are reported as the means ± standard deviations with ANOVA using Bonferroni comparisons taken to be significant when *P<0.05 and **P<0.01.

2.4.3 Results

As expected, we observe a significant decrease (about 60%) with the accumulated cellular density in the mast cell deficient mice, compared to the wild type controls. Histological evaluation however reveals that surprisingly, after only six weeks of subcutaneous mast cell reconstitution the biomaterial-mediate cellular responses are nearly completely restored (Figure 2-9). Similar results are obtained after analyzing the capsule thickness at (102 ± 9 μm) for the wild type, (87 ± 9 μm) with reconstitution and only a thickness of (64 + 3 μm) with mast cell deficiency (Figure 2-10). Further analysis of the collagen content with aniline blue from masson trichrome staining reveals a 40% reduction in total collagen with mast cell deficiency. Additionally, a 17% reduction in the tissue collagen type 1 content is observed in mast cell deficient animals in comparison with the controls using picrosirius red staining (Figure 2-10). Interestingly, not only is the total collagen content restored but specific collagen type I percentages are also restored with mast cell reconstitution (45.8 ± 4.5% for reconstitution and 43.4 ± 3.2% for the control wild type). These results further support our hypothesis that mast cell reconstitution has restored the histological tissue response after the observed reduction with mast cell deficiency. We therefore continued our analyses to determine if mast cell deficiency was also altering the fibrocyte/ myofibroblasts response.

Indeed, we again observe significantly altered cellular reactions within the fibrotic capsule in mast cell deficient animal models. In each of the target cell groups, leukocyte (CD45), fibrocyte (CD45/Col), and myofibroblasts (CD45/α-SMA) we see an approximate 50% reduction in cell density with mast cell deficiency. Even more impressive however is that by simple subcutaneous mast cell reconstitution we see an approximate full recovery in the fibrocyte (287 ± 34 cells/mm^2 for control and 273 ± 80 cells/mm^2 for reconstituted) and the fibrocyte-derived myofibroblast (522 ± 166 cells/mm^2 for control and 485 ± 30 cells/mm^2 for reconstituted) cellular densities (Figure 2-11).

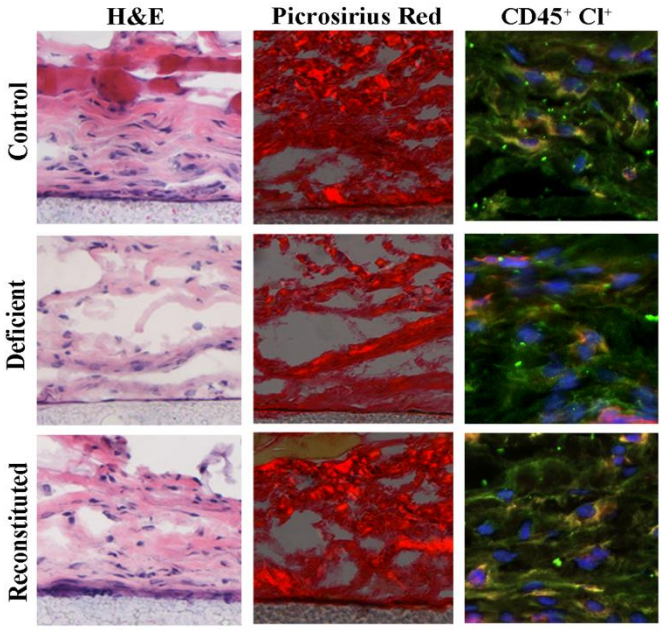

Figure 2.9 Histological staining for mast cell deficiency and reconstitution. Panel shows representative images of histological staining for H&E (left column) and picrosirius red collagen 1 content (middle column) surrounding PLGA films after subcutaneous implantation for 2 weeks. Immunohistochemical staining for CD45/Col1 reveals the presence of fibrocytes (yellow) (right column). The figure is adapted from reference number [105]

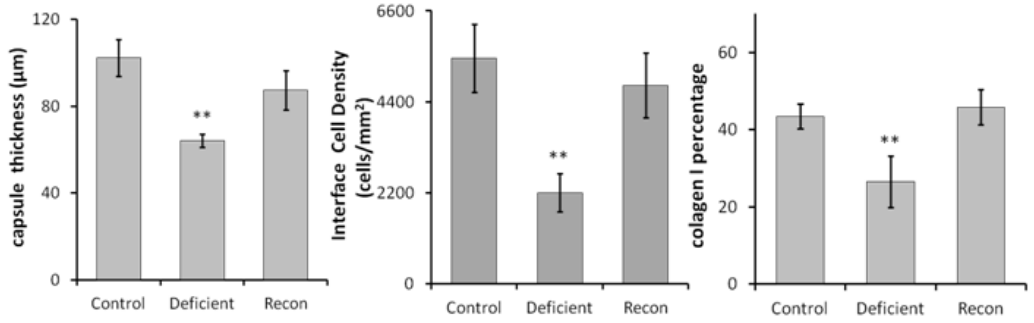

Figure 2.10 Histological responses for mast cell deficiency and reconstitution. Histograms show quantification of capsule thickness, cell density, and collagen 1 percentage in the fibrotic capsule surrounding PLGA films after subcutaneous implantation for 2 weeks. Results are from n=6 mice. Significant differences were calculated by ANOVA with Dunnett comparisons and taken as significant at *P<0.05 and **P<0.01. The figure is adapted from reference [105]

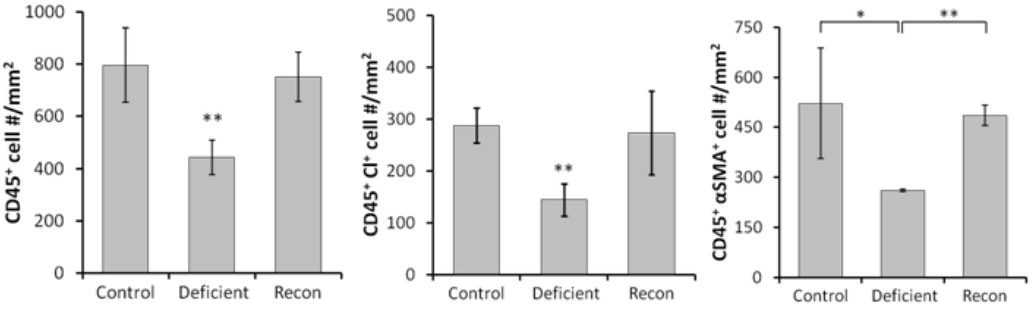

Figure 2.11 Cellular responses for mast cell deficiency and reconstitution. Histograms show quantification of leukocyte numbers (CD45), fibrocyte numbers (CD45/CI), and myofibroblast numbers (CD45/α-SMA) in the fibrotic capsule surrounding PLGA films after subcutaneous implantation for 2 weeks. Results are from n=6 mice. Significant differences were calculated by ANOVA with Dunnett comparisons and taken as significant at *P<0.05 and **P<0.01. The figure is adapted from reference [105]

2.4.4 Discussion

In the previous section, we showed that fibrocyte accumulation around a biomaterial implant seems to follow the influx of inflammatory cells. These fibrocytes were found to transmigrate from the bone marrow and correlate directly with the production of collagen in the developing fibrotic matrix. These findings are supported by previous

observations of the relationship between the extent of fibrocyte recruitment and collagen production in other fibrotic models such as lung fibrosis [124]. Here, for the first time, we present evidence that mast cell activation is responsible for facilitating biomaterial-mediated fibrotic responses through fibrocyte interactions.

In two separate models mast cell stabilization or deficiency failed to prompt fibrotic tissue reactions to subcutaneous implants. In opposition, increased mast cell degranulation substantially increased fibrotic reactions and mast cell reconstitution restored fibrotic reactions to that of the control animals. Our results are supported by previous investigations of liver and lung fibrosis and several studies attributing persistent mast cell activation to fibrotic tissue responses [93, 125-128].

To the best of our knowledge, this initial study constitutes the first direct evidence that biomaterial-mediated fibrotic reactions are both mast cell- and fibrocyte-dependent. However the processes and factors governing these cellular responses are mostly undetermined. It has previously been shown in a pulmonary fibrosis model that fibrocytes traffic to the inflamed areas and migrate with inflammatory cells [124]. It is therefore generally assumed that inflammatory products provide some essential signals for fibrocyte immigration. In support of this, there is some evidence that the SDF-1α/CXCR4 axis is involved in fibrocyte recruitment to the site of inflammation and in the subsequent fibrocyte response in initializing fibrotic reactions [124, 129]. There are however several conflicting observations on the primary chemotactic regulation of fibrocytes with several factors implicated including CCL2, CCL21, and CCL12 [82, 130-132].

At this juncture, we still do not know the potential mechanisms governing mast cell activation and subsequent fibrocyte responses. It is likely however that biomaterial implantation prompted the activation of mast cells. Activated mast cells are known to secret a number of mediating cytokines, chemokines, and growth factors, such as

stromal cell-derived factor (SDF-1α), TGF-β, IL-1B, secondary lymphoid tissue chemokine (SLC), and monocyte chemoattractant proteins (MCP)'s, which can tiger further mast cell activation, as well as the onset of phagocyte and leukocyte migration [70, 116]. Some mast cell products, including histamine, TGF-β, TNF-α, MCP-1, and SDF-1α, may also trigger inflammatory cells and fibrocyte immigration as well [70-71, 75, 92, 124]. Additionally, as several homing axis's have been identified for fibrocyte recruitment, mast cells may contribute indirectly by exerting a dominant cofactor effect on one or more of these axis's such as the CXCL12/CXCR4 pathway [114, 133-134].

Regardless of the mode of activation it is clear that upstream modulation of mast cell responses can significantly reduce fibrocyte-mediated fibrotic responses at the biomaterial interface. This interaction implicates mast cells and fibrocytes as critical regulators of the biomaterial mediated fibrotic response. As mast cells are well known modulators of the inflammatory response, and macrophages are paramount to inflammation, we further hypothesized that inflammatory cells such as macrophages may be responsible for the activation of fibrocytes triggering a shift in the inflammatory or fibrotic potential of these highly plastic cells. We therefore continue our investigation of cellular interactions with a look at macrophage activation and polarization and the resultant fibrocyte response.

Chapter 3

Implant-Associated Macrophage Responses and Polarization

3.1 Introduction

Macrophages are well known as key modulators of immune/ inflammatory and fibrotic responses to biomaterial implants [3, 5, 27]. Importantly, implant-activated macrophages produce a wide variety of growth factors, including IL-1, TNF-α, and transforming growth factor-beta (TGF-β), interleukin-6 (IL-6), fibroblast growth factor (FGF) and platelet-derived growth factor (PDGF) [27]. While in general these factors are inflammatory in nature, some, namely TGF-β, FGF and PDGF, also show a tendency to regulate fibrotic responses [135-136]. In fact, it has been widely documented that macrophages may act as beneficial modulators of disease and tissue repair. The remarkable plasticity of macrophages has more recently been attributed to polarization of these cells dependent upon environmental factors leading to several diverse tissue specific macrophage populations [137]. In general, polarized macrophages are referred to having either an M1 (classically activated) or M2 (alternatively activated) phenotype. Several studies have identified that M1 and M2 cells have a profound impact on immune and tissue responses, such as tumorigenesis and angiogenesis, through differential cytokine production [95-96, 138-142]. It has further been suggested that these cells exert opposite effects on the adaptive immune response triggering either tissue destruction or regeneration [32]. This has been observed in models such as pulmonary fibrosis, metastatic disease, and infectious disease [96, 139-141, 143]. Unfortunately however there is a lack of evidence on the interplay between polarized macrophages and biomaterial-mediated fibrotic responses.

In an earlier study, we identified that CD11b inflammatory cells (mainly macrophages) arrived at the implant site earlier than fibrocytes. We thus assume that

macrophage responses influence subsequent fibrotic reactions. In this chapter we investigate the influence of macrophages on fibrocyte-mediated fibrotic responses. To first determine a link connecting macrophages to fibrocytes we employ a macrophage depletion model. From this model we extrapolate the change in the influx of fibrocytes to the implant and the resultant influence on the acute phase of inflammation and transition to fibrosis.

Secondly, as M1 and M2 polarized macrophages are known to exert opposite effects on disease and tissue repair outcomes, we hypothesized polarized macrophages and associated products would alter the fibrocyte activation pathway. In support of this, an increased M2 over M1 response was found to be associated with more positive remodeling outcomes to biologically derived surgical mesh materials after implantation [30]. While these previous results are promising, there has yet to be a connection made between M1/M2 macrophages and fibrocyte reactions around a biomaterial implant. To begin our investigation on the interactions of polarized macrophages we developed an imaging probe modality capable of monitoring macrophage polarization *in vivo*. We subsequently characterize these probes and demonstrate their effectiveness in an extreme model of implant infection and a subtle model of biocompatible biomaterial implants.

Thirdly, as mentioned above, M1 and M2 cells are associated with differential cytokine production and inflammatory/ immune regulators. Some of these various cytokines are known to participate in different stages of tissue repair. For instance, a rapid up-regulation of IL-1β and TNF-α has been shown after adhesion of monocytes and neutrophils to material surfaces [27, 144]. IL-1β is also a potent mitogen for fibrocytes [62], while both IL-1β and TNF-α are well known inflammatory agents [145]. IL-1β, may also function to maintain fibrocytes in a pro-inflammatory state driving further recruitment

of inflammatory cells [63]. On the other hand, TGF-β has been shown to promote the migration and proliferation of fibrocytes during lung fibrosis [42, 79, 82], and promote pro-fibrotic and wound healing responses [42, 135, 146]. TGF-β also leads to myofibroblast differentiation of resident tissue fibroblasts and circulating fibrocytes and can perpetuate extensive collagen production [37-38, 67]. We hypothesized that these opposing roles may be substantially altered by the dominating state of macrophage polarization. Along these lines, we have identified two antagonistic agents SB203580 and SB431542 that target either M1 or M2 specific products that may alter subsequent activation of fibrocytes.

3.2 Macrophage Depletion Leads to Reduced Fibrocyte Responses and Collagen Production

3.2.1 Purpose

Immune/ inflammatory cell interactions, such as those of macrophages, are known to be key modulators of downstream fibrotic responses [3, 5, 27]. To further understand a possible connection between macrophage and fibrocytes, we have performed limited studies using an induced macrophage depletion model.

3.2.2 Materials and Methods

3.2.2.1 Macrophage Depletion Animal Model

Macrophage depletion studies were performed by depleting macrophages with daily iv injection (100 µl) of a rabbit anti-mouse macrophage antibody (Accurate Chemical & Scientific Corp.) starting 48 hours prior to subcutaneous implantation of a PLA model biomaterial implant. Subcutaneous implantations were performed four hours after the prior injection of the same day. Neutralizing injections were continued out once daily during the acute macrophage depletion study for 3 days. Poly-L-lactic acid (PLA)

microspheres (10% w/v in 50 µl in saline) were used as model biomaterial implants to mimic biomaterial-mediated inflammatory/fibrotic responses as described earlier [107].

3.2.2.2 Imaging Fibrocyte Migration

For fibrocyte tracking studies, splenic derived fibrocytes were grown in culture for 7 days before incubation with a NIR fluorophore Xsight 761 as previously described. Following labeling $2x10^6$ cells in 200µl PBS were administered by iv injection as previously described [102-103]. The in vivo imaging approach used for tracking fibrocyte migration has previously been established by our group, and explained earlier in the previous chapter [103-104] (Please see 2.2.2.2).

3.2.2.3 Histological and Immunohistochemical Evaluation

Histological and immunohistochemical methods have similarly previously been described (Please see 2.3.2.3). In brief, fibrocytes were identified in the explanted tissue by staining for CD45 and Collagen 1 markers. Similarly masson trichrome staining was used to observe and quantify the total collagen content surrounding the implants. Both fibrocyte numbers and collagen staining was performed during the acute inflammatory phase 5 days after implantation.

3.2.2.4 Statistical Analysis

GraphPad (La Jolla, CA) was used for all statistical operations. Results are reported as the means ± standard deviations. Students t-test was performed for data with single group comparisons. All data was considered significant when *P<0.05 or **P<0.01.

3.2.3 Results

To first determine a potential link between macrophages and fibrocyte reactions at the implant, we examined the influence of macrophage depletion on overall foreign body reactions. macrophage depleted mice and controls were subcutaneously implanted with PLA microspheres as a model biomaterial implant. Near infra-red (NIR) labeled

fibrocytes were then injected intravenously and their migration was monitored for 72 hours as previously described. [102-103]. Fibrocytes were found to transmigrate to the site of the biomaterial implant in both depleted and control mice, however in depleted mice the number of migrated fibrocytes was reduced by 10 fold on average over 72 hours (Figure 3.1). To further study the influence of the reduced fibrocyte numbers on the acute inflammatory response and the resultant shift to fibrosis the implants were excised after five days.

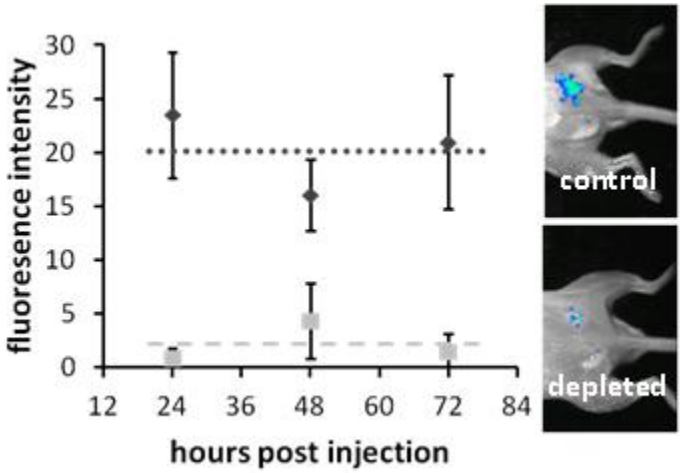

Figure 3.1 NIR labeled fibrocyte migration to control and macrophage depleted mice Results are shown as the means ± standard deviations for n=3 animals. Following labeling of fibrocytes, $2x10^6$ cells in 200µl PBS were injected iv. Migration to PLA microsphere implant sites was monitored by fluorescent intensity using the Kodak in vivo FX pro system. On average, migration of fibrocytes to macrophage depleted animals was reduced by 10 fold (dotted lines) in comparison to the controls over 72 hours. This figure is adapted from reference [110] currently in submission.

Histological analysis at the five day time point demonstrates drastic differences in the tissue response. First, immunohistochemical shows an almost complete lack of fibrocytes (yellow/orange staining) in the response of macrophage depleted animals (Figure 3.2). Quantification of fibrocyte numbers reveals a similar trend as observed with

in vivo imaging with an approximate 8.5 fold difference between controls and macrophage depletion (Figure 3.3). Secondly, a normal foreign body response with organized layers of cells and the formation of collagen bands, identified by aniline blue from masson trichrome staining, is observed in the control animals (Figure 3.2). However, in the depleted animals, only random cell organization and minimal collagen formation are observed. Again, a significant reduction of the collagen content, approximately 3 fold, was found in the depleted animals. Interestingly, the cellular density was not observed to change between the control and the macrophage depleted response. Although the overall number of cells present in the response does not drastically change, the cellular phenotypes and activation are clearly altered with a reduction in the fibrocyte response and a significant decrease in matrix and collagen production.

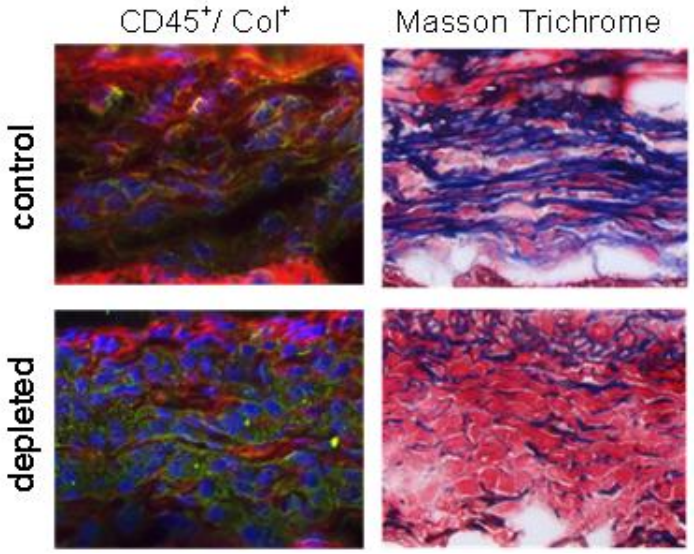

Figure 3.2 Histological identification of fibrocytes and collagen production
The panel shows representative images for fibrocytes (left column) and collagen staining (right column) for control and macrophage depleted animals five days after subcutaneous implant of PLA microspheres. Fibrocytes are identified by dual staining for $CD45^+$ and Collagen 1^+ (yellow). Collagen is identified by analine blue in the Masson Trichrome stain. The study was performed with n=3 animals. This figure is adapted from reference [110] currently in submission.

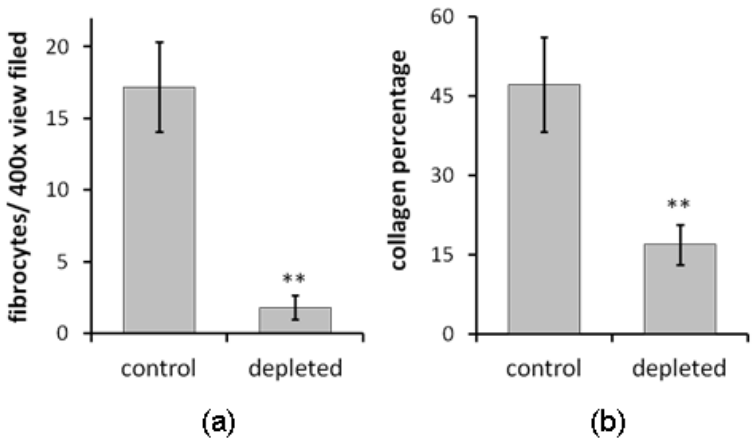

Figure 3.3 Histograms of fibrocyte and collagen response to macrophage depletion (a) Number of fibrocytes per 400x view field taken as the average of n=3 view fields for each animal (b) Collagen percentage within the developing fibrotic capsule. Data is presented as the average of n=3 animals per treatment. Statistics are performed with student's t-test and take as significant at **P<0.01. This figure is adapted from reference [110] currently in submission.

3.2.4 Discussion

There is profound evidence to support that macrophages are, at least partially, responsible for the recruitment and subsequent activation of fibroblasts during healing [27, 147]. In understanding and potentially altering this reaction we first focused on macrophage depletion to determine if a link exists to the fibrocyte response. Our results indicate that macrophage depletion significantly reduces fibrocyte immigration to the implant. Macrophages secrete a host of inflammatory factors that may recruit fibrocytes to the implant such as SDF-1α, MCP-1 and SLC [148]. These homing axes, CXCL12, CCL2, and CCL21 respectively, have all been previously suggested to play a role in fibrocyte recruitment [74, 82, 85].

Five days after injection of fibrocytes, the histological results show drastic differences in the foreign body response with little to no collagen production in depleted animals and minimal accumulation of fibrocytes. While the cellular density does not seem

to be changed, it is clear that the tissue response is significantly altered with macrophage depletion. As a result, the fibrocyte recruitment to the site of implantation is diminished and inadvertently the healing or initial fibrotic response is significantly reduced. These results suggest that fibrocyte accumulation at the implant site is closely related to macrophage activation, as in agreement with previous findings [143], however the mechanisms for communication between cells are unclear. With this initial link established, we further investigate the interactions of macrophages and fibrocytes specifically focusing on the macrophage polarization paradigm.

3.3 Development of Optical Imaging Probes for Monitoring Macrophage Polarization

3.3.1 Introduction

Classically activated M1 macrophages are pro-inflammatory and induced by interferon gamma (IFN-γ) often in combination with lipopolysaccharide (LPS) or TNF-α [32, 137]. These cells produce inflammatory cytokines, reactive oxygen species, and induce nitric oxide synthase, as well as Th1 type inflammatory responses [137]. On the other hand, alternatively activated M2 macrophages are produced by exposure to IL-4 and IL-13 in conjunction or by elevated levels of IL-10. M2 cells are primarily anti-inflammatory and involved in Th2 reactions such as tissue healing and regeneration. While this broad description of M1 and M2 cells is generally accepted it represents a simplified depiction of the true nature of macrophages. In vivo, macrophages exist within a spectrum of activation states between the M1 and M2 extremes. In support of this, studies have shown that macrophages can be re-polarized (convert from M2 back to M1 and vice versa) by secondary Th1 or Th2 cytokine signals altering regulation of cytokine secretion [140]. Nevertheless, this simplified description provides a platform to study and interpret the diverse roles of macrophages in tissue remodeling.

Despite of the improvements in understanding immune/ inflammatory responses, the interaction between polarized macrophages and fibrotic responses are mostly unclear. This is partially due to the lack of method to monitor and quantify the relative polarity of macrophages in real time. Due to the mounting evidence that supports the differential role of M1 and M2 macrophage in tissue regeneration, the development of an imaging modality to distinguish these cells *in vivo* is paramount for advancing our knowledge of these dynamic cellular interactions. In fact, macrophages are known to have a plethora of receptors enabling them to responds to various signals in the wound environment. Some of these receptors, such as folate and mannose, have been previously used to distinguish subsets different macrophages.

The folate receptor has been shown to be up-regulated and specific for macrophages activated by an inflammatory stimulus [149], as well as activated synovial macrophages in rheumatoid arthritis [150], and in macrophages in the pathogenesis of arthrosclerosis. [151]. In one study it was found that only an activated macrophage subset and not the resident macrophages, granulocytes, lymphocytes, or erythrocytes, expressed up-regulated folate receptors [149]. In addition these M1 macrophages were found to produced reactive oxygen species and express TNF-α [149]. Most interestingly, the folate receptor is only expressed in low or undetectable levels in normal tissues (with some exceptions such as the kidney, placenta, and malignant tissues) [150-151], making it a potential candidate to identify M1 macrophages *in vivo*.

Alternatively, the mannose receptor has previously been used as a target ligand for M2 alternatively activated macrophages. As an endocytic receptor mannose functions as a clearance system for tissue plasminogen activator, myeloperoxidase, thyroglobulin, and some microbial ligands up-regulated during inflammation [97, 152]. In addition to macrophages the mannose receptor is expressed by select endothelial and activated

dendritic cells, but not by monocytes or neutrophils [97]. In addition, most dendritic cells do not constitutively express the mannose receptor *in vivo* [152]. Furthermore the mannose receptor can be substantially up-regulated on macrophages by stimulation with IL-4, IL-10, and IL-13 [97, 152-153]. Coincidentally, expression of the mannose receptor is diminished by the presence of IFN-γ which is a hallmark initiator of M1 responses [97]. The contrast between expression of the folate and mannose receptors on macrophages may therefore provide a window to monitor macrophage polarization *in vivo*.

To illuminate the process of macrophage polarization and investigate the effects on fibrocyte-mediate reactions we therefore developed analogous imaging probes coupled with distinct NIR indicators to simultaneously monitor the up-regulation of the folate and mannose receptors. By comparing NIR probe fluorescence intensities and histological evaluation, we explore the possibility of using folate- and mannose-based probes to monitor and quantify the extent of inflammatory and fibrotic reactions to biomaterial implants.

3.3.2 Materials and Methods

3.3.2.1 Fabrication of Folate- and Mannose-based Near Infrared Probes

All chemicals were purchased from Sigma-Aldrich (St Louis, MO) unless otherwise specified. For the folate-based probe fabrication folic acid (50 mM) was dissolved in dimethylsulfoxide, and then 1-Ethyl-3-(3-(dimethlaminopropyl) carbodiimide (EDC) (150 mM) and N-hydroxysuccinimide (NHS) (150 mM) were added to the folic acid solution. The mixture was incubated for 24hrs at room temperature. The activated folic acid was then precipitated by adding diethyl ether, washed three times with tetrahydrofuran (THF) and dried under vacuum. *t*-BOC-PEG-NH_2 (Mw:5k, JenKem Technology USA Inc. Allen, TX)(4 mM) and the prepared activated folic acid (80 mM) were dissolved in dimethylsulfoxide for 12hrs at room temperature to couple folic acid to

the amine group of *t*-BOC-PEG-NH_2 (*t*-BOCPEG-FA). Residual folic acid was removed by dialysis against dimethylsulfoxide and then against DI water. The dried conjugates were further dissolved in Dichloromethane and then treated with trifluoroacetic acid to cleave *t*-BOC groups (NH_2-PEG-FA). After purifying against DI water and lyophilizing, the folate-based probe was prepared by incubating Oyster800 TFP ester (Boca Scientific Inc. Boca Raton, FL) and NH_2-PEG-FA (molar ratio:1.5/1) in PBS buffering solution (pH:8.2) for 24 hrs at room temperature. The probe was purified with dialysis, freeze dried and stored at 4^oC for further use.

For the mannose-based probe fabrication, a similar method was carried out using an established EDC procedure [154-155]. Briefly, Oyster680 TFP ester (Boca Scientific Inc. Boca Raton, FL) and NH_2-PEG-COOH (Mw:5k, JenKem Technology USA Inc. Allen, TX) (molar ratio: 1.5/1) were incubated in PBS buffering solution (pH:8.2) for 24 hrs at room temperature to obtain Oyster680-PEG-COOH. After dialysis and freeze drying, EDC was added to 4-aminophenyl α-D-mannopyranoside and Oyster680-PEG-COOH PBS buffering solution (pH:4.8) (molar ratio: Oyster680-PEG-COOH/EDC/4-aminophenyl α-D-mannopyranoside=1/35/30). The solution was then incubated for 24 hrs at room temperature to obtain the mannose-based probe. The probe was further purified thorough dialysis and freeze drying before use. Chemical structures of both folate- and mannose-based probes were characterized using Nicolet 6700 FT-IR Spectrometer (Thermo Nicolet Corp., Madison, WI). Optical properties of two probes were analyzed using a microplate reader (Infinite® M200; Tecan Group Ltd, Mannedorf, Switzerland).

3.3.2.2 Bone Marrow Macrophage Isolation and Culture

Primary murine macrophages were obtained as previously described [156-157]. Briefly, the bone marrow from the femur and tibia of 6-8wk old Balb/c mice was flushed with Dulbeco's modified eagle medium (DMEM) (Sigma) supplemented with 20% fetal

bovine serum (FBS) (Atlanta Biologicals). Cells were plated into 25cm^2 tissue culture flasks with a bone marrow macrophage media (10%FBS, 10%L929 fibroblast conditioned medium, 1% HEPES, 1%non-essential amino acids (Life Tech, Grand Island, NY.), 1% sodium pyruvate, and 1% penicillin-streptomycin in DMEM) [157]. Macrophages were allowed to mature for 10 days before further subculture and separation into well plates at specified densities from 2000 to 50,000 cells/well. For cytotoxicity studies 3T3 Swiss albino fibroblasts were obtained from American Tissue Culture Collection (ATCC, Manassas, VA.) and cultured in DMEM with 10%FBS and 1% penicillin-streptomycin. All cells were cultured at an ambient temperature of 37^{o}C in 5% CO_2 in a Nuair incubator.

3.3.2.3 Differentiation of Macrophages to M1 and M2 Populations

All macrophages were first cultured for 10 days with a bone marrow macrophage media. Some macrophages were then differentiated to classically activated M1 cells by the addition of lipopolysaccharide (from E-coli, Sigma St. Louis MO) (1µg/ml) for 24 hours according to previous publication [158]. Another population of macrophages was differentiated to alternatively activated M2 cells by the addition of IL-4 and IL-13 to the bone marrow macrophage media (10ng/ml IL-4 and 10ng/ml IL-13 for 24 hours) as previously described [159-160]. After 24 hours of differentiation, cell subsets were confirmed morphologically and through immunohistochemical staining (M1 phenotype- CD80$^+$, M2 phenotype- CD206$^+$) as previously described [30, 161].

3.3.2.4 In Vitro Analysis of Folate- and Mannose-based Probes

M1 and M2 differentiated cells were used to assess the specificity and efficacy of the imaging probes *in vitro*. For this, a competition binding study was devised in which both imaging probes (25 µg/ml) were added to a specific cell lineage and incubated for 30 minutes (established in preliminary studies). The cells were then washed thrice with Hank's buffered salt solution. Fluorescent intensities were then read on a Tecan Infinite

M 200 plate reader (San Jose, CA) at excitation 730 emission 800, and excitation 630 emission 700 for the folate- and mannose-based probes respectively.

Cytotoxicity studies were performed with 3T3 fibroblasts as described earlier [104]. Briefly, 5,000 cells were plated into wells of a 96 well plate, cells were allowed to adhere overnight before the addition of folate- or mannose-based probes at specified concentrations from 0 to 62.5 µg/ml. The toxicity assessment was run for 24 hours after which an MTS assay (CellTiter96, Promega, USA) was run on the cell samples. Percent cell survival was compared to controls (0 µg/ml probe, taken as 100%). Measurement of absorbance was performed on a SpectraMax 340 spectrophotometer (Molecular Devices, USA).

3.3.2.5 Animal Models of Biocompatible Biomaterials and Biomaterial-mediated Infection

All mice used in this study were female Blab/c mice purchased from Taconic Farms (German town NY). All animal experiments were approved by the University of Texas at Arlington Animal Care and Use Committee (IACUC). Poly (N-isopropylacrylamide) (PNIPAM, D:100nm) and poly-lactic acid (PLA,D: 5–10 µm) particles were used as model biomaterial implants and prepared as previously described. [104, 162] For all *in vivo* studies, particles (100ul, 10% wt/vol in saline) were implanted subcutaneously on either side of the dorsal region in mice via a 25 gauge needle.

As an infection model lipopolysaccharide (LPS) (5% solution in saline) was mixed with PLA particles to yield a final concentration of 10% PLA and 0.2% LPS. Similarly in the bacterial model, 10%PLA w/v was mixed into a 1ml saline solution containing 1.6 x 10^8 cfu *Staphylococcus aureus* -Xen29 bacteria (Caliper LifeSciences, Alameda CA) prior to subcutaneous transplantation with a 25 gauge needle.

3.3.2.6 In Vivo Imaging Analysis of Folate- and Mannose-based Probes

In vivo imaging of biomaterial-mediated tissue responses and mock infection were performed four days and one day after subcutaneous implantation, respectively. The four day time point was established in a preliminary study as the critical time-point to observe both M1 and M2 responses to a PLA implant (Figure 3.4). This study assessed the time-course influx of M1 and M2 cells in response to PLA implants over 14 days. The four day time point was identified as the switch point in the response, where the relative number of M1 to M2 cells changes, indicating a shift in the inflammatory response. For imaging infection related responses the one day time point was established from a previous infection model [163].

In both models NIR probes are administered simultaneously by iv. injection (total volume 100 µl, containing 10µl folate-based probe (1.0mg/ml) +10µl mannose-based probe (1.0mg/ml) + 80µl saline), twenty four hours prior to *in vivo* imaging. Whole body fluorescence images are then taken using the Kodak in-vivo FX Pro system (f-stop:2.5, 4x4 binning: Carestream Health, Rochester, NY). To simultaneously monitor the folate- and mannose-based probes an excitation filter 760nm: emission 830nm, and an excitation filter 630nm: emission 700 are used respectively. For all imaging analysis, the mean intensities for all pixels in the region of interest (ROI) (area surrounding and including the implantation location) are calculated. To normalize data, background correction is performed to an area of no fluorescence. All data analyses are performed with the Carestream Molecular Imaging software, network edition 4.5 (Carestream Health, Woodbridge, CT.)

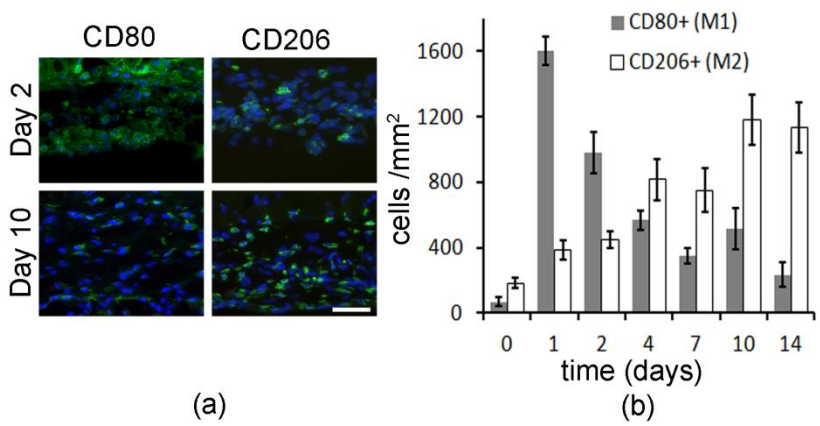

Figure 3.4 M1 and M2 cellular influx to PLA implants
(a) Representative images at day 2 and 10 for M1 (CD80) and M2 (CD206) cells at the interface. DAPI is used as a counter stain to show cell nucleus. The scale bar shows 50 µm. (b) Histogram shows mean and standard deviation of M1 and M2 counts. Data is shown for n=2 implants at each respective time point. From the histogram a shift in the response can be seen at day 4. This figure is adapted from reference [164] currently in submission.

3.3.2.7 Histological and Immunohistochemical Evaluation

After completion of *in vivo* imaging analysis, animals were euthanized and implants and surrounding tissues were isolated for further analysis. Hematoxylin and Eosin staining (H&E staining) (Sigma) was used in general to determine the extent of the inflammatory response to the implants. The capsule thickness was determined by measuring the distance from the biomaterial perpendicular toward the native healthy tissue of the hypodermis using NIH ImageJ software as previously described [105]. The degree of macrophage polarization surrounding implants was assessed though immunohistochemistry. All antibodies used were purchased from Santa Cruz Biotech (Santa Cruz, CA). Secondary antibodies were purchased from ProSci (Poway CA), and nuclei were stained with DAPI (Invitrogen, Carlsbad, CA). All cell densities were calculated as the number of positive cells per view area using equal areas for all counts.

All histological and immunohistochemical analysis was performed on a Leica microscope (Leica, Wetzlar Germany) and processed using NIH ImageJ software.

3.3.2.8 Statistical Analysis

All statistical operations were conducted with GraphPad (La Jolla, CA). Results are reported as the means ± standard deviations. Differences between treatment groups were assessed using ANOVA with Bonferroni comparisons for data with multiple group comparisons. The student's t-test was performed for data with single group comparisons. All data are considered significant when *P<0.05 or **P < 0.01. Linear regression analyses were also used to determine the correlation between group comparisons. Correlations were taken to be significant with a coefficient of determination R^2 >0.80.

3.3.3 Results

3.3.3.1 Confirmation of Folate- and Mannose-based Probe Fabrication

The folate and mannose based probes both use a polyethylene glycol (PEG) backbone with separate conjugation of NIR dyes and covalently linked ligands. To assess the conjugation of folate and mannose moieties into PEG samples were run through Fourier Transform infrared analysis (FTIR) (Figure 3.5). For PEG, characteristic IR absorption peaks are observed at 1100 and 1345 cm^{-1} corresponding to the C-O-C stretching, and at 950cm^{-1} for C-H bending [165].The folate-based probe displays characteristic peaks at 1680 cm^{-1}, due to the amide link between PEG and folic acid, as well as 1600 and 1410 cm^{-1} which can be attributed to the benzene ring of the folate (Figure 3.5a) [165-166]. The mannose-based probe shows IR absorption peaks of a C=N stretch at 1660cm^{-1} demonstrating the conjugation of mannose to PEG as well as the presence of the amide bond at 1390cm^{-1} (Figure 3.5c) [167].

For simultaneous imaging of the folate- and mannose-based probes Oyster800 and Oyster680 were incorporated, respectively, with the individual probes. These dyes

were chosen due to their NIR characteristics and their distinct excitation and emission bands with little to no overlap in emission signals. This was confirmed post-conjugation by mixing the probes in an aqueous solution (PBS) and monitoring the excitation and emission spectra (Figure 3.5b & d). As expected the two probes show individual excitation/ emission spectra with maximal emission of the folate-based probe at 800nm and maximal emission of the mannose-based probe at 700nm wavelength.

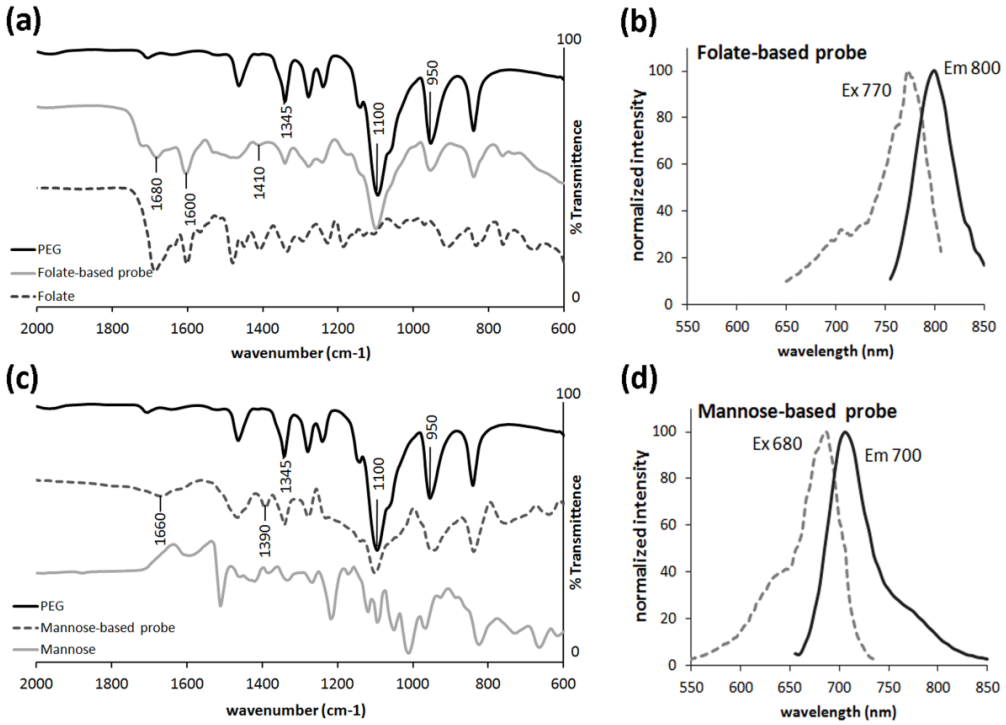

Figure 3.5 Characterization of folate- and mannose-based probes
(a) FTIR spectral comparison between PEG, folate-based probe, and folate. Characteristic PEG peaks are observed at 1100 and 1345 cm^{-1} corresponding to the C-O-C stretch, and at 950cm^{-1} for the C-H bending. Conjugation of PEG and folate is observed by characteristic peaks at 1680 cm^{-1}, (amide link), and 1600, 1410 cm^{-1} (benzene ring of folate). (b) Excitation/ emission wavelengths of the folate-based probe show maximal excitation and emission at 770 and 800nm respectively. (c) FTIR spectral comparison between PEG, mannose-based probe, and mannose. The appearance of peaks at 1660cm^{-1} and 1390cm^{-1} demonstrate the conjugation of mannose to PEG by the presence of C=N stretch and of the amide bond respectively. (d) Excitation/ emission wavelengths of the mannose-based probe shows maximal excitation and emission at 680 and 700nm respectively. This figure is adapted from reference [164] currently in submission.

3.3.3.2 In Vitro Analysis on the Efficacy of Folate- and Mannose-based Probes

The cytotoxicity of folate- and mannose-based probes was determined using 3T3 fibroblasts and a standard MTS assay as previously described (Figure 3.6) [168]. Both probes were well tolerated in 3T3 cells over the entire concentration range studied (up to 62.5µg/ml) with no statistical differences from the control.

Differentiation of M1 and M2 cells from bone marrow macrophages was confirmed by morphological and immunohistochemical analysis. As expected, after 24 hours of differentiation a spindle morphology with round nucleus and a high degree of spreading, as well as positive identification by the activation marker CD80, was observed for lipopolysaccharide activated M1 cells (Figure 3.6). These observations express a typical phenotype previously described for inflammatory macrophages [149]. In contrast, culture with IL-4 and IL-13 resulted in a broader round morphology with positive staining for CD206, a known M2 differentiation marker [30].

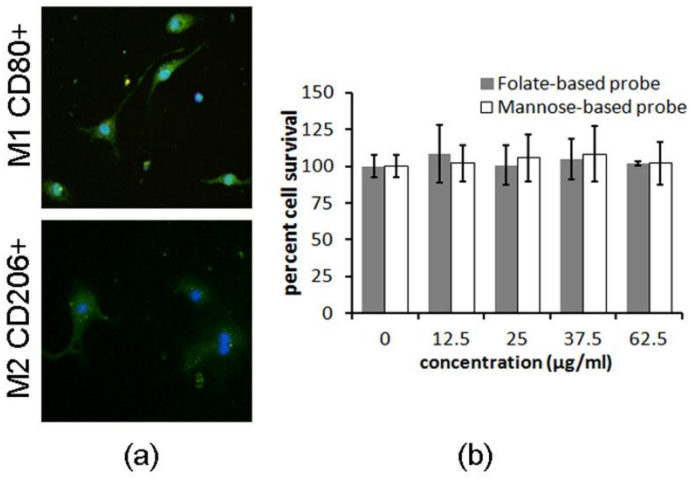

Figure 3.6 Differentiation of macrophage and cytotoxicity of imaging probes
(a) Fluorescent images of M1 and M2 cells in culture. Differentiation is confirmed through morphological analysis and positive staining for CD80 and CD206 respectively. (b) Toxicity results of folate-and mannose-based probes to 3T3 fibroblasts show no statistical differences from the control (0 µg/ml probe). Data is presented as the mean and standard deviation of n=8 replicates of 5000 cells in a 96 well plate, with toxicity studied after 24 hours. This figure is adapted from reference [164] currently in submission.

To investigate the probes' specificity to target either M1 or M2 cells, a competition binding test was performed. The hypothesis is that in a mixed solution of both folate- and mannose-based probes, only the folate-based probes would bind to a population of M1 cells, and only the mannose-based probes would bind to a population of M2 cells. As expected, both probes show good cellular specificity for their respective target phenotype (Figure 3.7). In both cases, the difference in uptake is enhanced by the increasing cell number in a near linear fashion (M1 cells and folate-based probe R^2=0.914, M2 cells and mannose-based probe R^2=0.941). As expected, again in both cases, the intensity of the opposing probe (mismatched with the cell phenotype) remains almost constant, indicating minimal to no binding and minimal phagocytosis within the short time frame (30 minutes). In addition the results suggest that the mannose-based probe can detect a significant difference (~2 fold in intensity) with as few as 15,000 cells.

Similarly the folate-based probe can detect the same difference with around 30,000 cells *in vitro*. This data supports our hypothesis that the folate receptor and mannose receptor may be used as target ligands to distinguish between M1 and M2 cell populations *in vitro*.

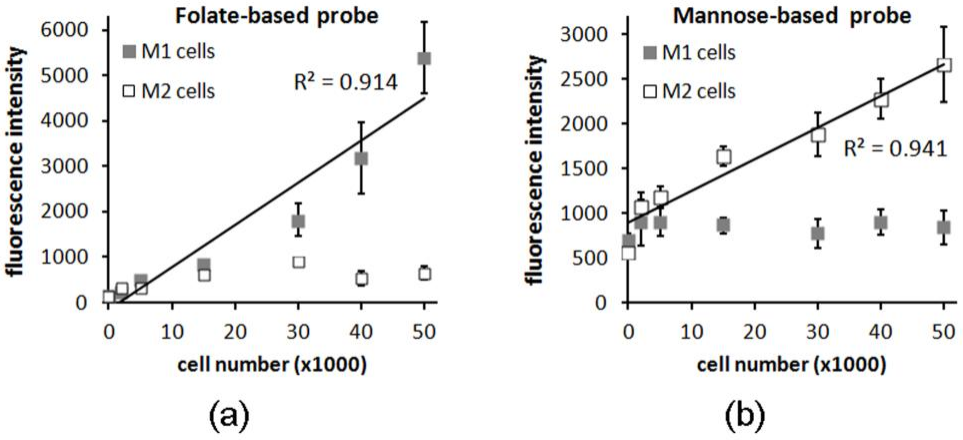

Figure 3.7 In vitro characterization of folate- and mannose based probes
In a competition binding study both probes were added equally to a population of either M1 or M2 cells. The results indicate good cellular specificity of the probes for their respective target phenotype. Linear correlations are observed for the folate-based probe and M1 cells (a) (R^2=0.914) and the mannose-based probe with M2 cells (b) (R^2=0.941). Data are presented as the means and standard deviation for n=6 replicates. This figure is adapted from reference [164] currently in submission.

3.3.3.3 In Vivo Analysis on the Efficacy of Imaging Probes to Monitor Polarized Macrophages to Biomaterial-mediated Infection

M1 macrophage responses are a vital part of the innate immune response to device-centered infection [169-171]. We therefore hypothesized that, in an extremes model of device-centered infection, the folate- and mannose-based probes would have a differential response to infected vs. bacteria-free implants. An implant-infection model was therefore devised in which some of the PLA particles were incubated with either lipopolysaccharide (+LPS) or live bacteria (+Bacteria) prior to implantation.

In the infection model, sites with subcutaneously injected LPS or Bacteria show a substantial increase in the folate-based probe accumulation over the PLA control (Figure 3.8a). This is offset by the reduced presence of the mannose-based probe at either infection site. In fact, quantification of the fluorescence intensity shows an approximate 3 fold increase with the folate-based probe during infection (Figure 3.8b). In contrast, the mannose-based probe shows an approximate 2 fold decrease with +LPS and a 3 fold decrease with +Bacteria (Figure 3.8b). Moreover, histological comparison confirms the trends observed in vivo by quantifying M1 and M2 accumulation around the implants (Figure 3.8c). To assess the accuracy of the probes to monitor M1 and M2 responses we performed a correlation between the average fluorescence intensity and the average cell count for both M1 and M2 cells. When compared with their respective probes, across each implant type studied (PLA, +LPS, +Bacteria), a coefficient of determination $R^2=0.916$ is achieved (Figure 3.8d).

It has previously been found that a higher M2/M1 macrophage ratio can be associated with more positive remodeling outcomes [30]. We therefore calculated the M2/M1 ratio form both the *in vivo* imaging fluorescence intensities and the histological cell numbers (Figure 3.8e). In both cases the PLA control has a substantially higher ratio suggesting, as expected that device centered infection reduces the repair and remodeling outcome. In confirmation of this, we observed that both +LPS and +Bacteria implants had a substantially increased capsule thickness at 133 ±13 µm and 132 ±27 µm respectively in comparison to the PLA controls at only 91 ±9.8 µm.

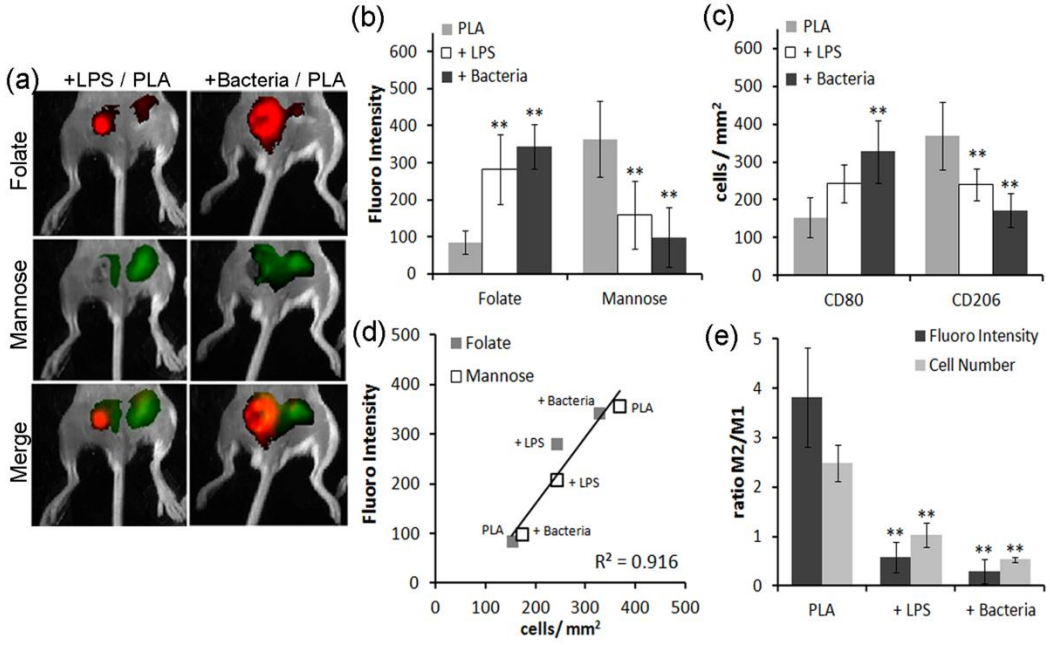

Figure 3.8 M1 M2 probe assessment in an extremes model of device-centered infection (a) Imaging analysis of two infection models (+LPS and +Bacteria) in comparison to PLA controls. In each image the control is on the right. Images are taken 24 hours after implantation. (b) Histogram showing the relative intensity measurements for probes in response to infection. (c) Histological analysis of M1 (CD80) and M2 (CD206) cell counts surrounding implants. (d) Correlation between fluorescence intensity and cell counts for each implant type (R^2=0.916) (e) M2/M1 ratio of fluorescence intensity and cell numbers. In all histograms statistical comparisons are made to the corresponding PLA controls. Statistics are performed with one way ANOVA with Bonferroni comparisons and are considered significant when *P<0.05 or **P<0.01. Each experiment (LPS infection and Bacterial infection) was run independently with n=5 mice. This figure is adapted from reference [164] currently in submission.

3.3.3.4 In Vivo Analysis on the Efficacy of Imaging Probes to Monitor Polarized Macrophages in Response to Biocompatible Biomaterial Implants

In an alternative model we analyzed the more subtle response of M1 and M2 macrophages to biocompatible biomaterial implants. Poly-L-lactic acid and poly(N-isopropylacrylamide) (PNIPAM) are both commonly employed micro and nano-particles for drug delivery and tissue engineering with distinct tissue reactivity. Although biocompatible, PLA microparticles are known to elicit an inflammatory response resulting

in the formation of a fibrotic capsule [172]. In contrast, PNIPAM has improved biocompatibility and does not lead to a chronic inflammatory response [173]. Particles were first implanted subcutaneously for 3 days, after which folate- and mannose-based probes were administered iv. and whole body images were then taken after an additional 24 hours. The results show a greater accumulation of both folate- and mannose-based probes around PLA implants compared to PNIPAM implants (Figure 3.9a & b). Interestingly, there is a significant 2 fold difference in the folate-based probe accumulation at the 4 day time point while the difference in the mannose-based probe accumulation is not significant. The M2/M1 ratio of fluorescent intensities on the other hand is statistically higher with the PNIPAM implants, indicating an increased healing response (Figure 3.9c). This is similarly supported by the observed decrease in capsule thickness around PNIPAM implants (49 ±8.9 μm compared to 82 ±12 μm for the PLA implants). As before, histological analysis of the M1 and M2 cell numbers confirms the trends observed with the imaging probes. A similar correlation between fluorescence intensities and counted cell numbers shows a linear trend with a coefficient of determination R^2=0.943 (Figure 3.10).

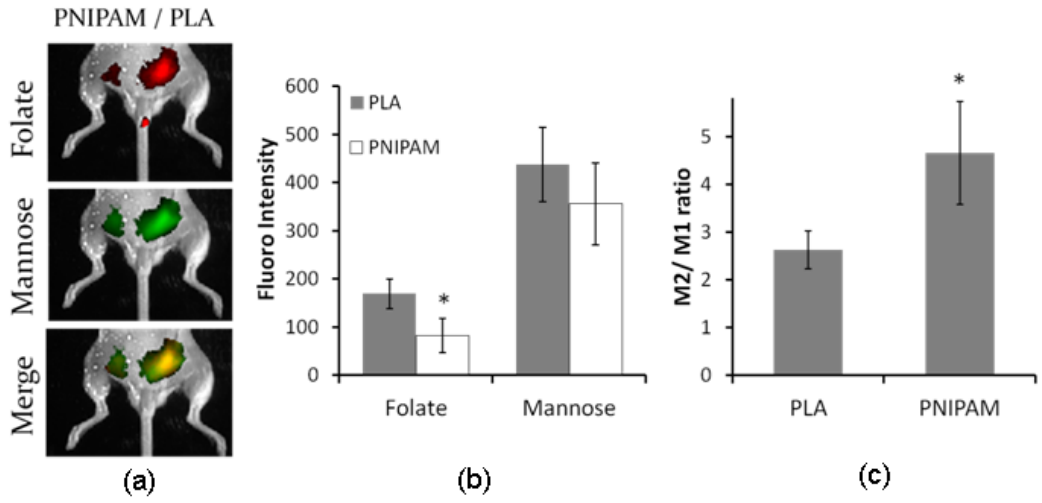

Figure 3.9 M1 M2 probe assessment in a subtle model of biomaterial responses (a) Imaging analysis of PNIPAM and PLA implants at 4 days. In each image the PLA implant is on the right. (b) Histogram of relative fluorescence intensity measurements. (c) M2/M1 ratio of fluorescence intensity. Statistics are performed with the student's t-test and take to be significant at *P<0.05 or **P<0.01. All data is presented as the average and standard deviation from n=4 mice. This figure is adapted from reference [164] currently in submission.

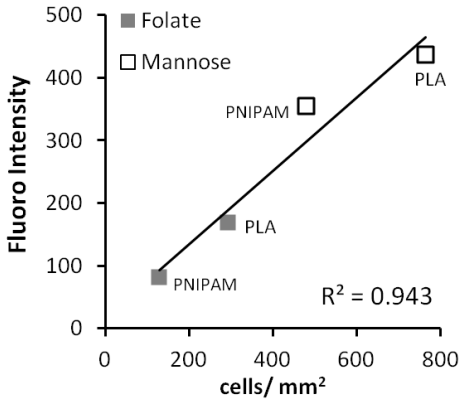

Figure 3.10 Correlation of folate- and mannose-based probe intensity with M1 M2 cells. The points represent the averaged value of probe fluorescence intensity with the corresponding averaged cell number. The correlation curve shows a linear trend with R^2=0.943. This figure is adapted from reference [164] currently in submission.

3.3.4 Discussion

Recently substantial efforts have been placed on investigating the influence of polarized macrophages to determine the balance between immune rejection and tissue regeneration responses [30, 161]. There is currently however no method which can provide fast, accurate, and minimally invasive assessment of M1 and M2 responses *in vivo*. By covalently linking folate and mannose with polyethylene glycol particles we have developed a dual probe imaging system to non-invasively and simultaneously evaluate M1 and M2 responses to biomaterial implants *in vivo*. Taken together, our data indicates that the folate- and mannose-based probes are able to accurately determine the relative degree of M1 and M2 cells across two distinct infection models and in more subtle biocompatible material responses.

The up-regulation of both the folate receptor and the mannose receptor on activated macrophages has been extensively studied for potential imaging modalities and drug delivery vehicles. In example, use of the folate receptor has been investigated in several arthritic and cancer models [150, 174-176]. Similarly use of the mannose receptor has been exploited for delivering drugs to macrophages either by direct conjugation [177], through mannose coated liposomes [178-179], or through polymer microspheres [167, 180]. While the use of mannose as an alternative activation marker is widely acknowledged, some evidence indicates that the folate receptor β can also be used to mark M2 regulatory cells [181]. While we do not dispute this claim, we can refer back to our previous statement that macrophages exist in a spectrum with M1 and M2 at the extremes and various overlap in the expression of surface markers. This may limit the use of the probes in specific cases. For instance, the probes' detection of M1/M2 would be hindered in cancer models where cancer cells also express the folate receptor. We temper the argument by referring to up-regulation during inflammation or regeneration.

Folate is up-regulated during inflammation while mannose is up-regulated during tissue repair, aiding the contrast and use of these markers in cases such as infection.

The developed folate-based and mannose-based probes are observed to have minimal cytotoxicity and are able to distinctly monitor stimulated M1 and M2 cells *in vitro*. This is confirmed by stimulating bone marrow macrophages with either LPS to induce M1 cells or by the addition of IL-4 and IL-13 to induce M2 cells. LPS is well known to activate macrophages through toll like receptor 4 (TLR4) resulting in cytokine production of M1 pro-inflammatory factors such as interferon gamma (IFN-γ), IL-2 and TNF-α [182]. Similarly, studies have shown that some macrophage cell lines such as RAW264.7 or U937 monocytes may be stimulated by LPS to express increased levels of folic acid receptor [151, 183]. Our *in vitro* results indicate that the folate receptor was similarly induced on bone marrow macrophages by the increased intensity of the folate-based probe but not the mannose-based probe in LPS activated macrophages. Had the folate receptor not been induced, it would be expected that the intensity of the folate-based probe and mannose-based probe would be similar due to nonspecific binding or phagocytosis. In contrast, our results show that the stimulated M1 cells specifically uptake the folate-based probe and that the M2 stimulated cells specifically uptake the mannose-based probe.

To initially test the efficacy of the imaging probe *in vivo,* we used an extremes model of device-centered infection. Device-centered infection is one of the common causes of implant failure due to chronic inflammatory responses [184-185]. Interestingly, *Staphylococcus aureus* can often be recovered from approximately 90% of clean wounds at the time of closure [184]. This indicates that even when all appropriate steps are taken, the possibility of infection remains high and should be regarded with concern. Pathogens, such as *Staphylococcus aureus* bacteria, are known to induce a range of activation

profiles priming macrophages to mount an increased immune response [186]. LPS is similarly known to prompt a localized inflammatory response with increased accumulation activated macrophages [187-189]. Using *Staphylococcus aureus* bacteria or LPS as a device-centered infection model we observed, as expected, a significant increase in M1 macrophage accumulation at the site of infection. In addition an increased M2/M1 ratio was observed for the control implants, corresponding to a smaller fibrotic capsule, indicating a more positive healing response. Finally, in a direct correlation the folate- and mannose-based probes were able to accurately represent the relative cellular density for M1 and M2 cells in each of the three implant types in the infection model.

Since infection models are known to prompt an increased M1 inflammatory response we further sought to test the probes in a more subtle model using biocompatible biomaterial implants. PLA and PNIPAM particles were chosen, since both are commonly used for fabricating tissue engineering scaffolds, drug delivery, and imaging agents [173, 188, 190-191]. In addition, PLA particles initiate a strong foreign body reaction while minimal inflammatory responses are induced by PNIPAM implants as previously established [102]. At the four day time point, we were able to observe significantly more folate- and mannose-based probe accumulated at the PLA particle implant sites than at the PNIPAM sites. Furthermore the imaging trends are confirmed by histological analysis of the M1 and M2 response.

These results, together with those from the infection models, present positive examples of the contrast between the folate- and mannose-based probes and the ability to differentially monitor M1/ M2 cellular interactions in the foreign body response. We believe that the twin probes could provide heightened sensitivity and reliability in the assessment of cellular responses to biomaterials. The use of real-time imaging probes such as these can enhance our understanding of the dynamic processes of macrophage

polarization, to provide new strategies in the diagnosis and mitigation of adverse responses to medical implants.

3.4 Influence of Macrophage Polarization on Fibrotic Reactions

3.4.1 Introduction

We have previously discussed the development of a dual probe imaging system to monitor M1 and M2 cellular events *in vivo*. As previously mentioned these cells express various cytokines and factors which are known to participate in different stages of biomaterial mediate tissue response. To explore the possibility of the alteration of fibrocyte responses in connection with macrophage polarization in vivo, we have chosen to focus on several of these factors, namely TGF-β, IL-1β, and TNF-α. In a general sense these factors represent the difference in pro-inflammatory (IL-1β / TNF-α), and pro-fibrotic (TGF-β) roles taken on by M1 and M2 macrophages respectively. Interestingly IL-1β may drive inflammatory reactions of fibrocytes while TGF-β induces a reparative/ fibrogenic role [63]. To investigate the potential influence of M1 and M2 macrophages on fibrocyte responses we designed drug releasing scaffolds to inhibit the production of IL1-β/TNF-α or TGF-β.

Porous PLGA tissue scaffolds were designed using a microbubble fabrication technique previously established by our laboratory [44]. These scaffolds are created by the use of an albumin or gelatin protein microbubble shell to generate an interconnected honeycomb-like porous structure. They may be modified to release growth factors or chemical agents by incorporation in either the protein shell or directly into the PLGA polymer. To alter macrophage responses and cytokine production, scaffolds were fabricated with either TGF-β inhibitor SB431542, or IL-1β/ TNF-α inhibitor SB203580. Both of these drugs, SB203580 and SB431542 have been shown to have good cytokine

specificity for IL-1β/TNF-α and TFG-β respectively [192-196]. SB203580 has been shown to suppress the development of endometriosis, alleviate arthritis, improve renal disease, and reduce bone resorption by down-regulating pro-inflammatory cytokines [196-198]. SB431542, on the other hand, has been shown to protect the cardiac conduction system in Chagas' disease, inhibit scar formation after glaucoma surgery, and inhibit extracellular matrix formation of fibronectin and collagen *in vitro* [194, 199-200]. Using scaffolds to localize the release of these inflammatory/ fibrotic chemokine inhibitors, we aim to explore both the acute and chronic response of M1/M2 cellular infiltration and fibrocyte involvement on the degree of biomaterial-mediated fibrotic reactions.

3.4.2 Materials and Methods

3.4.2.1 Porous Microbubble Scaffold Fabrication

All chemicals were purchased from Sigma Aldrich (St. Louis, MO) unless otherwise specified. The microbubble scaffold formation was based on a previous method for albumin (BSA) microbubble scaffolds developed in our lab [44]. Briefly, poly (D,L-lactic-co-glycolic acid) (75:25, 113kDa, Medisorb Inc., Birmingham, AL) was first dissolved in 1,4-dioxane at a 7.5% w/v ratio. Microbubbles of bovine gelatin (Sigma Aldrich) were then produced by ultra-sonication (20kHz for 10s) of a 10% w/v gelatin solution with the addition of nitrogen gas. The resulting nitrogen filled gelatin microbubbles were added into the polymeric solution at a 1:1 v/v ratio. The quasi-stable mixture is quickly agitated gently and quenched in liquid nitrogen. The scaffolds are then lyophilized (Freezone 12 lyophilizer, Labconco, Kansas City, MO) for 48 hours at 0.03 mbar vacuum to induce phase separation.

To stimulate inflammatory or wound healing signals, several inhibitor drugs were incorporated into and released from the microbubble scaffolds. Specifically, TGF-β inhibitor SB431542 (Selleck Chemicals) was loaded into scaffolds at a dose of 10 mg/kg

body wt/day [199]. IL-1β and TNF-α inhibitor SB203580 (a p38 MAPK inhibitor, Selleck Chemicals) was loaded into scaffolds at a dose of 15 mg/kg body wt/day [196]. For incorporation into scaffolds the drugs were first solubalized in dimethylsulfoxide and then blended with the polymer solution prior to the addition of the protein microbubbles. Scaffolds were cut into 5 x 5 x 5 mm cubes and stored at -20°C until implantation.

3.4.2.2 Method to Determine the Release Kinetics of Scaffold Incorporated Compounds

The release kinetics of SB203580 and SB431542 were measure by incubating scaffold sections in 1ml of PBS at 37^{o}C for various periods of time. At each respective time point (6 hours, 1, 3, 5, 7, 10, and 14 days) 1ml of PBS was removed and fresh PBS (1ml) was added back to the same scaffold section. The release kinetics for incorporated drugs were quantified by high performance liquid chromatography (HPLC). HPLC analysis was performed on a Waters 2695 separations module with a Waters 2996 Photodiode Array Detector (Waters Corp. Milford, MA). A Symmetry C18, 3.5µm 4.6 x75 mm column was used with a flow rate of 1ml/min. The mobile phase consisted of 90% water with 0.1% trifluoroacetic acid and 10% acetonitrile. The retention times of SB203580 and SB431542 were 4.6 and 5.1 minutes respectively (Figure 3.11). Separate standard curves of SB203580 and SB431542 were run to quantify release kinetics of compounds from scaffolds (concentrations for the standard curves ranged from 0.1 µg/ml to 20 µg/ml).

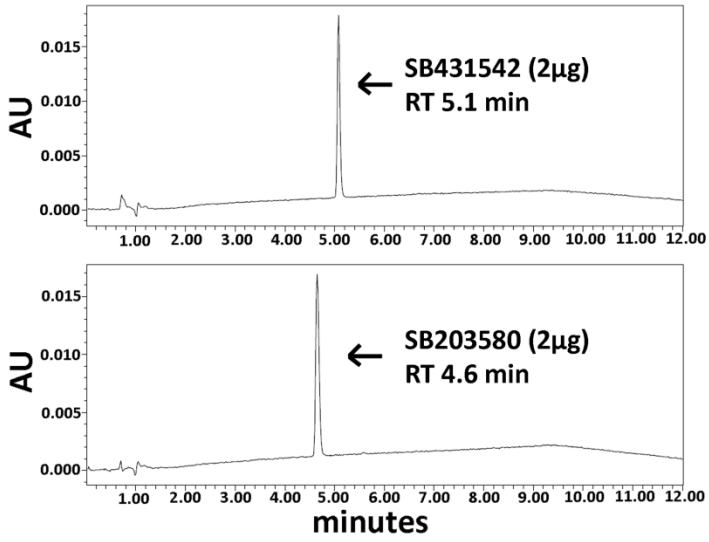

Figure 3.11 HPLC absorbance spectrum of SB431542 and SB203580
The data was processed on a Symmetry C18, 3.5µm 4.6 x75 mm column with a flow rate of 1ml/min. The mobile phase consisted of 90% water with 0.1% trifluoroacetic acid and 10% acetonitrile. Retention times (RT) were found to be 5.1 minutes for SB431542 and 4.6 for SB203580. This figure is adapted from reference [110] currently in submission.

3.4.2.3 Animal Model for Microbubble Scaffold Implants

For scaffold implantation, Balb/c mice (25g body weight) (Harlan, Indianapolis, IN) were anesthetized and a dorsal midline incision was created as previously described [103]. Briefly, each mouse was implanted with two scaffolds of equal treatment condition. The scaffolds were tucked into the subcutaneous space approximately 15mm away from the incision, placed laterally on either side of the mouse. The incision was then sutured closed. The mice were subsequently returned to housing, separated by implantation condition, and monitored daily for irritation around the implant. All animals were cared for in compliance with the protocols approved by the Institutional Animal Care and Use Committee at the University of Texas at Arlington.

3.4.2.4 Fibrocyte Culture and Labeling

Fibrocytes were isolated from the splenic reservoir of monocytes as established elsewhere and previously described [76] (Please see 2.2.2.1).

3.4.2.5 Imaging Model for Tracking Fibrocyte Migration

Whole body animal imaging analyses was carried out using the KODAK in vivo FX Pro system (Kodak, USA) as previously described (Please see 2.2.2.2). Migration of fibrocytes was studied out to 72 hours.

3.4.2.6 Histological and Immunohistochemical Evaluation

Histological and immunohistochemical methods have similarly previously been described within this chapter (Please see 3.3.2.7). In brief, cellular and tissue responses were quantified with ImageJ from H&E and Masson Trichrome staining as previously reported [105]. Cells were further analyzed using the following conventions: M1 macrophages (CD80+), M2 macrophages (CD206+), myofibroblasts (α-SMA+), fibrocytes (CD45+, collagen I+) [26, 105, 201-202].

3.4.2.7 Statistical Analysis

GraphPad (La Jolla, CA) was used for all statistical operations. Results are reported as the means ± standard deviations. Statistical analysis was performed with ANOVA using Bonferroni comparisons for data with multiple groups. The Student's t-test was performed for data with single group comparisons. All data were considered significant when *$P<0.05$ or **$P < 0.01$.

3.4.3 Results

3.4.3.1 Scaffold Formation and Release Kinetics of Incorporated Compounds

Characterization of gelatin microbubble scaffolds was performed as previously reported in our earlier works [44]. Briefly, cross sections were analyzed to confirm a macro-porous structure with pores ranging from 50-150 μm, interconnected with smaller

pores from lyophilization. Similarly SEM images were captured on freeze fractured scaffold to visualize scaffold structure (Figure 3.12a). Porosity of the microbubble scaffolds was similarly tested as previously described, using an ethanol displacement method, and found to be >90% porous [44, 203]. The release kinetics of incorporated compounds were characterized over a 14 day time span encompassing the length of the *in vivo* studies (Figure 3.12b & c). Release rates confirm sustained release of the incorporated drugs from the microbubble scaffold out to 14 days. On average the release rates of SB431542 and SB203580 were approximately 1 µM and 10 µM per day, respectively.

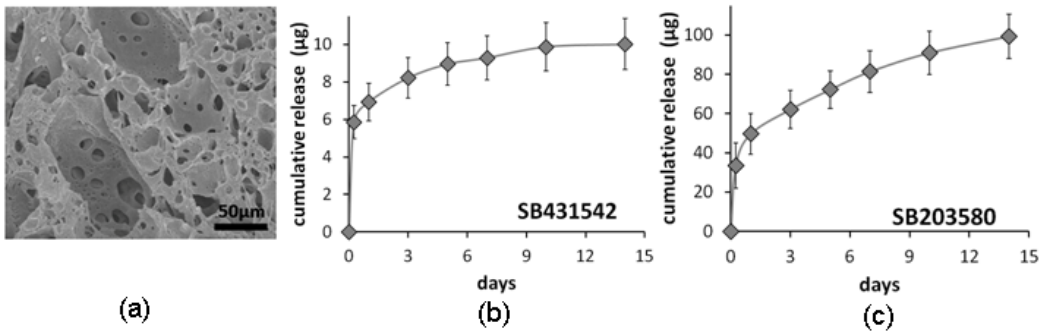

Figure 3.12 Scaffold fabrication and drug release kinetics
(a) SEM image for microbubble scaffold showing porous honeycomb-like structure. (b) Cumulative release in µg for SB431542 over 14 days. (c) Cumulative release in µg for SB203580 over 14 days. All data points are presented as the means ± standard deviation from n=6 replicates. This figure is adapted from reference [110] currently in submission.

3.4.3.2 Effect of Cytokine Antagonists on Fibrocyte Migration

Specific inhibitors SB203580 and SB431542 were used to block the production of known inflammatory modulators IL-1β and TNF-α, and fibrotic modulator, TGF-β respectively. It should be noted that these factors are each produced or expressed by macrophages at different stages of activation [27, 148, 204]. To assess the specific

influence of these modulators on fibrocyte responses we first preformed an analysis of the fibrocyte migration during the acute inflammatory response. Four hours after scaffold implantation NIR labeled fibrocytes were administered through iv. injection. Real time in vivo monitoring was then performed over the next 72 hours. As expected, fibrocytes readily migrate to the control scaffold (gelatin microbubble scaffold without drug) within 24 hours. Of the two inhibitors used however, it was found that only inhibition of the TGF-β signal reduced fibrocyte migration over 72 hours (Figure 3.13a).

Interestingly, the inflammatory cytokine inhibitors were also found to affect the relative degree of macrophage polarization during the acute response. Inhibition of TGF-β resulted in an increased M1 macrophage population, (939 ± 98 cells/mm2 in comparison to 469 ± 92 cells/mm2 for the control) of cells surrounding the implant during the acute response (Figure 3.13b). In contrast, inhibition of IL-1/TNF-α resulted in a decreased M1 macrophage population, (76 ± 34 cells/mm2) and an increased M2 population, (1022 ± 91 cells/mm2 in comparison to 647 ± 60 cells/mm2 for the control) (Figure 3.13b). This shows that general stimulation of inflammatory/ regulatory cytokine mediators may shift the macrophage population during the acute response.

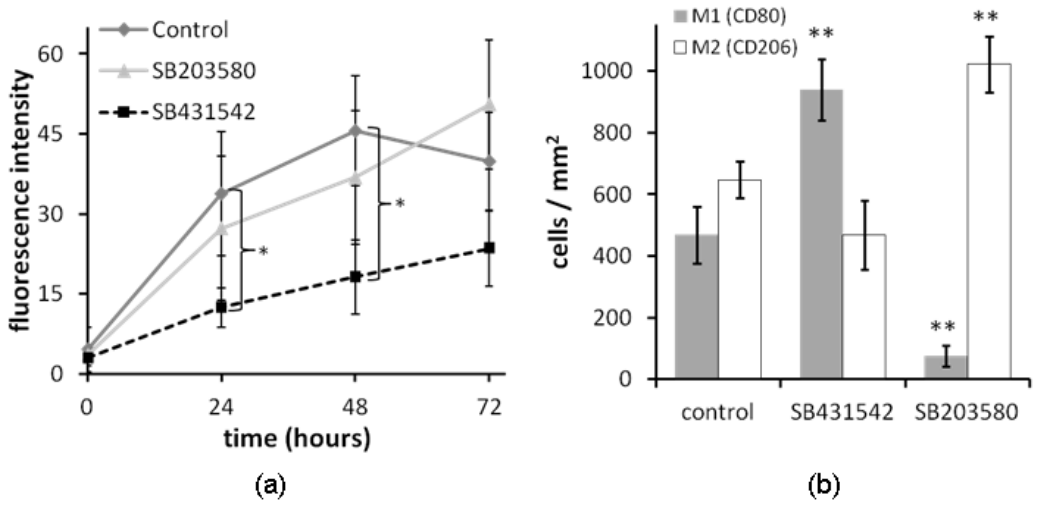

Figure 3.13 Effect of various cytokine antagonists on fibrocyte and polarized macrophage reactions in the acute response.
(a) Fluorescence intensity measurements of NIR labeled fibrocytes migrating to the implant. The localized release of SB431542 (TGF-β antagonist), but not SB203580 (IL-1 and TNF-α) shows significant reduction of fibrocyte migration from control at 24 and 48 hours. (b) Macrophage population density surrounding acute phase implants. Localized release of SB431542 resulted in increased M1 population from control with no statistical difference in the M2 population. Implants releasing SB203580 resulted in a decreased M1 and increased M2 population. Statistics are performed with ANOVA Bonferroni analysis and taken as significant in comparison to the control when *P<0.05, or **P<0.01. Data is presented as the means ± standard deviation for n=4 mice for each treatment group. This figure is adapted from reference [110] currently in submission.

3.4.3.3 Effect of Cytokine Antagonists on M1/M2 Cellular Responses at Two Weeks

The effect of cytokine antagonists on macrophage differentiation were studied at 14 days post implantation. In the control, we found that the majority of the macrophages in the tissue surrounding scaffold implants possesses M2 phenotypes by day 14, (563 ±78 cells/mm2) while ~ 30% of the macrophages express M1 marker (250 cells/mm2). The treatment of SB431542 (TGF-β inhibition) significantly reduced the presence of M2 (370 ± 55 cells/mm2) and M1 (131 ± 39 cells/mm2) macrophages at the implant sites (Figure 3.14). On the other hand, inhibition of IL-1/TNF-α with SB203580 does not show a significant difference from the control samples at day 14.

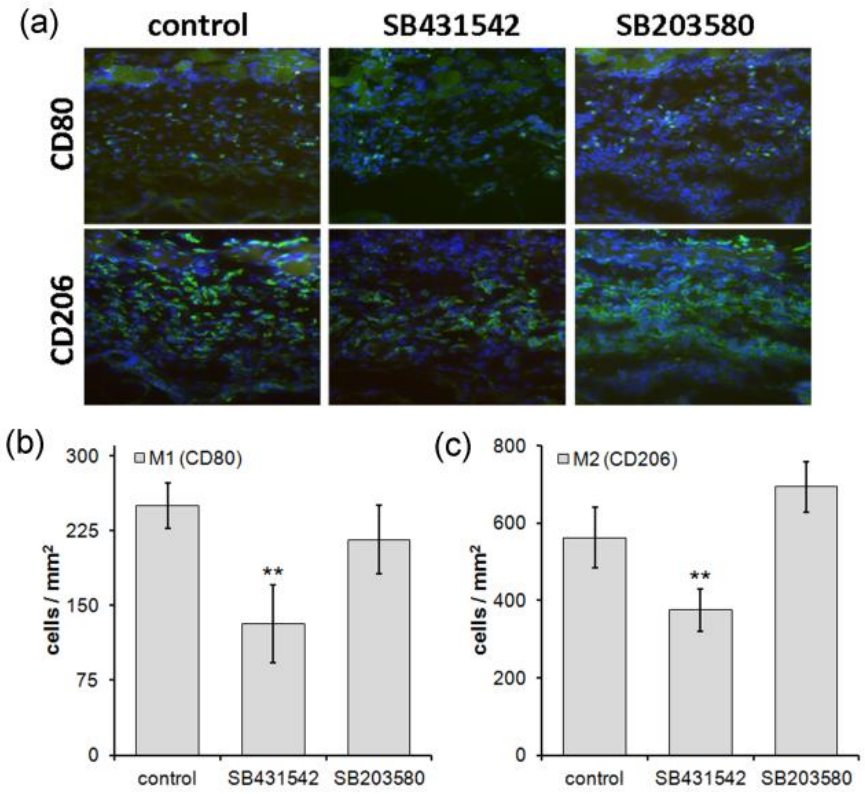

Figure 3.14 Chronic response of microbubble scaffold implants.
(a) Images are presented for immunohistochemical staining of M1/M2 comparing the SB431542 and SB203580 response at 14 days. Histograms show the resultant alternations in the (b) M1 (CD80) and (c) M2 (CD206) response to treatment groups at 14 days. It can be seen that both M1 and M2 are reduced by SB431542 from control where SB203580 shows a marked increase in the M2 response at day 14. Statistics are performed by ANOVA with Bonferroni comparison show to be significant at **P<0.01. Data is presented as the means ± standard deviation for n=4 mice for each treatment group. This figure is adapted from reference [110] currently in submission.

3.4.3.4 Effect of Cytokine Antagonists on Tissue Reactions at Two Weeks

We further investigated the effect of cytokine antagonists on the degree of implant-mediated fibrotic tissue reactions. In the chronic response we observe a reduction in the formation of the foreign body capsule thickness with the release of

SB431542, but not SB203580 (Figure 3.15). The microbubble scaffold control is observed to have the largest capsule thickness at 213 ± 23 μm. The treatment of SB431542 (TGF-β antagonist) significantly reduces the capsule thickness to 119 ± 14 μm. Surprisingly, inhibition of IL-1/TNF-α by SB203580, two well know inflammatory regulators vital in the role systemic or chronic inflammation, does not show a significant reduction in capsule thickness (180 ± 24 μm). Using the capsule thickness as a general indicator of the degree of fibrosis we continued to analyze the resultant degree of fibrocytes within the capsule at 14 days post implantation. Similar to the fibrotic capsule results, we observed a marked decrease in the number of fibrocytes surrounding the implants releasing SB431542, however no significant change with inhibition of IL-1/TNF-α by SB203580 (Figure 3.15).

Expression of α-SMA and collagen production are two hallmarks of activated fibrocytes. It is thought that migratory fibrocytes transition into myofibroblasts losing their hematopoetic expression of CD34 and CD45 and up-regulate α-SMA [39, 42]. To determine if these cytokine antagonists cause a shift if fibrocyte activation we further assessed the degree of α-SMA expression at the biomaterial interface and the relative amount of collagen production. Inhibition of TGF-β similarly reduced the α-SMA expression and the amount of collagen present in the foreign body capsule. The inhibition of IL-1/TNF-α did not show a significant reduction in α-SMA expression, although collagen levels were observed to be reduced.

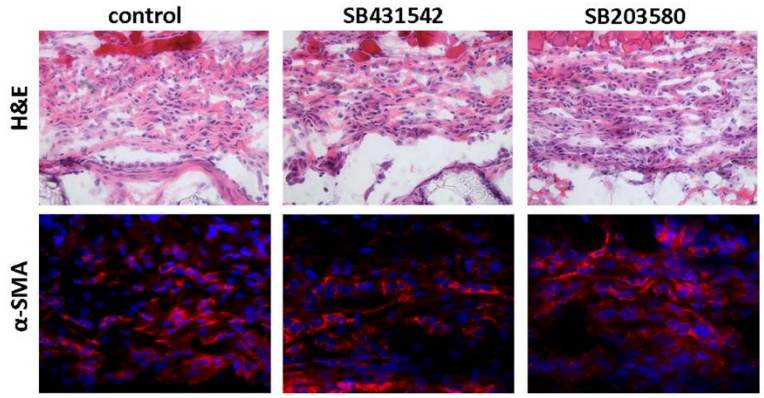

Figure 3.15 Two week histological response of SB431542 and SB203580
Images present the histological results H&E staining and α-SMA staining for the various treatments at 14 days. This figure is adapted from reference [110] currently in submission.

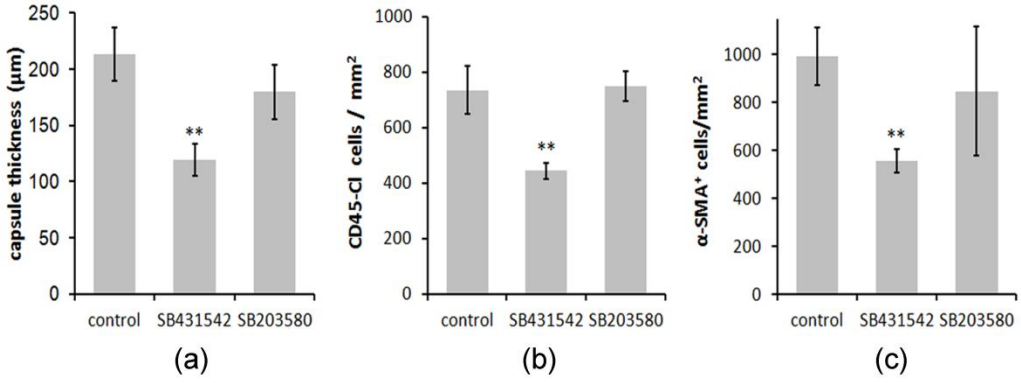

Figure 3.16 Two week histological response of SB431542 and SB203580
Histograms show the capsule thickness (a), the CD45-Cl fibrocyte response (b), and the degree of α-SMA positive cells present in the foreign body capsule (c). Statistics are performed by ANOVA with Bonferroni comparisons taken to be significant at **P<0.01. This figure is adapted from reference [110] currently in submission.

3.4.4 Discussion

To elucidate the potential mechanisms of cell communication we chose to focus on two key inflammatory cytokines IL-1β and TNF-α and the primary regulatory cytokine TGF-β which are up-regulated by macrophages during an inflammatory or wound healing

response [27]. The cellular responses resulting from the localized release of mediating inhibitors are summarized in Table 3.1. In the acute response, the TGF-β antagonist is observed to increase the macrophage M1 inflammatory cells around the implant. Acute inflammation is driven upwards, however the fibrocyte migration is reduced. We, and others have previously demonstrated that fibrocytes migrate to the site of injury following the inflammatory response [74, 105]. Our results indicate that continued or heightened inflammation may be detrimental to the migratory response of fibrocytes. It is well documented that pro-inflammatory interleukins such as IL-1β, IL-6, IL-12 and TNF-α are initially expressed in high quantities in response to a biomaterial implant [2, 36]. As inflammation shifts to regeneration there is also a shift in cytokine and growth factor release to more anti-inflammatory and pro-fibrotic cytokines such as IL-10 and TGF-β [2, 36]. The migratory response of fibrocytes may be dependent on this shift in signaling cues, such as increased TGF-β production. Indeed, studies have shown that TGF-β is potent on initiating fibrotic reactions, as well as stimulating fibroblasts and macrophage to express pro-fibrotic growth factors [146]. Along these lines, many recent studies have indicated that fibrocytes are responsive to TGF-β increasing accumulation and differentiation [62, 70, 75]. Coincidently this shift in cytokine signals has been shown to occur with the switch from M1 to M2 cells [26, 32]. On other hand SB203580 (IL-1/ TNF-α antagonist) had little to no effect on fibrocyte recruitment from control during the acute response. We do observe a significant decrease in M1cells and a resultant increase in the population of M2 cells around the implant. This indicates that a reduction in inflammatory mediators may help to ease the macrophage transition to M2 cells. The insignificant change in fibrocyte recruitment may indicate that the migratory response has reached a plateau for our control sample. In this case, additional stimulation would not be able to increase the migration any further. Nevertheless, inhibition of TGF-β and IL-

1/TNF-α did lead to significant differences in the acute response to the implant. Specifically the M1/M2 population is altered with both treatments, and the fibrocyte migration is reduced with the TGF-β antagonist. The long term effects of these changes were further investigated.

Table 3.1 Summary of localized release of cytokine antagonists on macrophage and fibrotic responses.
This table is adapted from reference [110] currently in submission.

Relative degree of tissue and cell responses in comparison to controls.

	Acute Response			Chronic Response		
	Control	SB431542	SB203580	Control	SB431542	SB203580
capsule thickness	+	-	-	+	-	+
Mϕ M1	+	++	- -	+	-	+
Mϕ M2	+	-	++	+	-	+
fibrocytes	+	-	+	+	-	+
α-SMA				+	-	-

The relative trend in the tissue or cellular response. (+) indicates an elevated response, while (-) indicates a reduced response. Similarly a (++) indicates a greater difference in the elevated response where (--) indicates a more significant reduction in the response.

During the chronic response inhibition of IL-1 and TNF-α had less effect on the capsule thickness and degree of fibrocyte infiltration to the implant than inhibition of TGF-β. IL-1 and TNF-α are known to be potent inflammatory mediators, however there is also some evidence that they can play a role in stimulating fibrosis and collagen production. In two separate studies of bleomycin induced pulmonary fibrosis both IL-1 and TNF-α were found to be stimulatory for the growth of fibroblasts and localized collagen deposition [205-206]. There is also some evidence which shows that IL-1 may function to maintain fibrocytes in an inflammatory state [63]. Our results indicate however that the inflammatory signal from IL-1 and TNF-α may not have a major influence on fibrocytes,

indicating that other pathways may be involved. Inhibition of TGF-β had a more significant impact on the chronic tissue response. We observe a significant decrease in capsule thickness as well as both M1 and M2 macrophage subsets. In addition the fibrocyte numbers decrease and the degree of α-SMA expression surrounding the implant is significantly reduced. This indicates that the differentiation of fibrocytes into α-SMA expressing myofibroblasts has also been reduced by inhibition of TGF-β. In a murine pulmonary fibrosis model, increased macrophage activation, specifically the M2 polarized subset, and greater fibrocyte recruitment was linked to increased fibrosis with IL-10 over expression [143]. On the contrary, higher ratios of M2/M1 cells have been demonstrated to be associated with more positive remodeling outcomes to biologically derived mesh materials [30]. These studies highlight an interesting concept of polarized macrophage interaction with fibrocytes. In our study, we have revealed that a reduced inflammatory signal from IL-1/ TNF-α may act to ease the transition of macrophage from M1 to M2 during the acute response. However the influence on fibrocytes with reduced IL-1 TNF-α is minimal. On the contrary inhibition of TGF-β reduces the number of recruited fibrocytes by 40%, resulting in an almost 50% reduction in capsule thickness at two weeks. This demonstrates that recruitment of fibrocytes to the biomaterial implant may be an important initiator of the fibrotic response.

Our results suggest that fibrocytes play a critical role in biomaterial mediated fibrosis and are augmented by macrophage polarized activities and TGF-β. In support of this fibrocytes have been shown to influence the fibrotic matrix production in several fibrotic disease models such as asthma, pulmonary fibrosis, proliferative vitreoretinopathy, scleroderma, and others, through differentiation to myofibroblasts [42, 66, 123, 207]. Similarly cultured fibrocytes are known to differentiate to myofibroblasts under TGF-β stimulation in vitro [42]. We similarly found that inhibition of the TGF-β

response reduces α-SMA expression, a hallmark for myofibroblast differentiation. Alternatively it has been theorized that fibrocytes have a role extending far beyond extracellular matrix production [35]. The early recruited fibrocytes may function in a pro-inflammatory role induced by immune signals and augmented by IL-1 [35]. While our results demonstrate the importance of fibrocytes in the foreign body response, we cannot exclude the participation and importance of resident tissue fibroblasts through similar or alternative mechanisms.

Chapter 4

Strategies to Alleviate Fibrocyte-Mediated Fibrosis

4.1 Introduction

Increasing evidence suggests that fibrocytes, circulating connective tissue cells, can be differentiated into a variety of cells with different functions and activities. However, little is known about how the microenvironment cues (physical and biological factors) affect such cellular responses. On the other hand, it is possible that specific cues and factors can be provided to stimulate preferable cellular responses. To test this hypothesis, we have explored the possibility of developing new strategies to modulate fibrocyte mediate fibrosis. The first strategy discussed is based on passive alteration of mechanosensing signals through specified topographical changes using polydimethylsiloxane (PDMS) micropillars. This approach is centered on the notion of cell-contact guidance, a cells ability to respond to surface features, which has been proven critical in manipulating cellular behavior. In fact, surface features as small as 10 nm are generally recognized to influence both protein adsorption and cellular responses [208]. Micro and nano-topography are therefore theorized to provide biomimetic cell–modulating signals similar to native cues of the extracellular matrix, altering cell attachment, migration, and proliferation for cells such as osteoblasts, fibroblasts, endothelial, epithelial and macrophages [208]. In example, micro-surface roughness has been shown to substantially enhance the mechanosensing of osteoblasts and increase bone formation [209]. Additionally, macrophage behavior is modulated by nanogrooves *in vivo* altering cytokine secretion and influencing the foreign body response [210].

Micropillars or pegs have several unique features that may enhance mechanosensing signals providing a significant influence on cellular reactions. The addition of micropillars to a surface can provide a unique flexibility or elasticity to surfaces

that otherwise would be highly rigid. In addition, the surface area may be greatly increased and the hydrophilicity/ hydrophobicity may be altered on an intrinsically nonadhesive surface [211]. Increased surface area may also enable cells to form more focal connections [211-212]. Furthermore, the stiffness of the pillars and the ability of the cells to exert contractile forces may have a significant influence on the cellular biology. In fact, it has been shown that micropost rigidity impacts stem cell morphology, focal adhesions, and cytoskeletal contractility leading to alterations in stem cell fate, or differentiation [213-214]. We postulate that by providing differential contact guidance, various micropillar arrays could enhance or reduce fibrocyte mediate responses to the implant. To investigate this strategy we design a series of dual sided micropillar arrays which are subsequently tested in vitro and in vivo for their ability to alter inflammatory and fibrotic tissue responses.

In our second strategy to alleviate fibrocyte driven fibrosis we attempt to force the differentiation of fibrocytes into non-fibrotic cells. *In vitro*, fibrocytes have been shown to possess differential plasticity, under specific stimulation, differentiating not only to myofibroblasts but also adipocytes, osteoblasts, and chrondocytes [67-69]. In further support of this paradigm, human fibroblasts have also been characterized to have myofibroblastic or lipofibroblastic phenotypes with Thy-1^+ and Thy-1^- subsets [215]. Despite these interesting findings the differentiation potential of fibrocytes has not been investigated *in vivo*. While the multi-potency of fibrocytes could potentially offer advantageous responses in different cases, such as improved chondrocyte differentiation during wear and inflammatory responses to hip and joint implants, we focus our investigation on the adipocyte differentiation potential of fibrocytes in the foreign body response. It has been shown *in vitro*, that differentiation of fibrocytes to adipocytes is driven by the peroxisome proliferator-activated receptor PPAR-γ and that TGF-β drives

fibrocyte-to-myofibroblast differentiation [67]. Interestingly the two pathways were found to have reciprocal inhibition of each other [67, 216]. We thus hypothesize that, up regulation of fibrocyte-to-adipocyte differentiation would substantially reduced fibrocyte-to-myofibroblast stimulation and indirectly reduce collagen production in the wound environment. This hypothesis was tested in several *in vitro* and *in vivo* models.

4.2 Topographical Cues and Alteration of Fibrocyte Responses

4.2.1 Introduction

There are at least three main modes of cell attachment and mediation to the biomaterial surface, focal adhesions, close contacts, and extracellular contacts. Cells are guided by focal adhesions, which in turn can be altered by the initial protein adsorption to the implant. Interestingly the composition, amount, and degree of host protein adsorption may be altered by specific topographical cues. Micropillars have been shown to alter the protein attachment at the interface based on topography. In example, patterning of PDMS surfaces with dot-like protrusions increased fibrinogen adsorption by 46% compared with the flat surface, while surface area was only increased by 8% [217]. Additionally, an intrinsically hydrophilic material may lose its resistance to protein binding based on geometry [218]. In contrast, a hydrophobic material may lose its resistance to cell adhesion. These properties as well as those previously discussed for micropillars, such as increased surface area and increased elasticity, may enhance mechanosensing signals, cell morphology, focal adhesions, and cytoskeletal contractility [213, 219]. We hypothesize that these mechanisms may similarly impact precursor fibrocytes in the foreign body response.

As a model for topographical features, we investigated three spatial arrangements of micropillars [98]. All pillars were 10μm in diameter in a hexagonal

arrangement. To investigate the tissue response to various geometries the interspaces and heights of the pillars were altered. Three spatial dimensions were investigated distancing the pillars from center to center at 20, 35, and 70 µm. Two pillar heights were investigated at 14, and 25 µm. Since macrophages and fibroblasts are thought to be the main cells responsible for foreign body reactions, we first studied how micropillar substrates affect the adhesion and proliferation of RAW 264.7 macrophage cells and 3T3 fibroblasts *in vitro*. Subsequently, double-sided micropillar substrates were implanted in the mice subcutaneous cavity for two weeks.

In vivo, we observe that higher micropillar substrates gather more granulocytes and fibroblasts. In fact, cellular density at the interface of taller pillar substrates increased more than 50% over the control. Additionally the capsule thickness was found to increase with pillar height but only becoming statistically significant when pillars were placed further apart. While the increase in cellular density may be closely related to a change in the tensile modulus or stiffness of the pillars, there is also a clear augmentation in the response resulting from the spacing or distance between pillars. Our results suggest that the greater distance and increased height had a substantial effect on the cellular activation and production of extracellular matrix. Taking a closer look at the tissue responses we similarly noticed that the granulation tissue (accumulation of granuloma cells), neoangiogenesis, and collagen production where all enhanced by the increasing pillar dimensions. Most interestingly we find that these responses have strong positive correlations with the number of recruited fibrocytes over fibroblasts or macrophages.

4.2.2 Materials and Methods

4.2.2.1 Materials

Polydimethylsiloxane (PDMS) was purchased from Dow Corning Corporation (Midland, MI). Mouse 3T3-Swiss albino fibroblasts and RAW 264.7 macrophages were

obtained from ATCC (Manassas, VA). A live cell tracer dye, carboxyfluorescein diacetate succinimidyl ester (CFDA-SE) was purchased from Invitrogen (Carlsbad, CA). All primary antibodies used were procured from Santa Cruz Biotech (Santa Cruz, CA). Secondary antibodies coupled with FITC or Texas Red were purchased from ProSci (Poway, CA). Nuclei stain - 4'6-diamino-2-phenylindole dihydrochrolide (DAPI) was obtained from Invitrogen (Carlsbad, CA). All other reagents were purchased form Sigma (St. Louis, MO).

4.2.2.2 Micropillar Fabrication and Characterization

The geometrical configurations of micropillar substrates used in this study were based off previous observations of cells grown on PDMS films [98]. Briefly, the height and spacing arrangements were designed to prompt cell adherence via single or multiple micropillars based on the observed size and spreading on fibroblasts and macrophage *in vitro*. PDMS was utilized for micropillar fabrication due to its desirable characteristics for machining and lithography (low glass transition temperature T_g ~ -125^{o}C, chemical stability, low change in shear elastic modulus with temperature, high compressibility, and stability over a wide temperature range) as well as relative biocompatibility [220-221]. The micropillars were fabricated using a molding method in which the polymer was cast on a SU-8 mold with micro-holes [222]. The pillar dimensions were set at 10 x 10 μm^2 with heights at either 14 or 25 μm (abbreviated as H_{14} or H_{25}) in a centered hexagonal array. Three initial arrangements of pillar orientation were studied with varying inter spaces at 20, 35, and 70 μm (abbreviated as S_{20}, S_{35}, or S_{70}). Samples were labeled based on their physical characteristics by spacing and height (S, H) for example ($S_{20}H_{25}$) refers to pillar interspacing of 20 μm and pillar height of 25 μm. A general schematic of the pillar orientations is presented in Figure 4.1.

Characterization of the micropillar substrates is performed by SEM imaging analysis with a Hitachi 3000N Scanning Electron Microscope (Hitachi High Tech Inc, Tokyo, Japan). For *in vitro* cell culture studies single sided pillar arrays (5 x 10 mm^2) were sectioned and used. For *in vivo* implantation two single-sided pillar arrays of similar micropillar orientation were fashioned together back to back by applying a thin layer of liquid PDMS followed by curing process. Micropillar substrates and PDMS smooth surface films (controls) were sterilized in 70% ethanol followed by 20 minutes UV exposure in a culture hood prior to in vitro and in vivo testing.

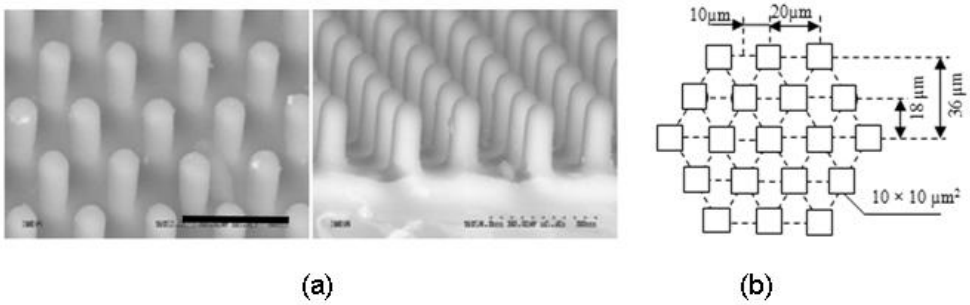

Figure 4.1 Overview of micropillar fabrication
(a) SEM images of micropillars showing the geometrical morphology and alignment as well as the consistency of the mold inversion process. (b) Schematic drawing of the 20 µm spacing pillar design. All subsequent designs are similar with differences in pillar spacing and height. The scale bar corresponds to 30 µm. This figure is adapted from reference [98].

4.2.2.3 In Vitro Analysis of Macrophages and Fibroblasts on Micropillar Substrates

For each cell type, 3T3 fibroblast or RAW 264.7 macrophages, a low density (2000 cells/10 µl) was seeded on 5 x 10 mm^2 micropillar samples so that the growth and morphology of the cell could be studied. Cells were maintained in Dulbecco's modified Eagle medium (DMEM) with 10% fetal calf serum and 1% antibiotics. Cellular growth and proliferation was monitored daily with a cell tracer dye CFDA-SE as previously described

[223]. Briefly, the number of adherent cells was quantified using fluorescence microscopy (Leica, Wetzlar, Germany) for 8 different areas covering the whole pillar substrate.

4.2.2.4 In Vivo Implantation of Dual Sided Micropillar Substrates

To assess the influence of surface topography on tissue reactions micropillar substrates were implanted in the dorsal subcutaneous region of BALB/c mice. The detailed surgical procedure is performed similarly to that previously described for scaffold implants. (Please see 3.4.2.3)

4.2.2.5 Histological and Immunohistochemical Evaluation

After implantation for 2 weeks, the implants and surrounding tissues were recovered for histological evaluation and quantification as previously described (Please see 2.3.2.3)

4.2.2.6 Statistical Analysis

The statistical significance between groups or sets of data was calculated using a One Way ANOVA analysis with a Bonferroni comparison using GraphPad (La Jolla, CA). All data is considered significant when P values of *P<0.05 or **P<0.01 were obtained. Linear regression analyses was used to assess the correlation between cell specific and tissue responses. For linear regression analysis, individual data points for each micropillar array were pooled together as opposed to using only the means. All correlations include multiple counts from the control and each pillar array. These counts are matched on a per-animal per-substrate basis, and then compiled as a whole for all substrates. For all correlations, a minimum of 20 samples, at least 4 animals per group, were matched together. The coefficient of determination (R^2) was calculated providing a measure of correlation.

4.2.3 Results

4.2.3.1 Micropillar Characterization

Characterization of the micropillar substrates is performed by SEM imaging analysis for at least three samples of each configuration. We confirmed that the pillars maintained heights at either 14.35 ± 0.29 or 25.39 ± 0.63 μm as well as held to consistent geometrical spacing in a centered hexagonal array. Table 4.1 summarizes the results of the dimensional analysis for each pillar arrangement expressed the means ± standard deviations. For all pillar arrangements, the pillar head diameter was found to be 10.22 ± 0.22 (length) x 9.87 ± 0.10 μm (width).

Table 4.1 Dimensional analysis of pillar substrates
Analysis was performed on a minimum of n=3 pillar samples for each arrangement measured from SEM images and presented as the means ± standard deviation. This table is adapted from reference [98]

Pillar head diameter (μm)		
10.22 +/- 0.22 X 9.87 +/- 0.10		
Width between center (μm)	**Length between center (μm)**	**Pillar height (μm)**
20.18 +/- 0.67	**18.81 +/- 0.30**	**14.35 +/- 0.29**
35.49 +/- 0.84	**31.32 +/- 0.57**	**or**
70.54 +/- 0.74	**62.81 +/- 0.73**	**25.39 +/- 0.63**

4.2.3.2 Differential Response of Fibroblasts and Macrophages to Micropillar Substrates In Vitro

Interestingly, a differential response was observed on the pillar substrates for fibroblast and macrophage cells. The presence of micropillars was generally found to reduce the adherence, spreading and proliferation of macrophages. Specifically, short and small-spaced micropillars ($S_{20}H_{14}$) were found to stimulate less cell attachment per area in comparison to PDMS controls and other micropillar substrates (Figure 4.2a). In

addition, short micropillar substrates ($S_{20}H_{14}$, $S_{70}H_{14}$) were also found with reduced macrophage growth compared to tall micropillar substrates of the same spacing ($S_{20}H_{25}$, $S_{70}H_{25}$). Intermediate spacing (S_{35}) of micropillars triggered similar responses at both heights (Figure 4.2a). Furthermore, only the tall and wide micropillar substrates ($S_{70}H_{25}$) show an increase over the control and are statistically higher than all other micropillar substrates.

In contrast, fibroblast proliferation shows a varying response based primarily on the pillar height (Figure 4.2b). In general, we find that all substrates with tall micropillars ($S_{20}H_{25}$, $S_{35}H_{25}$, $S_{70}H_{25}$) prompted significantly more fibroblast proliferation than the control substrate ($P<0.05$). Interestingly, there were no significant differences between the various pillar spacing arrangements. Both macrophages and fibroblasts show an intermediate response with the intermediate pillar spacing ($S_{35}H_{14}$, $S_{35}H_{25}$), we therefore decided to exclude this arrangement using only the S_{20} and S_{70} substrates that would prompt extreme cellular responses *in vivo*. This ethically reduced the number of animals required for *in vivo* studies.

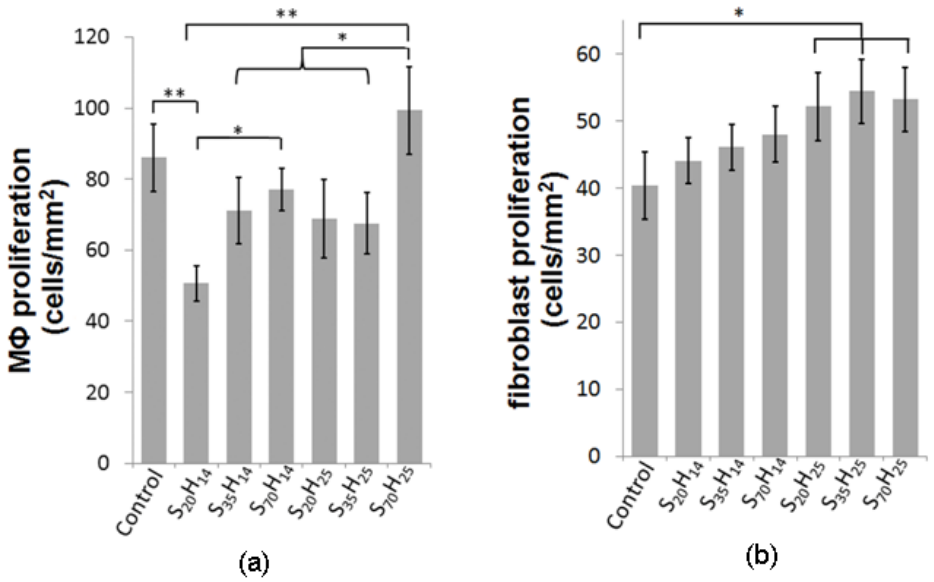

Figure 4.2 Analysis of differential *in vitro* response of macrophages and fibroblasts (a) Macrophage proliferation on micropillar surfaces shows a general decrease from the control smooth surface specifically with short and small-spaced micropillars. (b) Fibroblast proliferation on micropillar surfaces shows a general increase with pillar height. Data are presented as the mean ± standard deviation at 3 days in culture, for n=8 fluorescent images of cells on each respective substrate. Significance was calculated with a One Way ANOVA -Bonferroni comparisons test and taken to be significant at *P<0.05 or **P<0.01. This figure is adapted from reference [98].

In addition to monitoring cell proliferation with the live tracer CFDA-SE, SEM images were taken to observe the cell-substrate interactions. On the short small-spaced pillars macrophages tend to remain "rounded" in shape, forming small clusters of a handful of cells, connecting two or three H_{14} pillars together (Figure 4.3, top left, $S_{20}H_{14}$). With increased spacing however (and to some degree height as well) the cells become more branched and spindle shaped. With increased pillar height macrophages are observed to connect five or six pillars pulling them together and growing in more condensed colonies. Spacing is observed to amplify this effect where significantly larger colonies branch three or four pillars often with cells completely surrounding and covering the taller H_{25} pillars (Figure 4.3 top right, $S_{70}H_{25}$). Fibroblasts on the other hand are

observed to spread across the tops of the short small-spaced pillars. On large-spaced tall pillars however several fibroblasts grow around and often completely overtake the micropillars. With larger spacing, fibroblasts appear to be much larger, and induce significant matrix production (Figure 4.3 bottom right, $S_{70}H_{25}$).

Pillar distention is significantly influenced by pillar height, and limited pillar flexibility may in turn limit cell stretching or matrix production. In this study we observe significant deformation of the H_{25} pillars by colonies of both macrophages and fibroblasts. The spring constant (k) provides a measure of rigidity or stiffness of the pillars. The spring constant of the pillars is given by the formula

$$k = \frac{3\pi E(d^4)}{64L^3}$$

where E, L, and d are the Young's modulus of the PDMS, and the length and diameter of the pillars respectively [213, 224]. For the short pillars, H_{14} k= 402 nN/μm and for the tall pillars, H_{25} k= 70.68 nN/μm. The less rigid, lower spring constant, tall pillars are consistently observed to have larger colonies of cells and greater extracellular matrix secretion. We conclude that mechanical properties of the pillars have significant effects on the proliferation and the contractile forces of both macrophages and fibroblasts.

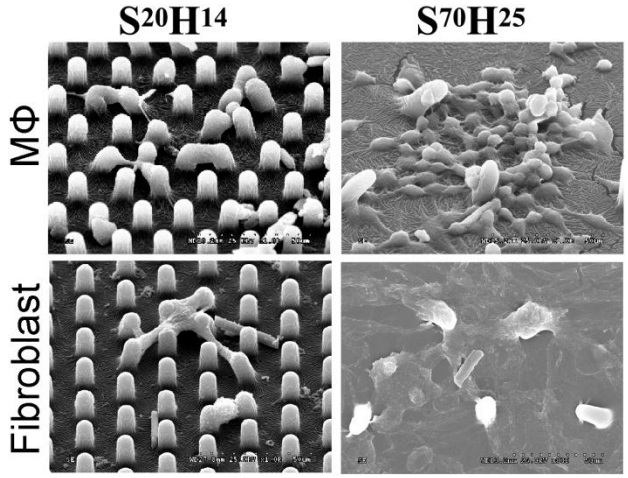

Figure 4.3 SEM images of cellular proliferation at 3 days for select pillar substrates SEM images show the cellular-substrate interactions in greater detail. The short small-spaced pillars (left column) are observed to limit macrophage proliferation while fibroblasts spread across the tops with limited matrix production. The tall large-spaced pillars (right column) show an increase in cellular proliferation and matrix production for both macrophage and fibroblasts. This figure is adapted from reference [98].

4.2.3.3 Cellular Accumulation and Tissue Responses to Micropillar Implants

To determine whether the physical characteristics of micropillars would affect the extent of fibrotic tissue reactions, double-sided micropillar substrates (spacing 20 and 70 μm only) were implanted in the subcutaneous cavities of mice for two weeks. Subsequently various tissue responses and cellular interactions were analyzed. The presence of micropillars was found to augment capsule cellular density and capsule thickness compared to PDMS smooth surface controls. We observed that the higher pillar substrates ($S_{20}H_{25}$, $S_{70}H_{25}$) accumulated more granulocytes and fibroblasts surrounding the pillars while the lower pillar substrates ($S_{20}H_{14}$, $S_{70}H_{14}$) retained smaller numbers and layers of inflammatory and fibrotic cells. In fact the cellular densities of the higher pillar substrates ($S_{20}H_{25}$, $S_{70}H_{25}$) are increased >50% over the control [98]. Interestingly, substrates with larger spacing ($S_{70}H_{14}$, $S_{70}H_{25}$) have a significant increase in capsule thickness, where the smaller-spaced pillars were not significant from the control.

We further examined how pillar height and spacing affect tissue properties such as granulation tissue formation, neoangiogenesis, and collagen production. The properties are common measures of regeneration in the foreign body response. Interestingly with higher pillars and larger spacing the accumulation of granuloma cells increased, as well as the number of blood vessels and the relative degree of collagen production (Figure 4.4). These results indicate that the tissue responses are in fact altered by the micropillar topography, however the cellular mechanisms governing such responses are unclear. To further investigate the relationship of inflammatory and fibrotic cells on micropillar-associated tissue reactions we used immunohistochemical staining to quantify cellular responses. While staining for $CD11b^+$ inflammatory cells shows a significant increase over the control for the micropillar arrays, there are minimal differences between pillar arrays (Figure 4.5a). Additionally, fibroblasts (stained with α-SMA as general marker for different types of fibroblasts) show an increased recruitment with spacing and height, although the difference is only significant with the $S_{70}H_{25}$ substrate (Figure 4.5b). Fibrocytes on the other hand ($CD45^+/\alpha\text{-}SMA^+$), show a significant difference in recruitment with increased micropillar height ($S_{20}H_{25}$ and $S_{70}H_{25}$) over controls and short micropillar substrates (Figure 4.5c).

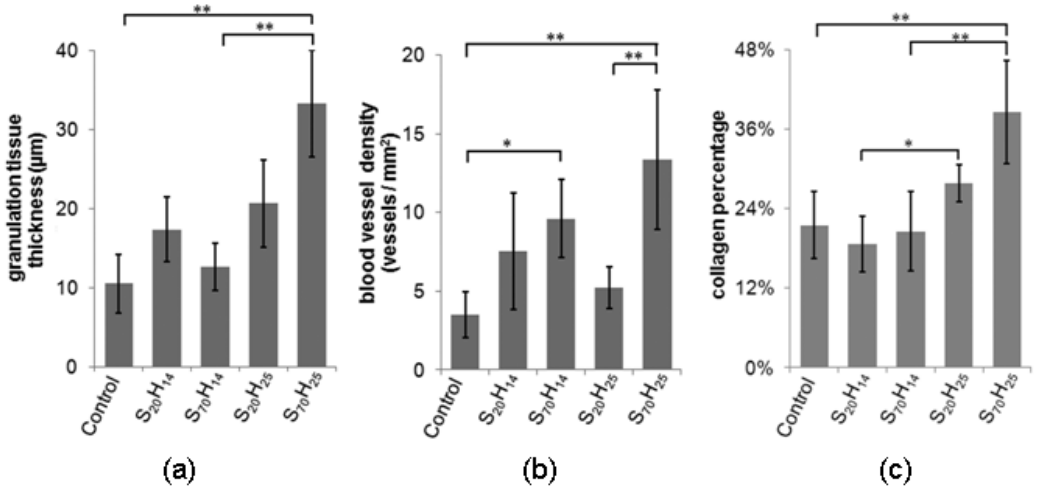

Figure 4.4 Histological analysis of tissue response to micropillar implants (a) Granulation tissue is measured by the thickness of the granuloma cell layer immediately adjacent to the implant (primarily increased with pillar height). (b) Neoangiogenesis is measured by the formation of new blood vessels within the fibrotic capsule (primarily increased with pillar spacing). (c) Collagen percentage is measured by the relative amount of aniline blue staining (primarily increased with pillar height). Statistics are performed with ANOVA Bonferroni comparisons test and taken to be significant at *P<0.05 or **P<0.01. This figure is adapted from reference [98].

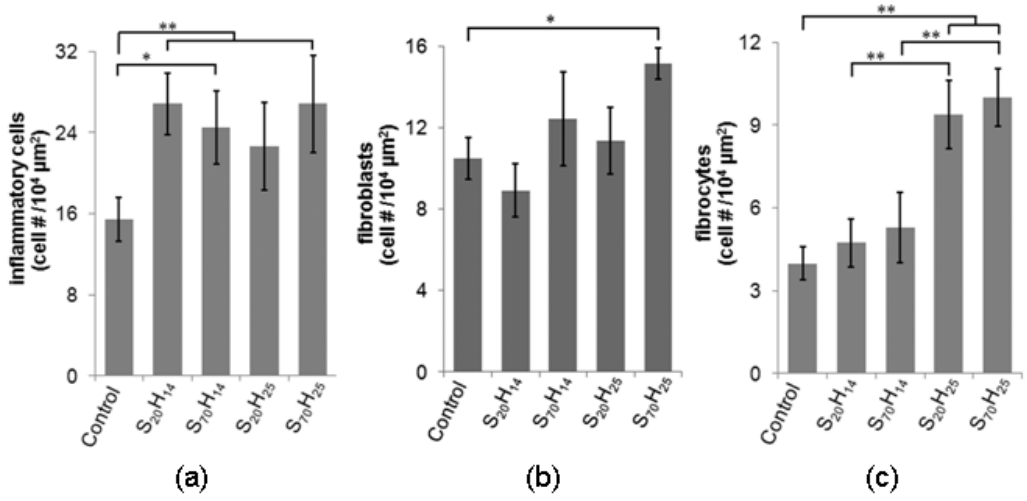

Figure 4.5 Analysis of cellular responses to micropillar implants
(a) The cellular density of inflammatory cells ($CD11b^+$) (b) The cellular density of fibroblasts (α-SMA^+) (c) The cellular density of fibrocytes ($CD45^+$/ α-SMA^+) Statistics are performed with ANOVA Bonferroni comparisons test and taken to be significant at *P<0.05 or **P<0.01. This figure is adapted from reference [98].

4.2.3.4 Assessment of Critical Cells Involved in Micropillar-mediate Responses

To determine the critical cells responsible for the observed differences to micropillar arrays, we ran a correlative assessment comparing histological results to the three cell types previously identified. These cell types, inflammatory cells (both macrophage and neutrophils, $CD11b^+$), general fibroblasts (α-SMA^+), and fibrocytes ($CD45^+$/α-SMA^+) were compared across the various tissue responses described including; capsule cell density, capsule thickness, granulation tissue thickness, blood vessel density, and collagen percentage. Across the board, the strongest positive relationships were found with fibrocytes in comparison to the fibrotic tissue responses studied (capsule cell density [R^2=0.82], granulation tissue thickness [R^2=0.76], and collagen percentage [R^2=0.76] (Figure 4.6)) [98]. In contrast, there were poor relationships between inflammatory cells and fibrotic responses (capsule cell density

[R^2=0.59], capsule thickness [R^2=0.48], granulation tissue thickness [R^2=0.44], blood vessel density [R^2=0.44], and collagen percentage [R^2=0.39]) to micropillar substrates. In addition fibroblast relationships were generally weak (capsule cell density [R^2=0.32], granulation tissue thickness [R^2=0.40], and blood vessel density [R^2=0.45]), although the fibroblast numbers correlate well with both capsule thickness (R^2=0.73) and collagen percentage (R^2=0.73) [98]. These results are summarized in Table 4.2 which presents the relative degree of tissue response and cell type as an elevated (+) or reduced (-) correlation.

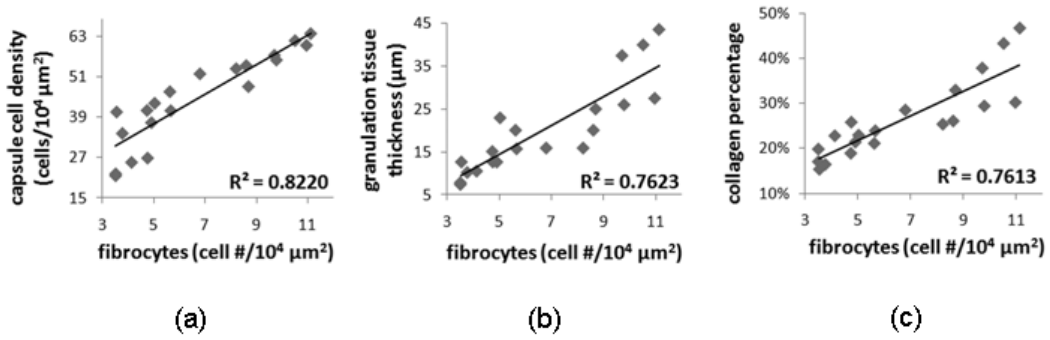

Figure 4.6 Selected correlations of fibrocytes with histological tissue responses. (a) Correlation of capsule cell density and fibrocyte numbers (R^2=0.82) (b) Correlation of granulation tissue thickness and fibrocyte numbers (R^2=0.76) (c) Correlation of collagen percentage and fibrocyte numbers (R^2=0.76). This figure is adapted from reference [98].

Table 4.2 Summary of tissue response to micropillar implants.
This table is adapted from reference [98]

Relative degree of tissue and cell correlation			
	inflammatory cells	resident fibroblasts	fibrocytes
capsule cell density	+	--	+++
capsule thickness	-	+	+
granulation tissue	-	-	++
blood vessel density	-	-	-
collagen percentage	--	+	++

The relative degree of linear correlation measured by the coefficient of determination (R^2). (+) indicates an $R^2 > 0.5$, while (-) indicates an $R^2 < 0.5$. Similarly (++) $R^2 > 0.7$, (--) $R^2 < 0.4$, (+++) $R^2 > 0.8$.

4.2.3.5 Manipulation of Collagen Alignment with Micropillar Implants

Several studies have suggested that the alterations of focal adhesions and directional organization of the cells can have an additional impact on the later organization of the extracellular matrix. In addition, it has been found that the initial organization of cells, resulting in alignment of cellular extracellular matrix, can impact further orientation of additional cell layers *in vitro* which more closely resemble the native tissue [225]. As previously discussed, it is possible that increased focal contacts, resulting from altered pillar dimensions would enhance the mechanochemical feedback to the cell. Based on the geometrical constraints, the extracellular matrix would assemble in a manner resembling the initial cell attachment. Therefore, with precise control of the micropillar parameters, it may be possible to engineer the orientation of the extracellular matrix.

Interestingly investigation into specific collagen fiber alignment with polarized light microscopy demonstrates that the specific pillar orientation alters the layout of the collagen fibrils. Figure 4.7 presents birefringent images from picrosirius red staining for collagen I, as well as representative vectors of fibril orientation for each sample studied. The collagen fibrils of the control sample are observed to orient in parallel with the substrate. As might be expected, this response is also observed to translate though the fibrotic capsule mimicking the same fiber directions. As the pillars become further spaced apart the collagen fiber orientation shifts becoming more segregated, almost reaching opposing directions in subsequent layers through the fibrotic capsule. In the 35um spacing arrangement there is clear organization at the implant interface. In the 70um spacing the fibers seem disconnected with a greater percent at opposing angles to the adjacent fibers. Interestingly, these observations show that the micropillar configurations influence the direction and orientation of the extracellular matrix as well as the fibrotic outcome.

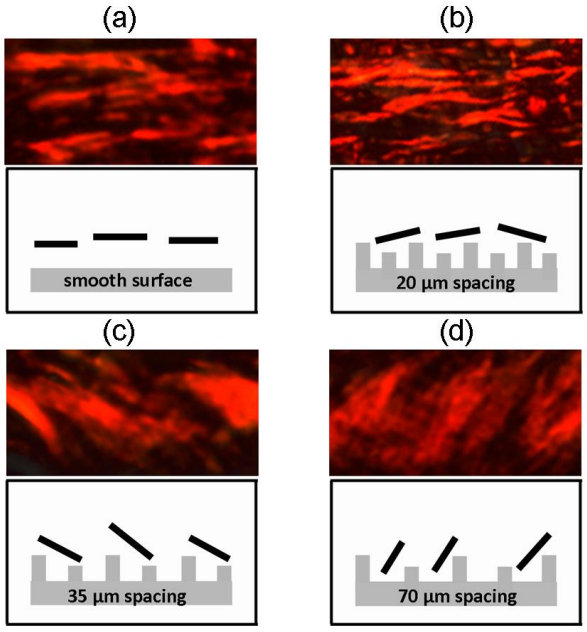

Figure 4.7 Collagen alignment to micropillar implants
Representative samples of observed *in vivo* collagen alignment with micropillar samples. The birefringent images show collagen 1 fibril orientation for the various pillar spacing and smooth sample control. Underneath each image black vectors outline the general orientation of collagen fibrils observed in the samples. This figure is adapted from reference number [226].

4.2.4 Discussion

To determine the role of fibrocytes on biomaterial-associated fibrotic tissue formation, poly-dimethylsiloxane micropillars with different surface morphology (pillar heights and pillar distances) were implanted in the subcutaneous cavity [98]. Surprisingly, we have uncovered that different types of cells prompt varying responses to the same micropillar substrates. Specifically, we found that the increase of pillar height, but not pillar spacing, substantially enhances fibroblast proliferation while macrophage proliferation is inhibited by substrates with small pillar spacing, but not pillar height. Pillar height-dependent fibroblast proliferation is in agreement with several recent observations. First, several studies have revealed that fibroblasts alter their mode of attachment, cell

shape, and migration patterns in response to topographical cues [211-212, 224, 227]. Second tall pillars may provide more spatial surface area for extracellular matrix production and subsequent activation. Lastly, the influence of pillar height may be dependent on the substrate properties such as pillar diameter and material properties such as the tensile modulus or stiffness. These interactions result in the rigidity of the pillar and subsequent cell signaling. It has recently been observed that cell shape, focal adhesion structure, and cytoskeletal tension are closely coupled with rigidity sensing [213]. In addition it has been observed that there are significant differences in the micro and nano scale interactions. A recent study suggests that the adhesion and mechanical cues provided by the pillars alters the microenvironment enhancing adhesive interactions with cells and the production of proteins that form mechanochemical feedback [228]. The alteration of these cues can have a profound influence on cellular behavior.

The properties of micropillar surfaces offer several unique features that have the potential to passively alter cellular interactions. The potential for increased protein adsorption, greater surface area, and increased elasticity resulting in enhanced cellular mechanosensing may provide a favorable environment for cellular attachment and activation at the implant interface. We unexpectedly found however that there were weak relationships between extent of fibrotic responses (capsule cell density, granulation tissue, and blood vessel density) and numbers of fibroblasts in general. This further led us to study fibrocytes. Comparisons of inflammatory cells, general fibroblasts, and fibrocytes reveal that fibrocytes have a stronger correlation with the capsule cell density, granulation tissue thickness and relative collagen percentage around the micropillar implants. Fibrocytes were observed to have a weaker correlation with capsule thickness R^2=0.50 than fibroblasts R^2= 0.73. This however is not entirely unexpected as $CD45^+$ α-SMA^+ fibrocytes are known to transition into $CD45^-$ α-SMA^+ myofibroblasts [39].

Therefore the capsule thickness may be more indirectly related to the fibrocyte recruitment with transition to fibroblasts and myofibroblasts. In addition to the augmentation of the fibrotic outcomes the micropillar configurations were also observed to influence the direction and orientation of the resultant extracellular matrix produced throughout the fibrotic capsule. This notion may open up additional uses for micropillar implants where it may be possible to orient the collagen fibers in applications such as anisotropic tissues for which collagen alignment is of utmost importance to the function of the tissue. Additionally, in another sense, taller pillars may lead to increased collagen production and granulation maturation and therefore enhance wound healing [9]. On the other hand, shorter more densely packed pillars may prompt minimal inflammatory reactions prolonging the lifespan of medical implants such as breast implants and intraocular lenses [9].

4.3 Fibrocyte to Adipocyte Differentiation and the Fibrotic Response

4.3.1 Introduction

The identity and regulation of the adipocyte precursor cell and its progenitor cell has been intensely studied for several years [229]. More recently a chimeric bone marrow study identified the trafficking and differentiation of bone marrow-derived circulating progenitor cells to adipose tissue and multilocular adipocytes [230]. This was observed in mice under a high fat diet or stimulation with anti-diabetic agents such as thiazolidinediones. In contrast, however a separate study was unable to verify this potential showing that bone marrow progenitor cells do not transdifferentiate into adipocytes *in vivo* and instead retain a macrophage phenotype [231]. Interestingly several studies have further shown that fibrocytes function as circulating progenitor cells

that can differentiate into an adipocyte *in vitro* adding a new dimension to this area of research [67, 99].

The differentiation of fibrocytes to adipocytes may be advantageous in the context of the foreign body response. Normal adipose tissue is a primary site for energy storage and functions to regulate energy homeostasis. The tissue is highly vascularized, and constitutively expresses several angiogenic factors such as leptin, VEGF and HGF [232]. In fact, adipogenesis and angiogenesis are known to be reciprocally regulated events [229]. Additionally stimulation of adipogenesis with agents such as thiazolidinediones typically increases the number of small multilocular adipocytes, (which are transitory in nature) decreasing the larger unilocular cells responsible for obesity [229]. Furthermore, the stimulation of fibrocytes to adipocytes in vivo was observed to decrease α-SMA expression which is a hallmark of myofibroblasts differentiation and collagen production [67]. In this alternative paradigm, differentiating fibrocytes toward an adipocyte lineage and away from the traditional myofibroblast may lead to a substantial reduction in the collagen formation in the foreign body response. It is however unclear whether fibroctyte differentiation is a viable strategy to reduce collagen production and scar tissue formation in vivo.

Adipogenesis of stem cells, and recently described fibrocytes, may be achieved by stimulation with an induction media often containing dexamethasone and insulin among other stimulants. Several induction media products however are commercially available supplied as differentiation kits for MSC's. In example Invitrogen (StemPro) and American Tissue Culture Collection ATCC (PCS-500) offer comparable adipogenesis differentiation kits demonstrated to reproducibly induce MSCs into the adipogenic lineage. The multi-potency of fibrocytes and adipogenic potential may offer an alternative strategy to passivate the fibrocyte response during fibrosis, or to enhance regeneration of

tissue specific implants. This study therefore primarily focuses on the potential for directing fibrocyte differentiation surrounding implants *in vivo*. After confirming differentiation potential *in vitro*, we utilized mini-osmotic pumps to study fibrocyte differentiation and the resultant tissue responses *in vivo*.

4.3.2 Materials and Methods

4.3.2.1 Cell Culture and Differentiation of Fibrocytes to Adipocytes

All chemicals and reagents were purchased from Sigma (St. Louis, MO) unless otherwise specified. Fibrocytes were cultured from the spleens of Balb/c mice as previously described [76]. This method has been explained in detail in the previous chapters (Please see 2.2.2.1). After culture for 7 days in media containing M-CSF and IL-13, the fibrocytes are subcultured and re-plated in 24 well plates on glass cover slips for the differentiation assays. The seeded cells, plated at 10,000 cells /well, are allowed to adhere to the cover slip overnight in the original culture media before supplementation of adipogenic media. For adipogenesis differentiation, StemPro Adipogenesis Differentiation Kit A10070-01 (Invitrogen, Grand Island, NY) was used as per the manufacturer's instruction. Briefly, the differentiation medium containing 10% adipogenesis supplement in basal medium was supplied to the cells. New differentiation media was supplemented every 3 days by removing half the old media and replacing with an equal volume of new media. In this process it is important that the cell monolayer is not exposed to air to ensure that the developing lipid vesicles do not burst. Differentiation of fibrocytes to adipocytes was carried out for 14 days following the initial supplementation of differentiation media. For controls, cells were similarly seeded into 24 well plates on glass cover slips. However for controls, use of the original media containing M-CSF and IL-13 was maintained with similar supplementation of half the media every 3 days.

To confirm adipocyte differentiation cells were subsequently fixed in 10% formalin and stained with Oil Red O to assess lipid accumulation or Sirius Red to assess protein accumulation. Images of cells on cover slips are then captured with a Leica microscope (Leica, Wetzlar, Germany) using a CCD camera (Retiga EXi, Qimaging, Surrey BC, Canada) to assess morphological characteristics. In addition quantification of the Oil Red O (positive for adipocyte differentiation) or Sirius Red (negative for adipocyte differentiation) was achieved by colorimetric absorbance microassays as previously described [233-234]. Briefly, the Oil Red O dye was extracted from the cells by the addition of 1ml of isopropyl alcohol. The absorbance of the dye was then read at a wavelength of 510nm on a microplate reader (Infinite® M200; Tecan Group Ltd, Mannedorf, Switzerland). For the Sirius Red assay, the dye was extracted by the addition of 0.3ml of 0.1 N sodium hydroxide solution and read at a wavelength of 550nm on the microplate reader [234].

4.3.2.3 Microbubble Scaffold Fabrication

Protein microbubble scaffolds were fabricated as previously described [44]. This method was described in detail in the previous chapter (Please see 3.4.2.1). Briefly, porous PLGA scaffolds are fabricated by mixing bovine gelatin protein microbubbles into the polymer solution. The quasi-stable mixture is quenched under liquid nitrogen before lyophilizing to induce phase separation. Scaffold sections are then cut into 5x5x5 mm cubes. For the differentiation studies an 18 gauge needle was subsequently used to drill a small hole into the center of the scaffold. This hole was further used to connect a polyvinyl chloride catheter to the scaffold for differentiation studies.

4.3.2.4 Animal Implantation Model and Delivery of Differentiation Media to Implanted Scaffolds

To achieve sustained delivery of differentiation factors *in vivo*, mini-osmotic pumps (Alzet Model 1002,Alza Corporation, Palo Alsot, CA) were used as previously described [103]. These pumps are capable of delivering incorporated factors at a rate of 0.25 ng/h for over two weeks. For *in vivo* differentiation a concentrated solution of the adipocyte differentiation media (StemPro, Invitrogen) (40% adipogenesis supplement in basal medium) was released from the pumps (established in preliminary studies). The pump is connected to the center of the scaffold via a polyvinyl chloride catheter (Alzet, Durect Corporation, Cupertino, CA). Both the pump and connected scaffold are then implanted in the subcutaneous cavity of Balb/C mice. For implantation a vertical incision was made down the midline of the back. The osmotic pump was tucked into the subcutaneous space away from the incision toward the hind limb. The accompanying scaffold was similarly tucked away from the incision resting in the center of the back on the same side as the pump. Control scaffolds were placed contralateral to the test scaffold sample. At the end of the two week study animals were sacrificed by CO_2 inhalation. Scaffolds and surrounding tissue was subsequently isolated and embedded in optimal cutting temperature compound for histological analysis.

4.3.2.5 Histological and Immunohistochemical Evaluation

To determine the extent of fibrotic responses to the scaffold implants some slides were stained with H&E or Masson Trichrome per the manufacturer's instructions as previously described (Please see 2.3.2.3). Furthermore Oil Red O staining was performed to evaluate the accumulation and formation of lipids in the tissue. Briefly, frozen sections are cut at 8 µm and fixed in 10% formalin. After rinsing in 60% isopropanol the sections are stained with the working solution of Oil Red O for 15 to 20

minutes. The samples are then counterstained with hematoxylin and mounted in a glycerine jelly mounting medium (5g Gelatin, 30ml DI water, 35 ml Glycerol, 0.125g Phenol). To identify the relative amount of fibrocyte response fibrocytes were stained with CD45 and Collagen 1 as previously described (Please see 2.3.2.3).

4.3.2.6 Statistical Analysis

Results are reported as the means ± standard deviations. The statistical significance between single group comparisons was performed with the student's t-test using MS Excel. All data are considered significant when *P<0.05 or **P < 0.01.

4.3.3 Results

4.3.3.1 In Vitro Fibrocyte to Adipocyte Differentiation

To investigate the potential of fibrocyte differentiation as an alternative strategy to mitigate fibrosis, we first confirm that stimulation of fibrocytes with an adipogenic medium is capable of spurring differentiation. After two weeks in culture with adipogenic medium we observe positive staining of fibrocyte-derived adipocytes with Oil Red O (Figure 4.8). Morphologically the fibrocyte-derived adipocytes are larger and rounder than the spindle shaped fibrocytes. The derived adipocytes are observed to accumulate intracellular lipids as evidenced by Oil Red O staining. In fact, by extracting the dye with isopropanol after cell staining, we observe an approximate 6 fold increase in the amount of lipid accumulation in the fibrocyte derived adipocyte cell cultures over the controls (Figure 4.8c). In addition, we also investigated the amount of collagen produced by the fibrocytes and fibrocyte derived adipocytes using a Sirius red staining protocol. Interestingly, the increase in lipid accumulation is mirrored by a 3 fold decrease in the amount of collagen production in fibrocyte-derived adipocyte cultures (Figure 4.8d). These findings are in agreement with previous reports indicating that the adipocyte and myofibroblasts differentiation pathways of fibrocytes have reciprocal inhibition of each other [67, 216].

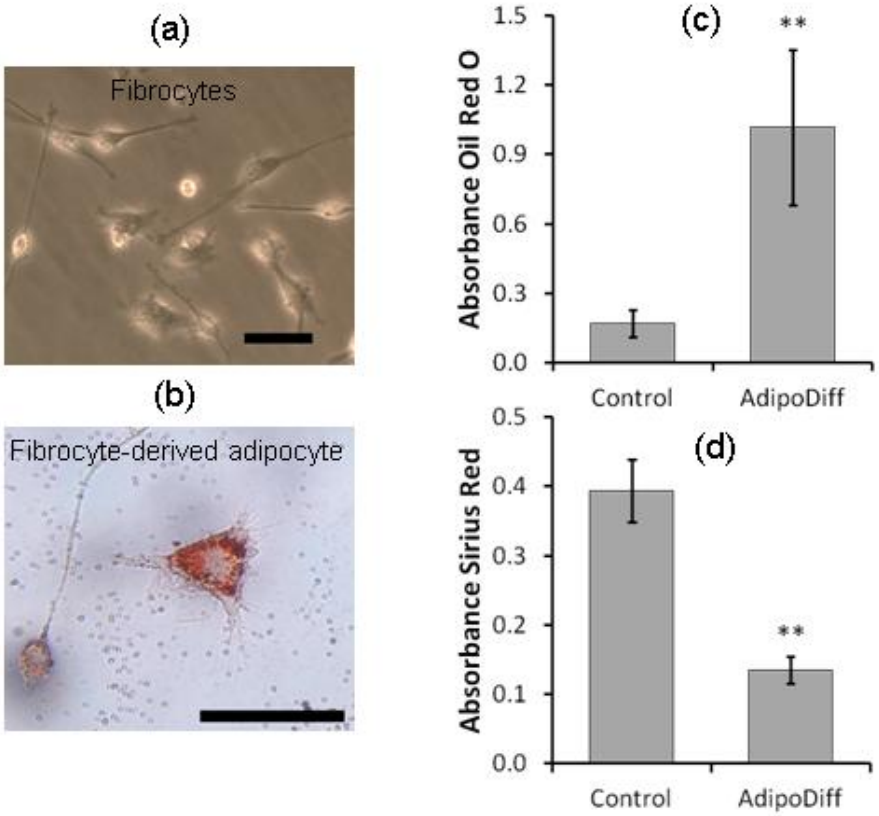

Figure 4.8 In vitro differentiation of fibrocytes to adipocytes.
(a) Fibrocytes show typical spindle shape morphology at 7 days in culture prior to stimulation with adipogenic media. (b) Fibrocyte differentiation to adipocytes at 2 weeks is shown by larger more circular cells with increased staining for intracellular lipids by Oil Red O. (c) Extraction of oil red oil after cellular staining shows a 6 fold increase in the amount of lipid staining after stimulated adipocyte differentiation. (d) Alternatively, staining for collagen shows a 3 fold decrease from controls with fibrocyte-derived adipocyte cultures. Each staining modality was performed on n=6 replicates of adipocyte differentiation with n=3 controls. Each scale bars represents 50 μm. Statistics are performed with the student's t-test and taken as significant at **P<0.01. This figure is adapted from reference [110] currently in submission.

4.3.3.2 Tissue Response to Adipogenic Stimulation

After confirming that cultured fibrocytes can be stimulated to fibrocyte-derived adipocytes *in vitro,* we continued our investigation of the differentiation capability in vivo. Scaffold implants were used as a model biomaterial implants known to induce an

inflammatory response and the recruitment of fibrocytes. To deliver constant and sustained differentiation stimulus, mini-osmotic pumps were connected to scaffold implants via catheter tubes. The tissue response to adipogenic stimulation was assessed at two weeks. A panel of representative histological images is presented in Figure 4.9. H&E images show an increased degree of disassociated tissue with reduced fibrous formation extending through the matrix. The Oil Red O imaging reveals a significant increase in the lipid droplet accumulation (small red circles) throughout the developing tissue, consistent with an increase in adipogenesis. Furthermore, collagen staining by aniline blue in the masson trichrome stain shows a significant reduction in overall collagen formation with small single fibers running through the tissue in contrast to the large bundles typically observed in the control.

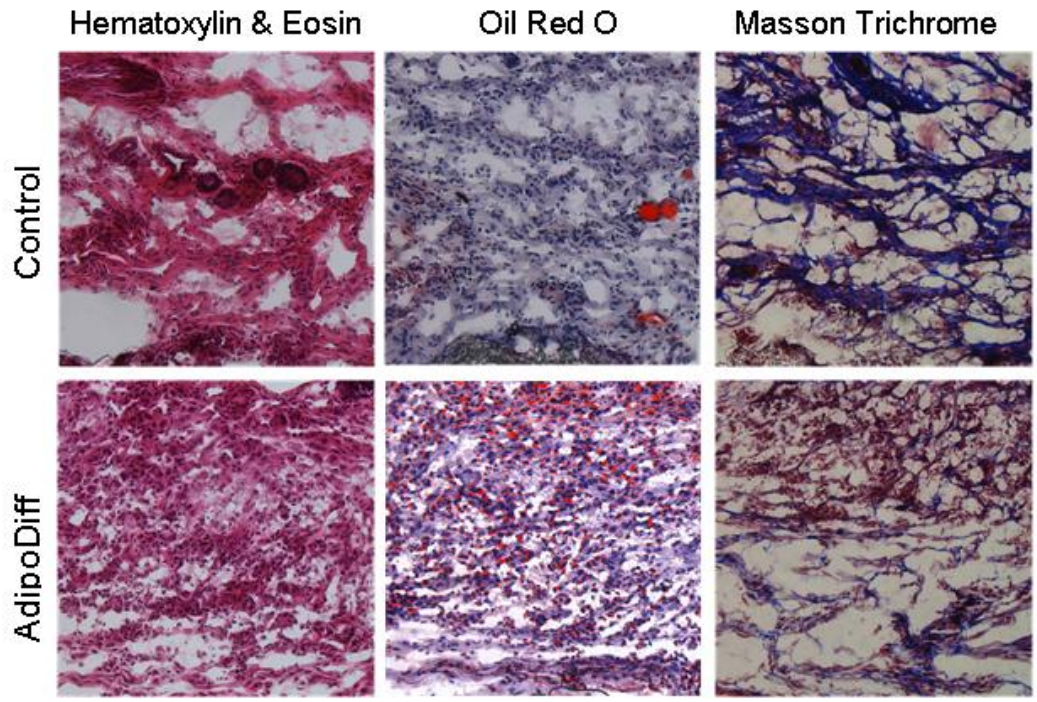

Figure 4.9 Histological analysis of fibrocyte to adipocyte differentiation
The panel presents H&E (left), Oil Red O (Center), and Masson Trichrome (right) staining for control and adipogenic scaffold implants at 2 weeks. Under adipogenic stimulation the tissue response shows a disorganized matrix with increased lipid accumulation dispersed throughout the capsule and reduced collagen formation. The study was performed with n=6 mice. This figure is adapted from reference [110] currently in submission.

Further imaging analysis was conducted with ImageJ to evaluate the overall degree of the tissue responses. Interestingly, the lipid and collagen accumulation show similar trends *in vivo* as previously observed for *in vitro* with fibrocyte-derived adipocytes. The percentage of lipid staining shows as expected an increased response with adipogenic stimulation. In fact, over two weeks of differentiation there is an observed 2.8 fold increase in the lipid production (Figure 4.10). On the other hand the collagen percentage is again shown to mirror the increased formation of lipids with a 2.3 fold reduction during adipogenic stimulation.

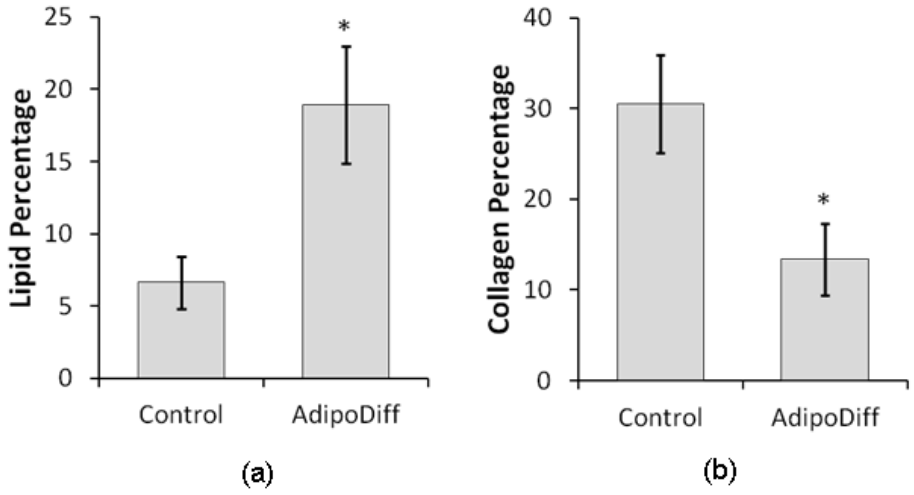

Figure 4.10 Analysis of lipid and collagen accumulation surrounding implants (a) The lipid percentage measured by the degree of Oil Red O shows a 2.8 fold increase after adipogenic stimulation for 2 weeks. (b) The collagen percentage measured by the degree of aniline blue staining shows a 2.3 fold decrease after adipogenic stimulation for 2 weeks. Statistics are performed with the student's t-test and taken to be significant at *P<0.05. The study was performed with n=6 mice. This figure is adapted from reference [110] currently in submission.

4.3.3.3 The Response of Fibrocytes During Adipogenic Stimulation In Vivo.

Our in vitro studies indicate, as supported by previous works, that fibrocytes possess the ability to differentiate to an adipocyte-like lineage with specific stimulation. We further investigate this potential in vivo by assessing both the acute (5 day) and chronic (14 day) response of fibrocytes during adipogenic stimulation (Figure 4.11). Our results suggest that fibrocytes are indeed recruited to the implant during adipogenic stimulation. In the acute response fibrocytes are observed primarily away from the implant toward the hypodermis in both the control and the adipogenic samples. As the response continues, fibrocytes are found throughout the capsule in the control, however only a minimal presence at the biomaterial interface is observed in the adipogenic samples. While fibrocytes remain prevalent in the control over 14 days, as previously demonstrated in the time course response to biomaterial implants, their presence has

been reduced by 4.5 fold from the control during adipogenic differentiation (Figure 4.12). In addition to the reduction of fibrocyte numbers in the capsule we also observe a 51% decrease in the α-SMA staining for myofibroblasts with in the adipogenic samples (Figure 4.13).

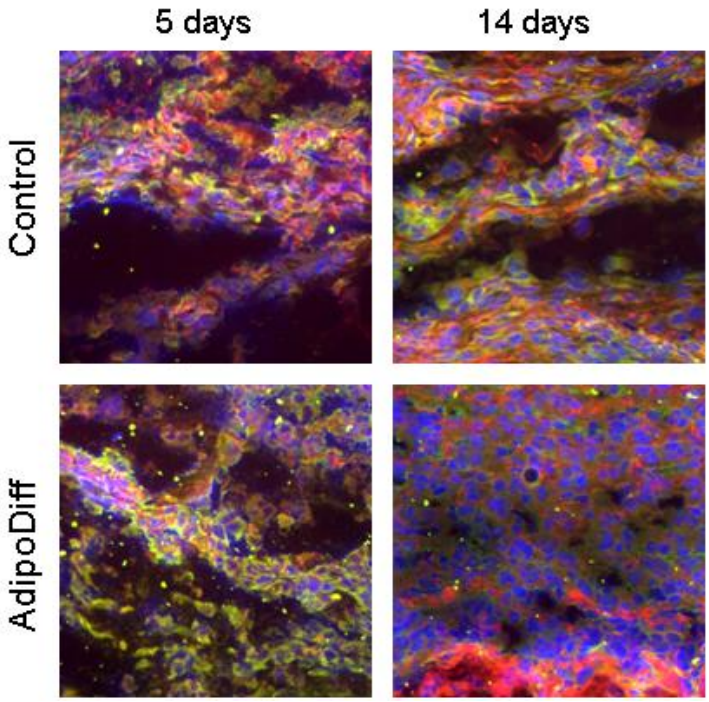

Figure 4.11 Identification of fibrocytes during adipogenic differentiation in vivo. Fibrocytes are identified by the overlay of $CD45^{+}$/ Col^{+} staining (yellow). At the 5 day time point fibrocytes are primarily located toward the hypodermis, away from the implant for both the control and adipogenic samples. By day 14 fibrocytes are found throughout the capsule in the controls however have been significantly reduced and limited to the implant interface during adipogenic differentiation. The study was conducted with n=6 mice. This figure is adapted from reference [110] currently in submission.

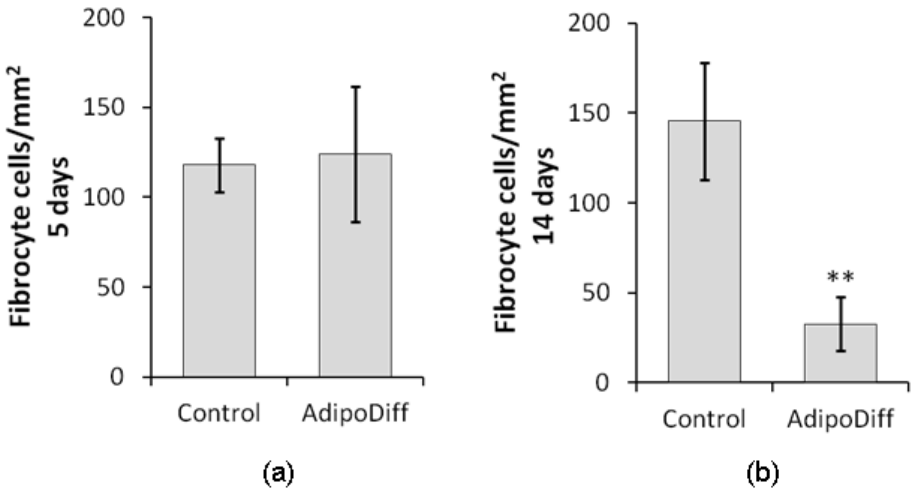

Figure 4.12 Quantification of fibrocytes during adipogenic differentiation
(a) Acute response of fibrocytes shows approximately equal recruitment to both control and adipogenic samples. (b) 2 week response of fibrocytes shows a significant reduction of fibrocyte accumulation in adipogenic samples. Statistics are preformed with the student's test and taken to be significant at **P<0.01. Data are presented as the means and standard deviations from n=6 animals. This figure is adapted from reference [110] currently in submission.

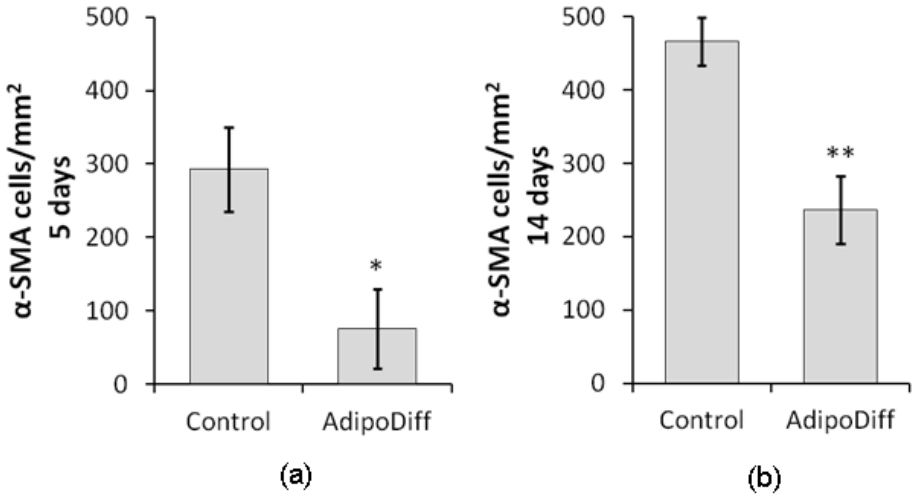

Figure 4.13 Quantification of myofibroblasts during adipogenic differentiation
(a) Acute response of myofibroblasts shows a reduced response to adipogenic samples. (b) 2 week response of myofibroblasts similarly shows a significant reduction of myofibroblast accumulation in adipogenic samples. Statistics are preformed with the student's test and taken to be significant at *P<0.05 or **P<0.01. Data are presented as the means and standard deviations from n=6 animals. This figure is adapted from reference [110] currently in submission.

4.3.4 Discussion

In our current investigation we have confirm that fibrocytes possess progenitor like properties with the capability of differentiation into adipocytes under specific environmental cues. These cells were observed to increase in size and adapt a round morphology as opposed to the spindle shaped fibrocytes in control media. Furthermore, Oil Red O staining verifies the presence of intracellular lipids in fibrocyte-derived adipocytes. These findings are supported by several previous studies discussing the multi-potency of fibrocytes with in vitro differentiation to myofibroblasts, chondrocytes, osteoblasts, and adipocytes [67, 99-100]. Additionally, we observed that with the increase in lipid production by fibrocyte-derived adipocytes, there is a corresponding decrease in collagen production. In support of this observation, a previous study has indicated that

the fibrocyte-to-adipocyte differentiation is driven by PPARγ which was shown to reduce α-SMA expression [67]. Furthermore, stimulation with TGF-β (a known activator of myofibroblasts and collagen production) was shown to inhibit fibrocyte-to-adipocyte differentiation. These interactions present an enhanced potential of fibrocytes where the resulting reduction in collagen with adipocyte differentiation could have a beneficial influence on reducing fibrotic responses and scar tissue formation. Additionally, enhancing the predisposition of fibrocytes to differentiate into myofibroblasts could potentially aid in treatment of certain conditions such as accelerated healing of acute tissue injuries like burns or lung tissue damage resulting from inhalation of toxic agents [235]. The ability of fibrocytes to truly enhance healing through differentiation however remains unproven due to the lack of investigative *in vivo* studies. A previous study did show the formation of human adipose tissue in SCID mice after 4 weeks with the implantation human fibrocyte-derived adipocytes [99]. In this study however fibrocytes were first stimulated in vitro to adipocytes prior to in vivo implantation. Nevertheless the study does indicate that fibrocyte-derived adipocytes can develop adipose tissue *in vivo* [99]. This study however did not investigate the differentiation potential of fibrocytes in vivo.

Our *in vivo* investigations suggest that fibrocytes may indeed be stimulated to differentiate into adipocytes around subcutaneous biomaterial implants. We present several lines of evidence which support this claim, however we cannot currently conclusively demonstrate a fibrocyte-derived adipocyte in vivo. In support of our hypothesis, fibrocytes were first indentified to migrate to the adipogenic samples during the acute inflammatory response. Subsequently while the control fibrocyte numbers increase over two weeks, the adipogenic samples show a significant decrease in fibrocyte numbers. This would be expected with adipocyte differentiation as fibrocytes are

known to decrease expression of hematopoietic markers CD45 and CD34 during differentiation [72-74]. In addition the decrease in fibrocyte numbers is not associated with differentiation to myofibroblasts due to a similar reduction of α-SMA expression in the adipogenic samples. The observed reduction in α-SMA expression is further confirmed by the significant decrease in collagen production around the adipogenic samples. Finally fibrocyte-to-adipocyte differentiation is further supported by the observed increase in lipid accumulation within the capsule, which would result from an increase in the localized adipocyte population.

While these findings all support the in vivo differentiation of fibrocytes to adipocytes we cannot rule out other potential mediators. For instance it is possible that the resultant increase in lipid accumulation is a result of stem cell recruitment and subsequent differentiation to adipocytes rather than fibrocyte-derived adipocytes. To conclusively demonstrate the fibrocyte to adipocyte differentiation in vivo more in-depth studies such as chimeric models or labeled fibrocytes wound need to be conducted. We believe however that our results present the first evidence that the differentiation potential of fibrocytes in vivo is a viable strategy to alter fibrotic tissue responses to biomaterial implants. This technique may have additional enhanced potential for site specific modulation and regeneration of site specific tissue.

Chapter 5

Summary and Conclusion

5.1 Summary

In this dissertation, we have identified that a type of circulating fibroblasts, called fibrocytes, plays an important role in biomaterial-mediated fibrotic tissue reactions. In addition, specific imaging probes were developed to monitor and to assess the influence of macrophage polarization on foreign body reactions. Our studies also revealed the role of mast cells and macrophage responses on fibrotic tissue reactions. The complex interactions of mast cells and polarized macrophages, were found to dictate the migration, accumulation, and activation of fibrocytes. Furthermore two independent strategies were examined for their potential to reduce biomaterial-mediated fibrotic reactions through manipulation of the fibrocyte response.

While fibrocytes have gained widespread acceptance for their involvement in several disease and pathologic states, little attention has been paid to their potential influence on biomaterial-mediated fibrotic responses. We therefore initially investigated the influx and presence of fibrocytes at the biomaterial interface using cultured and NIR labeled fibrocytes. Injected fibrocytes were found to accumulate around the implant within 24 hours and continued to increase with time. More importantly however in an increased time course study we were able to correlate the influx of transmigrated fibrocytes with the amount of collagen production around the implant. The main focus of my dissertation work is therefore to investigate the mechanism(s) governing biomaterial-mediated fibrocyte responses and their effects on foreign body reactions.

Our results show that mast cells play an important role on eliciting fibrocyte responses. Interestingly, we find that the fibrocyte accumulation, myofibroblast differentiation and total collagen production were all significantly reduced by stabilizing

mast cells with Cromolyn. In contrast, the activation of mast cell substantially increases fibrotic reactions . The role of mast cells on fibrotic tissue reactions was confirmed using c-kit deficient mice. Indeed, mast cell deficiency significantly reduced all previously observed fibrocyte responses. Furthermore, simple mast cell reconstitution of c-kit deficient mice was able to fully restore the level of fibrocyte-mediated tissue response. These studies demonstrate that upstream modulation of mast cell responses can reduce the percentage of fibrocytes and fibrocyte-driven fibrotic responses.

Macrophages are likely to be responsible for translating mast cell responses to fibrotic tissue formation. This assumption is supported by several lines of observations. First, the depletion of macrophages would blunt fibrotic tissue reactions to the implant. Second, increasing evidence supports that macrophage polarization prompts distinct tissue reactions. Third, using localized release of various inflammatory cytokine antagonists, we find that the reduction of TGF-β would substantially reduce fibrotic tissue reactions to biomaterial implants. We further determined that TGF-β (one of the macrophage products), is potent on influencing fibrocyte responses and fibrotic tissue production. Finally, via newly fabricated imaging probes, we are able to real time monitor the recruitment and activity of M1 and M2 macrophages on promoting inflammatory responses and tissue regeneration, respectively.

Based on the results of this work, we have now determined that the following sequence of cellular events occurs during foreign body reactions.

1. Biomaterial implant prompts the activation of mast cells to release pro-inflammatory cytokines.

2. Localized release of cytokines trigger the recruitment of inflammatory cells, including neutrophils and macrophages. Activated macrophages lean towards an M1 phenotype.

3. Activated neutrophils and M1 macrophages release many inflammatory products and enzymes to destroy surrounding tissue which are followed by fibrocyte recruitment.

4. Immigrated fibrocytes proliferate at the implant site in an inflammatory setting and are further stimulated to differentiate into myofibroblasts producing collagenous tissues.

5. With the change of microenvironment, an increasing percentage of macrophages possesses the M2 phenotype. The release products of M2 macrophages then slow down fibrotic tissue production to form permanent fibrotic capsules.

Substantial efforts have also been placed during my thesis study for developing novel strategy to alter implant-associated fibrotic tissue reactions. First, we tested the possibility of using micropillar surface morphology to passively modify fibrocyte activation. From our initial *in vitro* investigations we found that the increase of pillar height (but not pillar spacing) enhance fibroblast proliferation while the decrease of pillar spacing (but not pillar height) reduce macrophage accumulation. Due to these extreme cellular responses *in vitro* we hypothesized that pillar implants would initiate differential tissue responses *in vivo*. Very interestingly fibrocytes were found to be more responsive to topographical changes, specifically spacing and height, than fibroblasts or macrophages. In comparison with control, micropillar substrates with high pillar height and large pillar spacing prompt the strongest fibrotic tissue reactions reflected by collagen production, cell accumulation and angiogenesis. Furthermore the cellular responses were found to correlate with the histological outcomes of fibrosis including granulation tissue formation and collagen production. These results indicate that fibrocytes are highly responsive to topographical changes. By manipulating extent the parameters of pillar spacing to pillar height it may be possible that a limited or beneficial tissue responses could be generated.

Lastly, it has recently been shown that fibrocytes possess a multi-potency for several lineages including adipocytes, osteoblasts and chrondocytes *in* vitro. It is unclear however whether fibrocyte differentiation is a viable strategy to reduce collagen production and scar tissue formation in vivo. Through the use of mini-osmotic pumps, we show that the fibrotic matrix may be stimulated to produce small pockets of adipose-like tissue by Oil-Red-O staining. In this same tissue the number of fibrocytes is significantly diminished suggesting, although not conclusive, that fibrocytes may be stimulated to become adipocyte-like in vivo increasing lipid production.

5.2 Future Perspectives

In this dissertation we have begun to investigate the role of this dynamic cell (the fibrocyte) in response to biomaterial implants and foreign body reactions. While we have established the role and identified several important cellular interactions this remains only a first step toward fully understanding fibrocyte-mediate interactions. Continued analysis of several strategies presented in this work as well as the addition of clinically relevant models will be critical for connecting, modulating, and understanding the inflammatory and fibrotic interactions of fibrocytes.

Firstly, further development of the imaging probe would substantiate the role macrophage polarization as an indicator or predictor of chronic inflammatory or fibrotic outcomes to biomaterial implants. For this to be successful the probes need further investigation with clinically relevant models with well characterized M1 M2 responses. This could be performed in bacterial infection models such as tuberculosis, substantiating an M1 response, or parasitic infections such as schistosomiasis and other worm infections such as helminthic parasites, substantiating and M2 response [236-238].

We have further uncovered that fibrocytes may be driven to differentiate around a biomaterial implant. This technique has great potential for site specific modulation and regeneration of site specific tissue. For example by stimulating fibrocytes into adipocytes it may be possible to reduce fibrosis around breast implants or further reduce adherence of tissue after surgery as in intra-abdominal adhesions. Through possible chondrocyte or osteoblast differentiation it may be possible to enhance articular cartilage repair or bone resorption, especially in cases were inflammation is common such as the space between the prosthetic acetabular cup and neck of the femur in total hip replacement [239-240].

Lastly, micro- and nano- topography have a high potential to alter cellular and protein interactions at the material interface. Despite many exciting findings, several gaps remain in our understanding of the influence of surface topography on cellular responses. Collagen alignment with micropillar topography is an area with the potential for significant impact on the design of medical implants with improved safety and/or tissue reactivity. For example, many load-bearing soft tissues are subject to a high degree of mechanical anisotropy, including heart valves, blood vessels, tendons, skin, cartilage, myocardium and pericardium [241-242]. It is believed that the basis for the anisotropy is the collagen fiber structure. While there are several models that exist to study the nature of the collagen formation and alignment, the development of a substrate to direct cell function and matrix production in a physiologically equivalent manner remains a difficult challenge. Micropillars and the dictation of a controlled fibrocyte response may offer an alternative approach in the design of anisotropic collagen fibril formation with concise design parameters to control the cells, matrix production, and alignment.

References

1. Bucala R, Spiegel LA, Chesney J, Hogan M, Cerami A. Circulating fibrocytes define a new leukocyte subpopulation that mediates tissue repair. Mol Med. 1994;1(1):71-81.
2. Anderson JM, Rodriguez A, Chang DT. Foreign body reaction to biomaterials. Semin Immunol. 2008;20(2):86-100.
3. Tang L, Eaton JW. Natural responses to unnatural materials: A molecular mechanism for foreign body reactions. Mol Med. 1999;5(6):351-358.
4. Franz S, Rammelt S, Scharnweber D, Simon JC. Immune responses to implants - a review of the implications for the design of immunomodulatory biomaterials. Biomaterials. 2011;32(28):6692-6709.
5. Tang L, Eaton JW. Inflammatory responses to biomaterials. Am J Clin Pathol. 1995;103(4):466-471.
6. Tang L, Ugarova TP, Plow EF, Eaton JW. Molecular determinants of acute inflammatory responses to biomaterials. J Clin Invest. 1996;97(5):1329-1334.
7. Schmid-Schonbein GW. Analysis of inflammation. Annu Rev Biomed Eng. 2006;8:93-131.
8. Soder BL, Propst JT, Brooks TM, Goodwin RL, Friedman HI, Yost MJ, et al. The connexin43 carboxyl-terminal peptide ACT1 modulates the biological response to silicone implants. Plast Reconstr Surg. 2009;123(5):1440-1451.
9. Tang L, Hu W. Molecular determinants of biocompatibility. Expert Rev Med Devices. 2005;2(4):493-500.
10. Chang DT, Jones JA, Meyerson H, Colton E, Kwon IK, Matsuda T, et al. Lymphocyte/macrophage interactions: biomaterial surface-dependent cytokine, chemokine, and matrix protein production. J Biomed Mater Res A. 2008;87(3):676-687.
11. Luttikhuizen DT, Dankers PY, Harmsen MC, van Luyn MJ. Material dependent differences in inflammatory gene expression by giant cells during the foreign body reaction. J Biomed Mater Res A. 2007;83(3):879-886.
12. Mendes JB, Campos PP, Ferreira MA, Bakhle YS, Andrade SP. Host response to sponge implants differs between subcutaneous and intraperitoneal sites in mice. J Biomed Mater Res B Appl Biomater. 2007;83(2):408-415.
13. Patil SD, Papadimitrakopoulos F, Burgess DJ. Dexamethasone-loaded poly(lactic-co-glycolic) acid microspheres/poly(vinyl alcohol) hydrogel composite coatings for inflammation control. Diabetes Technol Ther. 2004;6(6):887-897.
14. Patil SD, Papadmitrakopoulos F, Burgess DJ. Concurrent delivery of dexamethasone and VEGF for localized inflammation control and angiogenesis. J Control Release. 2007;117(1):68-79.
15. Butler KR, Jr., Benghuzzi HA. Immunohistochemical detection of cytokine expression in tissue-implant response associated with TCP bioceramic implants loaded with steroid hormones. Biomed Sci Instrum. 2003;39:541-546.
16. Butler KR, Jr., Benghuzzi HA. Morphometric analysis of the hormonal effect on tissue-implant response associated with TCP bioceramic implants. Biomed Sci Instrum. 2003;39:535-540.
17. Hickey T, Kreutzer D, Burgess DJ, Moussy F. In vivo evaluation of a dexamethasone/PLGA microsphere system designed to suppress the inflammatory tissue response to implantable medical devices. J Biomed Mater Res. 2002;61(2):180-187.

18. Trivedi A, Olivas AD, Noble-Haeusslein LJ. Inflammation and Spinal Cord Injury: Infiltrating Leukocytes as Determinants of Injury and Repair Processes. Clin Neurosci Res. 2006;6(5):283-292.
19. Braiman-Wiksman L, Solomonik I, Spira R, Tennenbaum T. Novel insights into wound healing sequence of events. Toxicol Pathol. 2007;35(6):767-779.
20. Lumelsky NL. Commentary: engineering of tissue healing and regeneration. Tissue Eng. 2007;13(7):1393-1398.
21. Oberyszyn TM. Inflammation and wound healing. Front Biosci. 2007;12:2993-2999.
22. Broughton G, 2nd, Janis JE, Attinger CE. The basic science of wound healing. Plast Reconstr Surg. 2006;117(7 Suppl):12S-34S.
23. Henry G, Garner WL. Inflammatory mediators in wound healing. Surg Clin North Am. 2003;83(3):483-507.
24. Tuan RS, Lee FY, Y TK, Wilkinson JM, Smith RL. What are the local and systemic biologic reactions and mediators to wear debris, and what host factors determine or modulate the biologic response to wear particles? J Am Acad Orthop Surg. 2008;16 Suppl 1:S42-48.
25. Jones JA, Chang DT, Meyerson H, Colton E, Kwon IK, Matsuda T, et al. Proteomic analysis and quantification of cytokines and chemokines from biomaterial surface-adherent macrophages and foreign body giant cells. J Biomed Mater Res A. 2007;83(3):585-596.
26. Kou PM, Babensee JE. Macrophage and dendritic cell phenotypic diversity in the context of biomaterials. J Biomed Mater Res A. 2010.
27. Thomsen P, Gretzer C. Macrophage interactions with modified material surfaces. Curr Opin Solid St M. 2001;5(2-3):163-176.
28. Kim J, Dadsetan M, Ameenuddin S, Windebank AJ, Yaszemski MJ, Lu L. In vivo biodegradation and biocompatibility of PEG/sebacic acid-based hydrogels using a cage implant system. J Biomed Mater Res A. 2010;95(1):191-197.
29. VandeVord PJ, Matthew HW, DeSilva SP, Mayton L, Wu B, Wooley PH. Evaluation of the biocompatibility of a chitosan scaffold in mice. J Biomed Mater Res. 2002;59(3):585-590.
30. Brown BN, Londono R, Tottey S, Zhang L, Kukla KA, Wolf MT, et al. Macrophage phenotype as a predictor of constructive remodeling following the implantation of biologically derived surgical mesh materials. Acta Biomater. 2012;8(3):978-987.
31. Stout RD, Suttles J. Functional plasticity of macrophages: reversible adaptation to changing microenvironments. J Leukoc Biol. 2004;76(3):509-513.
32. Martinez FO, Sica A, Mantovani A, Locati M. Macrophage activation and polarization. Front Biosci. 2008;13:453-461.
33. Darby IA, Hewitson TD. Fibroblast differentiation in wound healing and fibrosis. Int Rev Cytol. 2007;257:143-179.
34. Chan A, Filer A, Parsonage G, Kollnberger S, Gundle R, Buckley CD, et al. Mediation of the proinflammatory cytokine response in rheumatoid arthritis and spondylarthritis by interactions between fibroblast-like synoviocytes and natural killer cells. Arthritis Rheum. 2008;58(3):707-717.
35. Reilkoff RA, Bucala R, Herzog EL. Fibrocytes: emerging effector cells in chronic inflammation. Nat Rev Immunol. 2011;11(6):427-435.
36. Ward WK. A Review of the Foreign-body Response to Subcutaneously-implanted Devices: The Role of Macrophages and Cytokines in Biofouling and Fibrosis. Journal of Diabetes Science and Technology. 2008;2(5):768-777.

37. Tomasek JJ, Gabbiani G, Hinz B, Chaponnier C, Brown RA. Myofibroblasts and mechano-regulation of connective tissue remodelling. Nat Rev Mol Cell Biol. 2002;3(5):349-363.
38. Phan SH. Biology of fibroblasts and myofibroblasts. Proc Am Thorac Soc. 2008;5(3):334-337.
39. Mori L, Bellini A, Stacey MA, Schmidt M, Mattoli S. Fibrocytes contribute to the myofibroblast population in wounded skin and originate from the bone marrow. Exp Cell Res. 2005;304(1):81-90.
40. McAnulty RJ. Fibroblasts and myofibroblasts: their source, function and role in disease. Int J Biochem Cell Biol. 2007;39(4):666-671.
41. El-Asrar AMA, Struyf S, Van Damme J, Geboes K. Circulating fibrocytes contribute to the myofibroblast population in proliferative vitreoretinopathy epiretinal membranes. British Journal of Ophthalmology. 2008;92(5):699-704.
42. Schmidt M, Sun G, Stacey MA, Mori L, Mattoli S. Identification of circulating fibrocytes as precursors of bronchial myofibroblasts in asthma. J Immunol. 2003;171(1):380-389.
43. Tang L, Lucas AH, Eaton JW. Inflammatory responses to implanted polymeric biomaterials: role of surface-adsorbed immunoglobulin G. J Lab Clin Med. 1993;122(3):292-300.
44. Nair A, Thevenot P, Dey J, Shen J, Sun MW, Yang J, et al. Novel polymeric scaffolds using protein microbubbles as porogen and growth factor carriers. Tissue Eng Part C Methods. 2010;16(1):23-32.
45. Kamath S, Bhattacharyya D, Padukudru C, Timmons RB, Tang L. Surface chemistry influences implant-mediated host tissue responses. J Biomed Mater Res A. 2008;86(3):617-626.
46. Wang C, Yu B, Knudsen B, Harmon J, Moussy F, Moussy Y. Synthesis and performance of novel hydrogels coatings for implantable glucose sensors. Biomacromolecules. 2008;9(2):561-567.
47. Yu B, Ju Y, West L, Moussy Y, Moussy F. An investigation of long-term performance of minimally invasive glucose biosensors. Diabetes Technol Ther. 2007;9(3):265-275.
48. Giurgiutiu V, Friedman H, Bender J, Borg T, Yost M, Newcomb W, et al. Electromechanical impedance sensor for in vivo monitoring the body reaction to implants. J Invest Surg. 2004;17(5):257-270.
49. Fournier E, Passirani C, Montero-Menei CN, Benoit JP. Biocompatibility of implantable synthetic polymeric drug carriers: focus on brain biocompatibility. Biomaterials. 2003;24(19):3311-3331.
50. Benghuzzi H, England B. Biocompatibility of steroid-HA delivery system using adult castrated rams as a model. Biomed Sci Instrum. 2001;37:275-280.
51. Haq I, Cruz-Almeida Y, Siqueira EB, Norenberg M, Green BA, Levi AD. Postoperative fibrosis after surgical treatment of the porcine spinal cord: a comparison of dural substitutes. Invited submission from the Joint Section Meeting on Disorders of the Spine and Peripheral Nerves, March 2004. J Neurosurg Spine. 2005;2(1):50-54.
52. Sargeant A, Goswami T. Pathophysiological aspects of hip implants. J Surg Orthop Adv. 2006;15(2):111-112.
53. Carro LP, Suarez GG. Intercondylar notch fibrous nodule after total knee replacement. Arthroscopy. 1999;15(1):103-105.
54. Adams WP, Jr., Haydon MS, Raniere J, Jr., Trott S, Marques M, Feliciano M, et al. A rabbit model for capsular contracture: development and clinical implications. Plast Reconstr Surg. 2006;117(4):1214-1219; discussion 1220-1211.

55. Poeppl N, Schreml S, Lichtenegger F, Lenich A, Eisenmann-Klein M, Prantl L. Does the surface structure of implants have an impact on the formation of a capsular contracture? Aesthetic Plast Surg. 2007;31(2):133-139.
56. Prantl L, Schreml S, Fichtner-Feigl S, Poppl N, Eisenmann-Klein M, Schwarze H, et al. Clinical and morphological conditions in capsular contracture formed around silicone breast implants. Plast Reconstr Surg. 2007;120(1):275-284.
57. Heatley CJ, Spalton DJ, Kumar A, Jose R, Boyce J, Bender LE. Comparison of posterior capsule opacification rates between hydrophilic and hydrophobic single-piece acrylic intraocular lenses. J Cataract Refract Surg. 2005;31(4):718-724.
58. Shirai K, Saika S, Okada Y, Oda S, Ohnishi Y. Histology and immunohistochemistry of fibrous posterior capsule opacification in an infant. J Cataract Refract Surg. 2004;30(2):523-526.
59. Seymour JP, Kipke DR. Neural probe design for reduced tissue encapsulation in CNS. Biomaterials. 2007;28(25):3594-3607.
60. Polikov VS, Tresco PA, Reichert WM. Response of brain tissue to chronically implanted neural electrodes. J Neurosci Methods. 2005;148(1):1-18.
61. Wisniewski N, Klitzman B, Miller B, Reichert WM. Decreased analyte transport through implanted membranes: differentiation of biofouling from tissue effects. J Biomed Mater Res. 2001;57(4):513-521.
62. Bellini A, Mattoli S. The role of the fibrocyte, a bone marrow-derived mesenchymal progenitor, in reactive and reparative fibroses. Lab Invest. 2007;87(9):858-870.
63. Chesney J, Metz C, Stavitsky AB, Bacher M, Bucala R. Regulated production of type I collagen and inflammatory cytokines by peripheral blood fibrocytes. J Immunol. 1998;160(1):419-425.
64. Balmelli C, Ruggli N, McCullough K, Summerfield A. Fibrocytes are potent stimulators of anti-virus cytotoxic T cells. J Leukoc Biol. 2005;77(6):923-933.
65. Chesney J, Bacher M, Bender A, Bucala R. The peripheral blood fibrocyte is a potent antigen-presenting cell capable of priming naive T cells in situ. Proc Natl Acad Sci U S A. 1997;94(12):6307-6312.
66. Quan TE, Cowper SE, Bucala R. The role of circulating fibrocytes in fibrosis. Curr Rheumatol Rep. 2006;8(2):145-150.
67. Hong KM, Belperio JA, Keane MP, Burdick MD, Strieter RM. Differentiation of human circulating fibrocytes as mediated by transforming growth factor-beta and peroxisome proliferator-activated receptor gamma. J Biol Chem. 2007;282(31):22910-22920.
68. Hong KM, Burdick MD, Phillips RJ, Heber D, Strieter RM. Characterization of human fibrocytes as circulating adipocyte progenitors and the formation of human adipose tissue in SCID mice. Faseb Journal. 2005;19(11):2029-+.
69. Choi YH, Burdick MD, Strieter RM. Human circulating fibrocytes have the capacity to differentiate osteoblasts and chondrocytes. Int J Biochem Cell B. 2010;42(5):662-671.
70. Metz CN. Fibrocytes: a unique cell population implicated in wound healing. Cell Mol Life Sci. 2003;60(7):1342-1350.
71. Herzog EL, Bucala R. Fibrocytes in health and disease. Exp Hematol. 2010;38(7):548-556.
72. Moore BB, Kolodsick JE, Thannickal VJ, Cooke K, Moore TA, Hogaboam C, et al. CCR2-mediated recruitment of fibrocytes to the alveolar space after fibrotic injury. Am J Pathol. 2005;166(3):675-684.

73. Quan TE, Cowper S, Wu SP, Bockenstedt LK, Bucala R. Circulating fibrocytes: collagen-secreting cells of the peripheral blood. Int J Biochem Cell Biol. 2004;36(4):598-606.
74. Phillips RJ, Burdick MD, Hong K, Lutz MA, Murray LA, Xue YY, et al. Circulating fibrocytes traffic to the lungs in response to CXCL12 and mediate fibrosis. J Clin Invest. 2004;114(3):438-446.
75. Abe R, Donnelly SC, Peng T, Bucala R, Metz CN. Peripheral blood fibrocytes: differentiation pathway and migration to wound sites. J Immunol. 2001;166(12):7556-7562.
76. Crawford JR, Pilling D, Gomer RH. Improved serum-free culture conditions for spleen-derived murine fibrocytes. J Immunol Methods. 2010;363(1):9-20.
77. Niedermeier M, Reich B, Rodriguez Gomez M, Denzel A, Schmidbauer K, Gobel N, et al. CD4+ T cells control the differentiation of Gr1+ monocytes into fibrocytes. Proc Natl Acad Sci U S A. 2009;106(42):17892-17897.
78. Wang CH, Huang CD, Lin HC, Lee KY, Lin SM, Liu CY, et al. Increased circulating fibrocytes in asthma with chronic airflow obstruction. Am J Respir Crit Care Med. 2008;178(6):583-591.
79. Mehrad B, Burdick MD, Strieter RM. Fibrocyte CXCR4 regulation as a therapeutic target in pulmonary fibrosis. Int J Biochem Cell Biol. 2009;41(8-9):1708-1718.
80. Moeller A, Gilpin SE, Ask K, Cox G, Cook D, Gauldie J, et al. Circulating fibrocytes are an indicator of poor prognosis in idiopathic pulmonary fibrosis. Am J Respir Crit Care Med. 2009;179(7):588-594.
81. Ishida Y, Kimura A, Kondo T, Hayashi T, Ueno M, Takakura N, et al. Essential roles of the CC chemokine ligand 3-CC chemokine receptor 5 axis in bleomycin-induced pulmonary fibrosis through regulation of macrophage and fibrocyte infiltration. Am J Pathol. 2007;170(3):843-854.
82. Moore BB, Murray L, Das A, Wilke CA, Herrygers AB, Toews GB. The role of CCL12 in the recruitment of fibrocytes and lung fibrosis. Am J Respir Cell Mol Biol. 2006;35(2):175-181.
83. Andersson-Sjoland A, de Alba CG, Nihlberg K, Becerril C, Ramirez R, Pardo A, et al. Fibrocytes are a potential source of lung fibroblasts in idiopathic pulmonary fibrosis. Int J Biochem Cell Biol. 2008;40(10):2129-2140.
84. Vakil V, Sung JJ, Piecychna M, Crawford JR, Kuo P, Abu-Alfa AK, et al. Gadolinium-containing magnetic resonance image contrast agent promotes fibrocyte differentiation. J Magn Reson Imaging. 2009;30(6):1284-1288.
85. Sakai N, Wada T, Yokoyama H, Lipp M, Ueha S, Matsushima K, et al. Secondary lymphoid tissue chemokine (SLC/CCL21)/CCR7 signaling regulates fibrocytes in renal fibrosis. Proc Natl Acad Sci U S A. 2006;103(38):14098-14103.
86. Wada T, Sakai N, Matsushima K, Kaneko S. Fibrocytes: a new insight into kidney fibrosis. Kidney Int. 2007;72(3):269-273.
87. Scholten D, Reichart D, Paik YH, Lindert J, Bhattacharya J, Glass CK, et al. Migration of fibrocytes in fibrogenic liver injury. Am J Pathol. 2011;179(1):189-198.
88. Medbury HJ, Tarran SL, Guiffre AK, Williams MM, Lam TH, Vicaretti M, et al. Monocytes contribute to the atherosclerotic cap by transformation into fibrocytes. Int Angiol. 2008;27(2):114-123.
89. Mathai SK, Gulati M, Peng X, Russell TR, Shaw AC, Rubinowitz AN, et al. Circulating monocytes from systemic sclerosis patients with interstitial lung disease show an enhanced profibrotic phenotype. Lab Invest. 2010;90(6):812-823.
90. Yang L, Scott PG, Giuffre J, Shankowsky HA, Ghahary A, Tredget EE. Peripheral blood fibrocytes from burn patients: identification and quantification of fibrocytes in

adherent cells cultured from peripheral blood mononuclear cells. Lab Invest. 2002;82(9):1183-1192.
91. Zdolsek J, Eaton JW, Tang L. Histamine release and fibrinogen adsorption mediate acute inflammatory responses to biomaterial implants in humans. J Transl Med. 2007;5:31.
92. Tang L, Jennings TA, Eaton JW. Mast cells mediate acute inflammatory responses to implanted biomaterials. Proc Natl Acad Sci U S A. 1998;95(15):8841-8846.
93. Tcacencu I, Wendel M. Collagen-hydroxyapatite composite enhances regeneration of calvaria bone defects in young rats but postpones the regeneration of calvaria bone in aged rats. Journal of Materials Science: Materials in Medicine. 2008;19(5):2015-2021.
94. Mosser DM, Edwards JP. Exploring the full spectrum of macrophage activation. Nat Rev Immunol. 2008;8(12):958-969.
95. Kodelja V, Muller C, Tenorio S, Schebesch C, Orfanos CE, Goerdt S. Differences in angiogenic potential of classically vs alternatively activated macrophages. Immunobiology. 1997;197(5):478-493.
96. Gordon S, Martinez FO. Alternative activation of macrophages: mechanism and functions. Immunity. 2010;32(5):593-604.
97. Gordon S. Alternative activation of macrophages. Nat Rev Immunol. 2003;3(1):23-35.
98. Baker DW, Liu X, Weng H, Luo C, Tang L. Fibroblast/fibrocyte: surface interaction dictates tissue reactions to micropillar implants. Biomacromolecules. 2011;12(4):997-1005.
99. Hong KM, Burdick MD, Phillips RJ, Heber D, Strieter RM. Characterization of human fibrocytes as circulating adipocyte progenitors and the formation of human adipose tissue in SCID mice. FASEB J. 2005;19(14):2029-2031.
100. Choi YH, Burdick MD, Strieter RM. Human circulating fibrocytes have the capacity to differentiate osteoblasts and chondrocytes. Int J Biochem Cell Biol. 2010;42(5):662-671.
101. Kisseleva T, von Kockritz-Blickwede M, Reichart D, McGillvray SM, Wingender G, Kronenberg M, et al. Fibrocyte-like cells recruited to the spleen support innate and adaptive immune responses to acute injury or infection. J Mol Med (Berl). 2011;89(10):997-1013.
102. Nair A, Shen J, Lotfi P, Ko CY, Zhang CC, Tang L. Biomaterial implants mediate autologous stem cell recruitment in mice. Acta Biomater. 2011;7(11):3887-3895.
103. Thevenot PT, Nair AM, Shen J, Lotfi P, Ko CY, Tang L. The effect of incorporation of SDF-1alpha into PLGA scaffolds on stem cell recruitment and the inflammatory response. Biomaterials. 2010;31(14):3997-4008.
104. Zhou J, Tsai YT, Weng H, Baker DW, Tang L. Real time monitoring of biomaterial-mediated inflammatory responses via macrophage-targeting NIR nanoprobes. Biomaterials. 2011;32(35):9383-9390.
105. Thevenot PT, Baker DW, Weng H, Sun MW, Tang L. The pivotal role of fibrocytes and mast cells in mediating fibrotic reactions to biomaterials. Biomaterials. 2011;32(33):8394-8403.
106. Thevenot P, Nair A, Dey J, Yang J, Tang L. Method to analyze three-dimensional cell distribution and infiltration in degradable scaffolds. Tissue Eng Part C Methods. 2008;14(4):319-331.
107. Zhou JT, Y. Weng, H. Tang, L. Noninvasive assessment of localized inflammatory responses. Free Radical Biology and Medicine. 2011.

108. Chesney J, Bucala R. Peripheral blood fibrocytes: mesenchymal precursor cells and the pathogenesis of fibrosis. Curr Rheumatol Rep. 2000;2(6):501-505.
109. Chesney J, Bucala R. Peripheral blood fibrocytes: novel fibroblast-like cells that present antigen and mediate tissue repair. Biochem Soc Trans. 1997;25(2):520-524.
110. Baker D, Tsai, YT., Weng, H., Shen, J., Tang, L. Fibrocytes respond to the macrophage population and may be differentiated to adipocytes to reduce collagen formation. 2013.
111. Keeley EC, Mehrad B, Strieter RM. Fibrocytes: bringing new insights into mechanisms of inflammation and fibrosis. Int J Biochem Cell Biol. 2010;42(4):535-542.
112. Frossi B, Gri G, Tripodo C, Pucillo C. Exploring a regulatory role for mast cells: 'MCregs'? Trends Immunol. 2010;31(3):97-102.
113. Theoharides TC, Kempuraj D, Tagen M, Conti P, Kalogeromitros D. Differential release of mast cell mediators and the pathogenesis of inflammation. Immunol Rev. 2007;217:65-78.
114. Ren SR, Xu LB, Wu ZY, Du J, Gao MH, Qu CF. Exogenous dendritic cell homing to draining lymph nodes can be boosted by mast cell degranulation. Cell Immunol. 2010;263(2):204-211.
115. Pietrzak A, Misiak-Tloczek A, Brzezinska-Blaszczyk E. Interleukin (IL)-10 inhibits RANTES-, tumour necrosis factor (TNF)- and nerve growth factor (NGF)-induced mast cell migratory response but is not a mast cell chemoattractant. Immunol Lett. 2009;123(1):46-51.
116. Brightling CE, Bradding P, Pavord ID, Wardlaw AJ. New insights into the role of the mast cell in asthma. Clin Exp Allergy. 2003;33(5):550-556.
117. Brightling CE, Symon FA, Holgate ST, Wardlaw AJ, Pavord ID, Bradding P. Interleukin-4 and -13 expression is co-localized to mast cells within the airway smooth muscle in asthma. Clin Exp Allergy. 2003;33(12):1711-1716.
118. Orenstein SB, Saberski ER, Klueh U, Kreutzer DL, Novitsky YW. Effects of mast cell modulation on early host response to implanted synthetic meshes. Hernia. 2010;14(5):511-516.
119. Dumont N, Lepage K, Cote CH, Frenette J. Mast cells can modulate leukocyte accumulation and skeletal muscle function following hindlimb unloading. J Appl Physiol. 2007;103(1):97-104.
120. Bytautiene E, Vedernikov YP, Saade GR, Romero R, Garfield RE. The effect of a mast cell degranulating agent on vascular resistance in the human placental vascular bed and on the tone of isolated placental vessels. Reprod Sci. 2008;15(1):26-32.
121. Thevenot PT, Nair AM, Shen J, Lotfi P, Ko C-Y, Tang L. The effect of incorporation of SDF-1[alpha] into PLGA scaffolds on stem cell recruitment and the inflammatory response. Biomaterials.In Press, Corrected Proof.
122. Mori L, Bellini A, Stacey MA, Schmidt M, Mattoli S. Fibrocytes contribute to the myofibroblast population in wounded skin and originate from the bone marrow. Experimental Cell Research. 2005;304(1):81-90.
123. Strieter RM, Keeley EC, Hughes MA, Burdick MD, Mehrad B. The role of circulating mesenchymal progenitor cells (fibrocytes) in the pathogenesis of pulmonary fibrosis. J Leukoc Biol. 2009;86(5):1111-1118.
124. Phillips RJ, Burdick MD, Hong K, Lutz MA, Murray LA, Xue YY, et al. Circulating fibrocytes traffic to the lungs in response to CXCL12 and mediate fibrosis. The Journal of Clinical Investigation. 2004;114(3):438-446.
125. Masuda T, Tanaka H, Komai M, Nagao K, Ishizaki M, Kajiwara D, et al. Mast cells play a partial role in allergen-induced subepithelial fibrosis in a murine model of allergic asthma. Clinical & Experimental Allergy. 2003;33(5):705-713.

126. Mori H, Kawada K, Zhang P, Uesugi Y, Sakamoto O, Koda A. Bleomycin-induced pulmonary fibrosis in genetically mast cell-deficient WBB6F1-W/Wv mice and mechanism of the suppressive effect of tranilast, an antiallergic drug inhibiting mediator release from mast cells, on fibrosis. Int Arch Allergy Appl Immunol. 1991;95(2-3):195-201.
127. Ayako S, Tohru T, Yukihisa F, Yasuo N, Nobuyuki T. Evaluation of role of mast cells in the development of liver fibrosis using mast cell-deficient rats and mice. Journal of hepatology. 1999;30(5):859-867.
128. Fairweather D, Frisancho-Kiss S, Yusung SA, Barrett MA, Davis SE, Gatewood SJL, et al. Interferon-{gamma} protects against chronic viral myocarditis by reducing mast cell degranulation, fibrosis, and the profibrotic cytokines transforming frowth vactor-{beta}1, interleukin-1{beta}, and interleukin-4 in the heart. Am J Pathol. 2004;165(6):1883-1894.
129. Quan TE, Cowper S, Wu S-P, Bockenstedt LK, Bucala R. Circulating fibrocytes: collagen-secreting cells of the peripheral blood. The International Journal of Biochemistry & Cell Biology. 2004;36(4):598-606.
130. Moore BB, Kolodsick JE, Thannickal VJ, Cooke K, Moore TA, Hogaboam C, et al. CCR2-mediated recruitment of fibrocytes to the alveolar space after fibrotic injury. Am J Pathol. 2005;166(3):675-684.
131. Lama VN, Phan SH. The extrapulmonary origin of fibroblasts: Stem/progenitor cells and beyond. Proc Am Thorac Soc. 2006;3(4):373-376.
132. Sakai N, Wada T, Yokoyama H, Lipp M, Ueha S, Matsushima K, et al. Secondary lymphoid tissue chemokine (SLC/CCL21)/CCR7 signaling regulates fibrocytes in renal fibrosis. Proceedings of the National Academy of Sciences. 2006;103(38):14098-14103.
133. Dy M, Schneider E. Histamine-cytokine connection in immunity and hematopoiesis. Cytokine Growth Factor Rev. 2004;15(5):393-410.
134. Godot V, Arock M, Garcia G, Capel F, Flys C, Dy M, et al. H4 histamine receptor mediates optimal migration of mast cell precursors to CXCL12. J Allergy Clin Immunol. 2007;120(4):827-834.
135. Bakhshayesh M, Soleimani M, Mehdizadeh M, Katebi M. Effects of TGF-beta and b-FGF on the potential of peripheral blood-borne stem cells and bone marrow-derived stem cells in wound healing in a murine model. Inflammation. 2012;35(1):138-142.
136. Seppa H, Grotendorst G, Seppa S, Schiffmann E, Martin GR. Platelet-Derived Growth-Factor Is Chemotactic for Fibroblasts. Journal of Cell Biology. 1982;92(2):584-588.
137. Brown BN, Ratner BD, Goodman SB, Amar S, Badylak SF. Macrophage polarization: an opportunity for improved outcomes in biomaterials and regenerative medicine. Biomaterials. 2012;33(15):3792-3802.
138. Sinha P, Clements VK, Ostrand-Rosenberg S. Reduction of myeloid-derived suppressor cells and induction of M1 macrophages facilitate the rejection of established metastatic disease. J Immunol. 2005;174(2):636-645.
139. Arora S, Olszewski MA, Tsang TM, McDonald RA, Toews GB, Huffnagle GB. Effect of cytokine interplay on macrophage polarization during chronic pulmonary infection with Cryptococcus neoformans. Infect Immun. 2011;79(5):1915-1926.
140. Gratchev A, Kzhyshkowska J, Kothe K, Muller-Molinet I, Kannookadan S, Utikal J, et al. Mphi1 and Mphi2 can be re-polarized by Th2 or Th1 cytokines, respectively, and respond to exogenous danger signals. Immunobiology. 2006;211(6-8):473-486.
141. Arora S, Hernandez Y, Erb-Downward JR, McDonald RA, Toews GB, Huffnagle GB. Role of IFN-gamma in regulating T2 immunity and the development of alternatively

activated macrophages during allergic bronchopulmonary mycosis. J Immunol. 2005;174(10):6346-6356.
142. Buhtoiarov IN, Lum H, Berke G, Paulnock DM, Sondel PM, Rakhmilevich AL. CD40 ligation activates murine macrophages via an IFN-gamma-dependent mechanism resulting in tumor cell destruction in vitro. J Immunol. 2005;174(10):6013-6022.
143. Sun L, Louie MC, Vannella KM, Wilke CA, LeVine AM, Moore BB, et al. New concepts of IL-10-induced lung fibrosis: fibrocyte recruitment and M2 activation in a CCL2/CCR2 axis. Am J Physiol Lung Cell Mol Physiol. 2011;300(3):L341-353.
144. Xing Z, Jordana M, Kirpalani H, Driscoll KE, Schall TJ, Gauldie J. Cytokine expression by neutrophils and macrophages in vivo: endotoxin induces tumor necrosis factor-alpha, macrophage inflammatory protein-2, interleukin-1 beta, and interleukin-6 but not RANTES or transforming growth factor-beta 1 mRNA expression in acute lung inflammation. Am J Respir Cell Mol Biol. 1994;10(2):148-153.
145. Dinarello CA. Therapeutic strategies to reduce IL-1 activity in treating local and systemic inflammation. Curr Opin Pharmacol. 2004;4(4):378-385.
146. Mulsow JJ, Watson RW, Fitzpatrick JM, O'Connell PR. Transforming growth factor-beta promotes pro-fibrotic behavior by serosal fibroblasts via PKC and ERK1/2 mitogen activated protein kinase cell signaling. Ann Surg. 2005;242(6):880-887, discussion 887-889.
147. Adamson R. Role of macrophages in normal wound healing: an overview. J Wound Care. 2009;18(8):349-351.
148. Mantovani A, Sica A, Sozzani S, Allavena P, Vecchi A, Locati M. The chemokine system in diverse forms of macrophage activation and polarization. Trends Immunol. 2004;25(12):677-686.
149. Xia W, Hilgenbrink AR, Matteson EL, Lockwood MB, Cheng JX, Low PS. A functional folate receptor is induced during macrophage activation and can be used to target drugs to activated macrophages. Blood. 2009;113(2):438-446.
150. Turk MJ, Breur GJ, Widmer WR, Paulos CM, Xu LC, Grote LA, et al. Folate-targeted imaging of activated macrophages in rats with adjuvant-induced arthritis. Arthritis Rheum. 2002;46(7):1947-1955.
151. Antohe F, Radulescu L, Puchianu E, Kennedy MD, Low PS, Simionescu M. Increased uptake of folate conjugates by activated macrophages in experimental hyperlipemia. Cell Tissue Res. 2005;320(2):277-285.
152. Martinez-Pomares L, Reid DM, Brown GD, Taylor PR, Stillion RJ, Linehan SA, et al. Analysis of mannose receptor regulation by IL-4, IL-10, and proteolytic processing using novel monoclonal antibodies. J Leukoc Biol. 2003;73(5):604-613.
153. Stein M, Keshav S, Harris N, Gordon S. Interleukin 4 potently enhances murine macrophage mannose receptor activity: a marker of alternative immunologic macrophage activation. J Exp Med. 1992;176(1):287-292.
154. Dube D, Francis M, Leroux JC, Winnik FM. Preparation and tumor cell uptake of poly(N-isopropylacrylamide) folate conjugates. Bioconjug Chem. 2002;13(3):685-692.
155. Nayak S, Lee H, Chmielewski J, Lyon LA. Folate-mediated cell targeting and cytotoxicity using thermoresponsive microgels. J Am Chem Soc. 2004;126(33):10258-10259.
156. Suzuki K, Kiyokawa N, Taguchi T, Takenouchi H, Saito M, Shimizu T, et al. Characterization of monocyte-macrophage-lineage cells induced from CD34+ bone marrow cells in vitro. Int J Hematol. 2007;85(5):384-389.
157. Godek ML, Sampson JA, Duchsherer NL, McElwee Q, Grainger DW. Rho GTPase protein expression and activation in murine monocytes/macrophages is not

modulated by model biomaterial surfaces in serum-containing in vitro cultures. J Biomater Sci Polym Ed. 2006;17(10):1141-1158.
158. Paul NE, Skazik C, Harwardt M, Bartneck M, Denecke B, Klee D, et al. Topographical control of human macrophages by a regularly microstructured polyvinylidene fluoride surface. Biomaterials. 2008;29(30):4056-4064.
159. Hesse M, Modolell M, La Flamme AC, Schito M, Fuentes JM, Cheever AW, et al. Differential regulation of nitric oxide synthase-2 and arginase-1 by type 1/type 2 cytokines in vivo: granulomatous pathology is shaped by the pattern of L-arginine metabolism. J Immunol. 2001;167(11):6533-6544.
160. Doyle AG, Herbein G, Montaner LJ, Minty AJ, Caput D, Ferrara P, et al. Interleukin-13 alters the activation state of murine macrophages in vitro: comparison with interleukin-4 and interferon-gamma. Eur J Immunol. 1994;24(6):1441-1445.
161. Badylak SF, Valentin JE, Ravindra AK, McCabe GP, Stewart-Akers AM. Macrophage phenotype as a determinant of biologic scaffold remodeling. Tissue Eng Part A. 2008;14(11):1835-1842.
162. Zhou J, Tsai YT, Weng H, Tang L. Noninvasive assessment of localized inflammatory responses. Free Radic Biol Med. 2012;52(1):218-226.
163. Zhou J, Tsai YT, Weng H, Tang EN, Nair A, Dave DP, et al. Real-time detection of implant-associated neutrophil responses using a formyl peptide receptor-targeting NIR nanoprobe. Int J Nanomedicine. 2012;7:2057-2068.
164. Baker D, Zhou, J., Tsai, YT., Patty, K., Weng, H.,Tang, E., Nair, A., Hu, WJ., Tang, L. Development of optical nanprobes for the detection of polarized macrophages during foreign body reactions. 2013.
165. Sun C, Sze R, Zhang M. Folic acid-PEG conjugated superparamagnetic nanoparticles for targeted cellular uptake and detection by MRI. J Biomed Mater Res A. 2006;78(3):550-557.
166. Wang H, Zhao P, Liang X, Gong X, Song T, Niu R, et al. Folate-PEG coated cationic modified chitosan--cholesterol liposomes for tumor-targeted drug delivery. Biomaterials. 2010;31(14):4129-4138.
167. Nahar M, Jain NK. Preparation, characterization and evaluation of targeting potential of amphotericin B-loaded engineered PLGA nanoparticles. Pharm Res. 2009;26(12):2588-2598.
168. Sohaebuddin SK, Thevenot PT, Baker D, Eaton JW, Tang L. Nanomaterial cytotoxicity is composition, size, and cell type dependent. Part Fibre Toxicol. 2010;7:22.
169. Benoit M, Desnues B, Mege JL. Macrophage polarization in bacterial infections. Journal of Immunology. 2008;181(6):3733-3739.
170. Mills CD, Kincaid K, Alt JM, Heilman MJ, Hill AM. M-1/M-2 macrophages and the Th1/Th2 paradigm. J Immunol. 2000;164(12):6166-6173.
171. Liew FY, Li Y, Moss D, Parkinson C, Rogers MV, Moncada S. Resistance to Leishmania major infection correlates with the induction of nitric oxide synthase in murine macrophages. Eur J Immunol. 1991;21(12):3009-3014.
172. Jiang WW, Su SH, Eberhart RC, Tang L. Phagocyte responses to degradable polymers. J Biomed Mater Res A. 2007;82(2):492-497.
173. Weng H, Zhou J, Tang L, Hu Z. Tissue responses to thermally-responsive hydrogel nanoparticles. J Biomater Sci Polym Ed. 2004;15(9):1167-1180.
174. Paulos CM, Turk MJ, Breur GJ, Low PS. Folate receptor-mediated targeting of therapeutic and imaging agents to activated macrophages in rheumatoid arthritis. Adv Drug Deliv Rev. 2004;56(8):1205-1217.

175. Lu Y, Stinnette TW, Westrick E, Klein PJ, Gehrke MA, Cross VA, et al. Treatment of experimental adjuvant arthritis with a novel folate receptor-targeted folic acid-aminopterin conjugate. Arthritis Res Ther. 2011;13(2):R56.
176. Turk MJ, Waters DJ, Low PS. Folate-conjugated liposomes preferentially target macrophages associated with ovarian carcinoma. Cancer Lett. 2004;213(2):165-172.
177. Basu MK, Lala S. Macrophage specific drug delivery in experimental leishmaniasis. Curr Mol Med. 2004;4(6):681-689.
178. Barratt GM, Nolibe D, Yapo A, Petit JF, Tenu JP. Use of mannosylated liposomes for in vivo targeting of a macrophage activator and control of artificial pulmonary metastases. Ann Inst Pasteur Immunol. 1987;138(3):437-450.
179. Muller CD, Schuber F. Neo-mannosylated liposomes: synthesis and interaction with mouse Kupffer cells and resident peritoneal macrophages. Biochim Biophys Acta. 1989;986(1):97-105.
180. Kassab R, Parrot-Lopez H, Fessi H, Menaucourt J, Bonaly R, Coulon J. Molecular recognition by Kluyveromyces of amphotericin B-loaded, galactose-tagged, poly (lactic acid) microspheres. Bioorg Med Chem. 2002;10(6):1767-1775.
181. Puig-Kroger A, Sierra-Filardi E, Dominguez-Soto A, Samaniego R, Corcuera MT, Gomez-Aguado F, et al. Folate receptor beta is expressed by tumor-associated macrophages and constitutes a marker for M2 anti-inflammatory/regulatory macrophages. Cancer Res. 2009;69(24):9395-9403.
182. Mukherjee S, Chen LY, Papadimos TJ, Huang S, Zuraw BL, Pan ZK. Lipopolysaccharide-driven Th2 cytokine production in macrophages is regulated by both MyD88 and TRAM. J Biol Chem. 2009;284(43):29391-29398.
183. Hattori Y, Sakaguchi M, Maitani Y. Folate-linked lipid-based nanoparticles deliver a NFkappaB decoy into activated murine macrophage-like RAW264.7 cells. Biol Pharm Bull. 2006;29(7):1516-1520.
184. Schierholz JM, Beuth J. Implant infections: a haven for opportunistic bacteria. J Hosp Infect. 2001;49(2):87-93.
185. Anderson JM. Mechanisms of Inflammation and Infection with Implanted Devices. Cardiovasc Pathol. 1993;2(3):S33-S41.
186. Nau GJ, Richmond JF, Schlesinger A, Jennings EG, Lander ES, Young RA. Human macrophage activation programs induced by bacterial pathogens. Proc Natl Acad Sci U S A. 2002;99(3):1503-1508.
187. Chen WT, Mahmood U, Weissleder R, Tung CH. Arthritis imaging using a near-infrared fluorescence folate-targeted probe. Arthritis Res Ther. 2005;7(2):R310-317.
188. Ruan G, Feng SS. Preparation and characterization of poly(lactic acid)-poly(ethylene glycol)-poly(lactic acid) (PLA-PEG-PLA) microspheres for controlled release of paclitaxel. Biomaterials. 2003;24(27):5037-5044.
189. Koning GA, Schiffelers RM, Wauben MH, Kok RJ, Mastrobattista E, Molema G, et al. Targeting of angiogenic endothelial cells at sites of inflammation by dexamethasone phosphate-containing RGD peptide liposomes inhibits experimental arthritis. Arthritis Rheum. 2006;54(4):1198-1208.
190. Michaelis M, Matousek J, Vogel JU, Slavik T, Langer K, Cinatl J, et al. Bovine seminal ribonuclease attached to nanoparticles made of polylactic acid kills leukemia and lymphoma cell lines in vitro. Anti-Cancer Drug. 2000;11(5):369-376.
191. Drury JL, Mooney DJ. Hydrogels for tissue engineering: scaffold design variables and applications. Biomaterials. 2003;24(24):4337-4351.
192. Hachet-Haas M, Balabanian K, Rohmer F, Pons F, Franchet C, Lecat S, et al. Small neutralizing molecules to inhibit actions of the chemokine CXCL12. J Biol Chem. 2008;283(34):23189-23199.

193. Lavoie P, Robitaille G, Agharazii M, Ledbetter S, Lebel M, Lariviere R. Neutralization of transforming growth factor-beta attenuates hypertension and prevents renal injury in uremic rats. J Hypertens. 2005;23(10):1895-1903.
194. Laping NJ, Grygielko E, Mathur A, Butter S, Bomberger J, Tweed C, et al. Inhibition of transforming growth factor (TGF)-beta1-induced extracellular matrix with a novel inhibitor of the TGF-beta type I receptor kinase activity: SB-431542. Mol Pharmacol. 2002;62(1):58-64.
195. Kagari T, Doi H, Shimozato T. The importance of IL-1 beta and TNF-alpha, and the noninvolvement of IL-6, in the development of monoclonal antibody-induced arthritis. J Immunol. 2002;169(3):1459-1466.
196. Badger AM, Bradbeer JN, Votta B, Lee JC, Adams JL, Griswold DE. Pharmacological profile of SB 203580, a selective inhibitor of cytokine suppressive binding protein/p38 kinase, in animal models of arthritis, bone resorption, endotoxin shock and immune function. J Pharmacol Exp Ther. 1996;279(3):1453-1461.
197. Zhou WD, Yang HM, Wang Q, Su DY, Liu FA, Zhao M, et al. SB203580, a p38 mitogen-activated protein kinase inhibitor, suppresses the development of endometriosis by down-regulating proinflammatory cytokines and proteolytic factors in a mouse model. Hum Reprod. 2010;25(12):3110-3116.
198. Jin N, Wang Q, Zhang X, Jiang D, Cheng H, Zhu K. The selective p38 mitogen-activated protein kinase inhibitor, SB203580, improves renal disease in MRL/lpr mouse model of systemic lupus. Int Immunopharmacol. 2011;11(9):1319-1326.
199. Waghabi MC, de Souza EM, de Oliveira GM, Keramidas M, Feige JJ, Araujo-Jorge TC, et al. Pharmacological inhibition of transforming growth factor beta signaling decreases infection and prevents heart damage in acute Chagas' disease. Antimicrob Agents Chemother. 2009;53(11):4694-4701.
200. Xiao YQ, Liu K, Shen JF, Xu GT, Ye W. SB-431542 inhibition of scar formation after filtration surgery and its potential mechanism. Invest Ophthalmol Vis Sci. 2009;50(4):1698-1706.
201. Muller U, Stenzel W, Kohler G, Werner C, Polte T, Hansen G, et al. IL-13 induces disease-promoting type 2 cytokines, alternatively activated macrophages and allergic inflammation during pulmonary infection of mice with Cryptococcus neoformans. Journal of Immunology. 2007;179(8):5367-5377.
202. Pechkovsky DV, Prasse A, Kollert F, Engel KMY, Dentler J, Luttmann W, et al. Alternatively activated alveolar macrophages in pulmonary fibrosis-mediator production and intracellular signal transduction. Clin Immunol. 2010;137(1):89-101.
203. Yang J, Shi G, Bei J, Wang S, Cao Y, Shang Q, et al. Fabrication and surface modification of macroporous poly(L-lactic acid) and poly(L-lactic-co-glycolic acid) (70/30) cell scaffolds for human skin fibroblast cell culture. J Biomed Mater Res. 2002;62(3):438-446.
204. Wolff RA, Tomas JJ, Hullett DA, Stark VE, van Rooijen N, Hoch JR. Macrophage depletion reduces monocyte chemotactic protein-1 and transforming growth factor-beta1 in healing rat vein grafts. J Vasc Surg. 2004;39(4):878-888.
205. Piguet PF, Collart MA, Grau GE, Kapanci Y, Vassalli P. Tumor Necrosis Factor Cachectin Plays a Key Role in Bleomycin-Induced Pneumonopathy and Fibrosis. J Exp Med. 1989;170(3):655-663.
206. Piguet PF, Vesin C, Grau GE, Thompson RC. Interleukin-1 Receptor Antagonist (Il-1ra) Prevents or Cures Pulmonary Fibrosis Elicited in Mice by Bleomycin or Silica. Cytokine. 1993;5(1):57-61.

207. Abu El-Asrar AM, Struyf S, Van Damme J, Geboes K. Circulating fibrocytes contribute to the myofibroblast population in proliferative vitreoretinopathy epiretinal membranes. Br J Ophthalmol. 2008;92(5):699-704.
208. Lord MS, Foss M, Besenbacher F. Influence of nanoscale surface topography on protein adsorption and cellular response. Nano Today. 2010;5(1):66-78.
209. Boyan BD, Lossdorfer S, Wang L, Zhao G, Lohmann CH, Cochran DL, et al. Osteoblasts generate an osteogenic microenvironment when grown on surfaces with rough microtopographies. Eur Cell Mater. 2003;6:22-27.
210. Chen S, Jones JA, Xu Y, Low HY, Anderson JM, Leong KW. Characterization of topographical effects on macrophage behavior in a foreign body response model. Biomaterials. 2010;31(13):3479-3491.
211. Schulte VA, Diez M, Moller M, Lensen MC. Surface topography induces fibroblast adhesion on intrinsically nonadhesive poly(ethylene glycol) substrates. Biomacromolecules. 2009;10(10):2795-2801.
212. Frey MT, Tsai IY, Russell TP, Hanks SK, Wang YL. Cellular responses to substrate topography: role of myosin II and focal adhesion kinase. Biophys J. 2006;90(10):3774-3782.
213. Fu J, Wang YK, Yang MT, Desai RA, Yu X, Liu Z, et al. Mechanical regulation of cell function with geometrically modulated elastomeric substrates. Nat Methods. 2010;7(9):733-736.
214. Teo BK, Ankam S, Chan LY, Yim EK. Nanotopography/mechanical induction of stem-cell differentiation. Methods Cell Biol. 2010;98:241-294.
215. Koumas L, Smith TJ, Feldon S, Blumberg N, Phipps RP. Thy-1 expression in human fibroblast subsets defines myofibroblastic or lipofibroblastic phenotypes. American Journal of Pathology. 2003;163(4):1291-1300.
216. Burgess HA, Daugherty LE, Thatcher TH, Lakatos HF, Ray DM, Redonnet M, et al. PPAR gamma agonists inhibit TGF-beta induced pulmonary myofibroblast differentiation and collagen production: implications for therapy of lung fibrosis. Am J Physiol-Lung C. 2005;288(6):L1146-L1153.
217. Chen H, Song W, Zhou F, Wu Z, Huang H, Zhang J, et al. The effect of surface microtopography of poly(dimethylsiloxane) on protein adsorption, platelet and cell adhesion. Colloids Surf B Biointerfaces. 2009;71(2):275-281.
218. Lensen MC, Schulte VA, Salber J, Diez M, Menges F, Moller M. Cellular responses to novel, micropatterned biomaterials. Pure Appl Chem. 2008;80(11):2479-2487.
219. Dickinson LE, Rand DR, Tsao J, Eberle W, Gerecht S. Endothelial cell responses to micropillar substrates of varying dimensions and stiffness. J Biomed Mater Res A. 2012;100(6):1457-1466.
220. Lotters JC, Olthuis W, Veltink PH, Bergveld P. The mechanical properties of the rubber elastic polymer polydimethylsiloxane for sensor applications. J Micromech Microeng. 1997;7(3):145-147.
221. Luo C, Meng F, Liu XC, Guo YY. Reinforcement of a PDMS master using an oxide-coated silicon plate. Microelectron J. 2006;37(1):5-11.
222. Liu XC, Luo C. Fabrication of super-hydrophobic channels. J Micromech Microeng. 2010;20(2):-.
223. Thevenot P, Nair A, Dey J, Yang J, Tang L. Method to Analyze Three-Dimensional Cell Distribution and Infiltration in Degradable Scaffolds. Tissue Eng Part C Methods. 2008;14(4):13.

224. Ghibaudo M, Trichet L, Le Digabel J, Richert A, Hersen P, Ladoux B. Substrate topography induces a crossover from 2D to 3D behavior in fibroblast migration. Biophys J. 2009;97(1):357-368.
225. Guillemette MD, Cui B, Roy E, Gauvin R, Giasson CJ, Esch MB, et al. Surface topography induces 3D self-orientation of cells and extracellular matrix resulting in improved tissue function. Integr Biol (Camb). 2009;1(2):196-204.
226. Baker DT, L. Effect of micro-topography on fibrocyte responses and fibrotic tissue reactions at the interface. In: Thomas Horbertt JLB, Willem Norde, editor. Proteins at Interfaces III State of the Art: American Chemical Society; 2012. p. 339-353.
227. Su WT, Liao YF, Lin CY, Li LT. Micropillar substrate influences the cellular attachment and laminin expression. Journal of Biomedical Materials Research Part A. 2010;93A(4):1463-1469.
228. Patel AA, Thakar RG, Chown M, Ayala P, Desai TA, Kumar S. Biophysical mechanisms of single-cell interactions with microtopographical cues. Biomed Microdevices. 2010;12(2):287-296.
229. Hausman GJ, Hausman DB. Search for the preadipocyte progenitor cell. J Clin Invest. 2006;116(12):3103-3106.
230. Crossno JT, Jr., Majka SM, Grazia T, Gill RG, Klemm DJ. Rosiglitazone promotes development of a novel adipocyte population from bone marrow-derived circulating progenitor cells. J Clin Invest. 2006;116(12):3220-3228.
231. Koh YJ, Kang S, Lee HJ, Choi TS, Lee HS, Cho CH, et al. Bone marrow-derived circulating progenitor cells fail to transdifferentiate into adipocytes in adult adipose tissues in mice. J Clin Invest. 2007;117(12):3684-3695.
232. Cao Y. Angiogenesis modulates adipogenesis and obesity. Journal of Clinical Investigation. 2007;117(9):2362-2368.
233. Ramirez-Zacarias JL, Castro-Munozledo F, Kuri-Harcuch W. Quantitation of adipose conversion and triglycerides by staining intracytoplasmic lipids with Oil red O. Histochemistry. 1992;97(6):493-497.
234. Tullberg-Reinert H, Jundt G. In situ measurement of collagen synthesis by human bone cells with a sirius red-based colorimetric microassay: effects of transforming growth factor beta2 and ascorbic acid 2-phosphate. Histochem Cell Biol. 1999;112(4):271-276.
235. Mattoli S, Bellini A, Schmidt M. The role of a human hematopoietic mesenchymal progenitor in wound healing and fibrotic diseases and implications for therapy. Curr Stem Cell Res Ther. 2009;4(4):266-280.
236. Kreider T, Anthony RM, Urban JF, Jr., Gause WC. Alternatively activated macrophages in helminth infections. Curr Opin Immunol. 2007;19(4):448-453.
237. Benoit M, Desnues B, Mege JL. Macrophage polarization in bacterial infections. J Immunol. 2008;181(6):3733-3739.
238. Herbert DR, Holscher C, Mohrs M, Arendse B, Schwegmann A, Radwanska M, et al. Alternative macrophage activation is essential for survival during schistosomiasis and downmodulates T helper 1 responses and immunopathology. Immunity. 2004;20(5):623-635.
239. Cobelli N, Scharf B, Crisi GM, Hardin J, Santambrogio L. Mediators of the inflammatory response to joint replacement devices. Nat Rev Rheumatol. 2011;7(10):600-608.
240. Fary C, Thomas GE, Taylor A, Beard D, Carr A, Glyn-Jones S. Diagnosing and investigating adverse reactions in metal on metal hip implants. BMJ. 2011;343:d7441.

241. Thomopoulos S, Fomovsky GM, Chandran PL, Holmes JW. Collagen fiber alignment does not explain mechanical anisotropy in fibroblast populated collagen gels. J Biomech Eng. 2007;129(5):642-650.
242. Engelmayr GC, Jr., Papworth GD, Watkins SC, Mayer JE, Jr., Sacks MS. Guidance of engineered tissue collagen orientation by large-scale scaffold microstructures. J Biomech. 2006;39(10):1819-1831.

Biographical Information

David William Baker received his Bachelor's Degree in Chemical Engineering from Clarkson University (NY) in May 2005. He then accepted a position as an Engineering Technician in research and development with Atrium Medical Corporation (Hudson NH). David was quickly promoted to an Associate Product Development Engineer where he worked primarily on a drug-eluting stent project, specializing in formulation research, accelerated aging and stability, and device design. Shorty after leaving Atrium to move to Texas, David began his work under Dr Liping Tang in pursuit of his PhD in Biomedical Engineering. Together, David and Dr Tang began investigating biomaterial surface interactions studying micropillar implants. This work revealed a critical and underestimated role of fibrocytes in biomaterial-mediated tissue responses. David and Dr Tang then began a series of projects to investigate fibrocyte-mediate responses. They further began to develop strategies to alleviate fibrocyte driven fibrotic responses, as discussed in this thesis. David currently has plans to continue his research into fibrocyte-mediated responses to biomaterials with the intention of co-editing a book with Dr Tang. However, David is also actively seeking employment opportunities in the greater Boston Area (MA) in product research and development.